Lake Qinghai, China: A multi-proxy investigation on sediment cores for the reconstructions of paleoclimate and paleoenvironment since the Marine Isotope Stage 3

Dem Fachbereich Material- und Geowissenschaften
der Technischen Universität Darmstadt
genehmigte Dissertation

zum Erlangen des akademischen Grades eines
Doktors der Naturwissenschaften
(Dr. rer. nat.)

von

JunQing YU

Darmstadt

Kurzfassung

Der Qinghai-See (auch bekannt als Koko Nor), das größte stehende Gewässer Chinas, liegt in der Nordostecke des Tibet-Qinghai Plateaus auf einer Höhe von 3193,7 m ü. NN. Er liegt in einem abflussloses Becken und hat eine Fläche von ungefähr 4437 km² und eine maximalen Tiefe von 26,5 m im Zentrum (gemessen im Jahr 1985). Das Einzugsgebiet des Sees ist etwa siebenmal so groß wie seine Oberfläche. Aufgrund des kalten und semiariden Klimas mit jährlichen Niederschlägen von 310-390 mm und einer jährlichen Verdunstung von 1460 mm ist das große Einzugsgebiet fast baumlos und größtenteils von Steppenvegetation bedeckt. Die Messungen aus den letzten 50 Jahren zeigen, dass der der Gesamtlösungsinhalt zwischen 12-14 g/l lag und sich der pH zwischen 9.1 und 9.4.bewegte. Karbonatminerale wie Aragonit und Calcit fallen heute direkt aus dem brackischen, alkalischen und karbonatübersättigten Wasser aus. Der sommerliche Niederschlag im Einzugsgebiet ist ein wichtiger Steuerungsfaktor für Änderungen des Seespiegels und der Wasserchemie. Weil der See heute am Rand des Monsungürtels liegt, wurden Klimaschwankungen, insbesondere Fluktuationen des Monsunregens, hochauflösend im Sedimentarchiv des Sees dokumentiert.

Die signifikante Reaktion des Tibet-Qinghai Plateaus auf den Einfluss globaler Zirkulationsmuster und des asiatischen Monsuns gab den Anstoß für die Untersuchung hochauflösender Paläoklimasignale in den Sedimentkernen des Qinghai-Sees. 1985 wurden während einer Geländekampagne mehr als 300 km hochauflösender seismischer Profile zur Untersuchung der Sedimentstrukturen im Seeuntergrund aufgenommen. Einige 5-6 m lange Sedimentkerne wurden mit einem Kullenberg-Zylinder-Kerngerät aus den 3 Beckenzentren entnommen. 1987 wurde ein 26 m langer Kern aus der Mitte des östlichen Teilbeckens erbohrt. Auf die Laboruntersuchungen der Sedimentkerne wurde ein Multi-Proxy-Ansatz angewandt, der lithologische, geochemische, paläobotanische, mineralogische und geophysikalische Parameter sowie die Untersuchung stabiler Isotope umfasste. Das Alter der Sedimente wurde mit ^{14}C-AMS-Datierungen an Pflanzenresten und an den jüngsten Sedimenten mit ^{210}Pb-Messungen bestimmt.

Diese Arbeit berichtet über neue Ergebnisse, die nach 1991 an zwei qualitativ hochwertigen Kernen, Q14B und Q16C, und an dem 26 m langen Bohrkern gewonnen wurden.. Das Ziel ist es, Paläoumweltdaten einer klimatischen Schlüssellokation als Beitrag zu PAGES (Past Gloabal Changes), dem Paläoklima-Kernprojekt von IGBP (International Geosphere-Biosphere Programme), für die Zeit seit dem seit dem Marinen Isotopenstadium 3 (MIS 3) beizusteuern. Ergebnisse und Schlussfolgerungen basieren auf den langjährigen Arbeiten des Autors und seinen Untersuchungen in den letzten 20 Jahren zur Paläoumwelt- und Paläoklimageschichte des Qinghai-Sees. Ein Teil der Ergebnisse wurden bereits publiziert, so Kapitel 5 im internationalen „Journal of Palaeolimnology" 28: 195-206, 2002, und in der europäischen Zeitschrift „GEOLINES" 11: 38-41, 2000. Kapitel 6 und Kapitel 7 werden als separate Artikel bei den internationalen Zeitschriften „Chemical Geology" beziehungsweise „Quaternary Science Reviews" eingereicht werden.

Ein Forschungsschwerpunkt der Dissertation war die mineralogische Untersuchung der postglazialen Karbonatabfolgen, mit welchen eine detaillierte Karbonatmineral-Stratigraphie aufgestellt werden konnte. Die Ergebnisse zeigen, dass die Variationen der Wasserchemie nicht nur eine Funktion des Seespiegels ist. Änderungen in

der Karbonatmineral-Zusammensetzung alleine oder in Kombination mit einer merklichen Änderung des Karbonatgehalts sind Folgen von Änderungen des Wasserhaushaltes und der Klimabedingngen. Dazu zählen die Intensität des Monsunregens und/oder der sommerlichen Verdunstung. Eine 13 cm mächtige Kalk-Dolomit-Schicht wurde unter karbonatischen Playa-Bedingungen um ~10,3-10 ka ^{14}C BP gebildet. Die Dolomit-Ablagerung zeigt eine starke negative Wasserbilanz des Playa-Sees in dieser Zeit an, die die Folge erhöhter sommerlicher Verdunstung ist, verstärkt durch andere kinetische Faktoren wie ein Mg/Ca-Verhältnis um 12 und in Zersetzung befindlichem organischen Material als Katalysator. Die postglaziale Karbonatsedimentation durchlief fünf Hauptphasen, von denen jede eine Periode eines bestimmten Niederschlags-Verdunstungs-Gleichgewichts repräsentiert. Die andauernde und vorherrschende Fällung von Aragonit resultierte in einer Anreicherung von Mg^{2+} und einer Abreicherung an Ca^{2+} und so zum graduellen Anstieg des Mg/Ca-Verhältnisses im Seewasser von ~12 am Beginn des Holozäns bis zu einem Gewichtsverhältnis von 82 im Jahre 1961.

Die Untersuchungen der stabilen Isotope in den kalkhaltigen Ablagerungen des großen Sees im Rahmen der Arbeit zeigt, dass der Trend der δ^{13}C-δ^{18}O Kovariante ein hilfreiches Werkzeug für die Rekonstruktion der paläohydrologischen Geschichte des lakustrinen Beckens ist. Diese Studie lieferte neue Daten, die zeigen, wie wichtig eine sorgfältige Auswahl der Karbonatproben für Isotopenuntersuchungen ist. Die Isotopenverhältnisse mancher primärer Karbonate, die in abflusslosen See-Becken gebildet werden, wie Aragonit-Laminae, unterliegen nicht dem Trend der δ^{13}C-δ^{18}O Kovariantion. Proben von primärem Dolomit zeigen die negativsten δ^{13}C-Werte und die Isotopenverhältnisse des Dolomits weichen vom Trend der Kovariantion ab. Trotzdem reflektieren weder die Isotopenverhältnisse der Aragonit-Laminae, die saisonale Oberflächenwasser-Ereignisse repräsentieren, noch die des primären Dolomits, die die Isotopeninformation einer mehrere hundert Jahre umfassenden Zeitspanne repräsentieren, eine Störung im Trend der δ^{13}C-δ^{18}O Kovariantion, des wesentlichen Isotopenmerkmals eines abflusslosen See-Beckens.

Ergebnisse eines seismischen Profils (Profil 1) und des 26 m langen Bohrkerns vom östlichen Teilbecken zeigen, dass der Qinghai-See sich um ca. 68,7 ka ^{14}C BP rasch vergrößerte, worauf bis etwa 28,8 ka ^{14}C BP feuchte, jedoch nicht vollglaziale Bedingungen herrschten. Die größte Ausdehnung des Sees war damals viel kleiner als im Holozän. Die Sedimente, die während dieser Periode gebildet wurden, zeigen eine Offlap-Abfolge, die auf ein generelles Schrumpfen des Sees bis zum Letzten Glazialen Maximum (LGM) hinweist. Die äolischen, löss-ähnlichen, sandigen Ablagerungen und die seismischen Daten weisen auf sehr kalte und aride Bedingungen im LGM (~28,8-18,3 ka ^{14}C BP) hin. Der 25 m lange Bohrkern im zentralen östlichen Becken enthielt keine Moränenablagerungen und deutet damit an, dass weder im MIS 3 noch im MIS 2 ein Gletschervorstoß in zentrale Teile des See-Beckens stattfand. Die Klimabedingungen während des MIS 3 waren nach dem Qinghai-See-Archiv wärmer als während des MIS 2, aber eindeutig kälter als im Holozän. Das, verglichen mit dem MIS 2, feuchtere Klima während des MIS 3 begünstigte deshalb nur einen regionalen Gletschervorstoß im nördlichen Tibet-Qinghai-Plateau.

Die Rekonstruktion des Seespiegels und des Paläoklimas am

Spätglazial-Holozän-Übergang schloss einen möglichen starken Schmelzwasserzufluss in den Qinghai-See aus. Das ist ein weiterer Hinweis auf einen geringen regionalen Gletschervorstoß während des LGM wegen des sehr ariden Klimas in der Region. Die Flachwasser-Bedingungen mit geringerer Karbonat-Produktion und geringerer organischer Produktivität deuten darauf hin, dass das Klima vor 11,6 ka ^{14}C BP viel kälter und trockener war als während des Holozäns. Der saisonale Zufluss von sedimentreichem Wasser stieg vor ~11,6 ka ^{14}C BP abrupt an und signalisiert damit einen höheren Niederschlag im Einzugsgebiet. Die Entwicklung eines karbonatischen Playa-Sees zwischen ~10,7 und 10 ka ^{14}C BP deutete auf das Fortbestehen einer negativen Wasserbilanz hin. Das Ende der Karbonat-Playa um ~10 ka ^{14}C BP war die Folge stärkeren Niederschlags und ein deutlicher Anstieg der organischen Produktivität markiert den abrupten Beginn des Holozäns. Das frühholozäne hydro-klimatische Regime zeichnet sich gegenüber allen späteren Stadien des Holozäns durch höhere sommerliche Verdunstung aus. Darauf weist eine höhere Karbonatproduktion bei gleichzeitiger höherer organischer Produktivität hin. Der frühholozäne Seespiegel lag etwa 20 m unter dem heutigen und deutet damit auf eine im Vergleich zur heutigen viel geringere effektive Feuchtigkeit hin.

Ein weiterer Anstieg der Monsunniederschläge ab ~8 ka ^{14}C BP wird von einer Abnahme der Karbonatproduktion und tieferen aquatischen Bedingungen angedeutet. Danach begann ein Anstieg des Baumpollenanteils. Um 7,5 ka ^{14}C BP erreichte dieser 50% des gesamten Pollenspektrums und blieb anschließend konstant bis etwa 4 ka ^{14}C BP. Dies deutet darauf hin, dass zwischen 7,5 und 4 ka ^{14}C BP die bewaldete Fläche im nordöstlichen Tibet-Qinghai-Plateau viel ausgedehnter war als heute. Die wärmeren und feuchteren Klimabedingungen zwischen ~8 und 4 ka ^{14}C BP wurden deshalb als das holozäne Klimaoptimum definiert.

Sediment-Daten weisen darauf hin, dass die Klimabedingungen seit ~4,1 ka ^{14}C BP im Allgemeinen den heutigen ähnlich waren. Klare Hinweise auf einen noch höheren Seespiegel während des mittleren Holozäns als im späten Holozän fehlen. Der Seespiegel schwankte zwischen fast vollständiger Austrocknung und einer Tiefe von ca. 30 m innerhalb der letzten 14 ka ^{14}C BP.

ABSTRACT

Lake Qinghai (also known as Koko Nor), the largest water body in China, lies on the northeast corner of the Tibet-Qinghai Plateau at the altitude of 3193.7 m above sea level. It is a closed-basin lake with an area of about 4437 km^2 and a maximal depth of 26.5 m at its center in 1985. Its catchment area is about 7 times larger than the lake size. Under a cold and semi-arid climate with an annual precipitation of 310-390 mm and an annual evaporation of 1460 mm, the large catchment is nearly treeless, covered mainly by steppe vegetation. In the past 50 years, the total dissolved solid of the lake was between 12 and 14 g/l and the pH was between 9.1 and 9.4. Carbonate minerals, such as aragonite and calcite, are precipitating today directly from the brackish, alkaline and carbonate-supersaturated water. Summer precipitation in the catchment exerts an important control on changes in both lake level and water chemistry. Because the lake today is situated at the outer margin of the Asian summer monsoon, past climate changes, fluctuations of monsoonal rainfall in particular, were sensitively documented in the sedimentary record of the lake.

The significance of the Tibet-Qinghai Plateau on influencing global circulation patterns and the Asian monsoon stimulated the investigation of high-resolution paleoclimate record from the sediment cores of Lake Qinghai. A field investigation took place in 1985. More than 300 km of high-resolution seismic profiles were recorded for the study of sub-bottom sediment structures. A number of 5-6 m long sediment columns were recovered with a Kullenberg piston corer from the three basin centers. In 1987, a 26 m long drill core was recovered from the middle of the eastern basin. A multi-proxy approach was applied to the laboratory investigation of sediment cores, including lithologic, geochemical, paleobotanical, mineralogical, geophysical logging, and stable-isotopic methods. Chronology is controlled by AMS radiocarbon dating of plant debris, in addition to ^{210}Pb dating of most recent sediments.

This thesis reports new results obtained after 1991 from two high quality cores, Q14B and Q16C, and on the 26 m drill core. It aims to provide key-site information for the international effort and database of the Past Global Changes (PAGES) community of the International Geosphere-Biosphere Program (IGBP) on regional paleoenvironmental and paleoclimate changes since the Marine Isotopic Stage 3 (MIS 3). Results and conclusions are based on the author's long-term effort and investigations in the past 20 years on the paleoenvironmental and paleoclimate history of Lake Qinghai. Part of the results has been published, such as Chapter 5, in the international "Journal of Paleolimnology" 28: 195-206, 2002, and in the European journal "GEOLINES" 11: 38-41, 2000. Chapter 6 and Chapter 7 will be submitted as two separate papers to the international journals "Chemical Geology" and "Quaternary Science Reviews", respectively.

One of the research foci of the dissertation is on mineralogical investigation on the postglacial calcareous succession, which established a detailed carbonate mineral stratigraphy. The results clearly indicate that the variations of water chemistry were not a simple function of lake levels. A marked change in carbonate mineral composition either alone or in combination with a noticeable change in carbonate content was most likely the consequence of a change in hydro-climate regime, such as a change of the intensity of monsoonal rainfall and/or of summer evaporation. A 13-cm-thick calcian dolomite layer was formed under a carbonate playa environment at ~10.3-10 ka ^{14}C BP. The dolomite

deposition reflects a strongly negative water balance of the playa lake at that time as a consequence of enhanced summer evaporation, in addition to effects from other kinetic factors such as a Mg/Ca ratio around 12, and decomposing organic matter as a catalyzer. The postglacial carbonate deposition underwent five main phases, each of them representing a distinguishable P-E balance period of the paleo-lake. The long-term and dominant precipitation of aragonite has resulted in the enrichment of Mg^{2+} and the deficiency of Ca^{2+}, so that the Mg/Ca ratio of the lake water increased gradually from ~12 at the onset of the Holocene to a weight ratio of 82 in 1961.

The stable isotope study of the thesis for the calcareous deposits of the large lake proved that the $\delta^{13}C$-$\delta^{18}O$ covariant trend is a useful tool for tracing the paleohydrological history of a lacustrine basin. This study provided new data showing the importance of a careful identification of carbonate samples used for isotopic study. The isotopic ratios of some primary carbonates formed in a closed-basin lake, such as aragonite laminae, do not fall into the $\delta^{13}C$-$\delta^{18}O$ covariant trend. Primary dolomite samples showed most negative $\delta^{13}C$ values and the isotopic ratios of the dolomite dissent from the covariant trend. Nevertheless, neither the isotopic ratios of aragonite laminae, which represent seasonal surface water events, nor those of primary dolomite, which reflect isotopic information spanning several hundred years, represents a breakdown of the $\delta^{13}C$-$\delta^{18}O$ covariant trend, the essential isotopic identity of the closed-basin lake.

Results from a seismic profile (Profile 1) and the 26 m drill core from the eastern basin reveal that Lake Qinghai expanded rapidly around 68.7 ka ^{14}C BP and remained in wet but not in full glacial conditions until about 28.8 ka ^{14}C BP. The largest extent of the paleo-lake size was much smaller than that of the Holocene. The sub-bottom sediment formed during this period of time show an offlap sequence, clearly indicating a general trend of shrinking in lake size towards the Last Glacial Maximum (LGM). The lake was in severely cold and arid conditions at the LGM (~28.8-18.3 ka ^{14}C BP), as suggested by the windblown loess-like sandy deposits and the seismic data. The 26 m drill core at the central eastern basin did not reveal moraine deposits, suggesting an exclusion of any glacial advance down to the central areas of the lake during both MIS 3 and MIS 2. Climatic conditions during the MIS 3, as indicated by the Lake Qinghai record, were warmer than during the MIS 2 but definitely colder than during the Holocene. The MIS 3 wetter climate therefore was comparatively more favourable for regional glacier advance rather than the MIS 2 in the northern Tibet-Qinghai Plateau.

The reconstruction of lake-level and paleoclimate across the Late Glacial/Holocene transition excluded the possibility of a large meltwater input into Lake Qinghai. This provided further evidence for a constrained regional glacier advance during the LGM due to the severity of arid climate in the region. The climate before 11.6 ka ^{14}C BP was much colder and drier than during the Holocene, as evidenced by a shallow lake environment with lower carbonate production and lower organic productivity. The seasonal inflow of sediment-laden water increased abruptly from ~11.6 ka ^{14}C BP, signaling an enhancement of precipitation in the large catchment. Between ~10.7 and 10 ka ^{14}C BP, a negative water balance persisted, as indicated by a development of a carbonate playa lake. At ~10 ka ^{14}C BP, the termination of the carbonate playa resulted from enhanced precipitation and a prominent increase in organic productivity marked abrupt onset of the Holocene. The early-Holocene hydro-climate regime is characterized by higher summer evaporation than

any later stages of the Holocene, as indicated by higher carbonate production alongside with high organic productivity. The early-Holocene lake level was about 20 m shallower than today, indicating that the effective moisture then was much lower than that of today.

A further increase in monsoonal precipitation occurred from ~8 ka ^{14}C BP, as suggested by a decrease in carbonate production and a deepened lake environment. Thereafter, tree pollen began to increase. It reached 50% of the total pollen around 7.5 ka ^{14}C BP and remained the high percentage until about 4 ka ^{14}C BP. This implies that between 7.5 and 4 ka ^{14}C BP, forested area in the N.E. Tibet-Qinghai Plateau was much more expanded than today. The warmer and wetter climate conditions between ~8 and 4 ka ^{14}C BP were therefore defined as the Holocene Climatic Optimum.

Sediment evidence indicates that climate conditions since ~4.1 ka ^{14}C BP remained generally similar to what it is today. Convincing evidence is lacking regarding whether the lake level was ever higher during the mid-Holocene than during the late Holocene. The lake level varied between near desiccation and a depth of ~30 m in the past 14 ka ^{14}C BP, as indicated by evidence from the Lake Qinghai cores.

Table of contents

1 Introduction

The Tibet-Qinghai Plateau, the largest elevated landmass and larruping topographic feature on Earth's surface (Figure 1.1), today exerts an important control on the global atmospheric circulation, and in particular on the pattern of the Asian monsoon. Paleoenvironmental changes on the Plateau and their relations to variations in Asian monsoon strength over the past 18,000 years are archived in diverse proxy records including sediment cores of modern lakes. Such high-resolution records can be obtained from closed-basin lakes because lake-level fluctuations respond sensitively to changes in the precipitation to evaporation balance in their catchments. These often relate to monsoon rainfall variations on regional scales. Climate proxy histories from the Tibet-Qinghai Plateau are indispensable for the global database used to test our understanding of the behavior of the climate system and as a guide to future conditions.

Lake Qinghai lies in an intermountain basin at $36^o54'N$, $100^o12'E$ on the northeast corner of the Tibet-Qinghai Plateau at an elevation of 3193.7 m a.s.l. in 1985. It is a closed-basin lake with a catchment area of 29,660 km^2. In spite of a cold/semiarid climate, the large catchment provides an annual surface runoff of more than 1.6 km^3 along with an estimated 0.64 km^3 groundwater input per year, maintaining a perennial lake of 4437 km^2 in size and a maximum water depth of 26.5 m (in 1985). It represents the largest water body now in the interior of China. Of the total annual catchment runoff today, about 1% is from meltwater of modern glaciers in the lake's upper catchment at altitudes above 4800 m a.s.l. The annual precipitation today is about 380 mm, of which about 65% falls in summer from June to September. The lake today is at the outer margin of the Asian summer-monsoon influence (Figure 1.2). Past changes in the monsoon circulation undoubtedly influenced the precipitation to evaporation balance of the lake and its catchment, resulting in substantial changes in lake level and water chemistry. The reconstructions of the lake levels and paleoclimatic change of Lake Qinghai could provide key-site information for the studies of the evolution of the Asian monsoon circulation and the past global change.

1.1 Previous investigations

1.1.1   1961-62 Expeditions to Lake Qinghai

A major study of Lake Qinghai has been carried out in 1961-1962. A number of scientists from four Institutes of the Chinese Academy of Sciences did a comprehensive field investigation on the lake, aiming at a systematic collection of geological, limnological, zoological and geochemical data. They attempted to study geological processes in the large closed-basin lake, including the deposition and preservation of organic matter and possible converting conditions towards petroleum source rock, and to provide an analogue for the study of sedimentary processes in ancient continental basins with respect to petroleum geology. During the field investigation, sediment cores retrieved from the modern lake bottom were limited to short cores of less than 1 m in length. Recovery of a continuous sediment record from the central basin of the lake was not the main focus of the 1961-62 investigations. However, the published monograph (Lanzhou Institute of Geology CAS, 1979) with substantial geological, limnological and zoological data provided a first

comparative framework for our later studies from 1985.
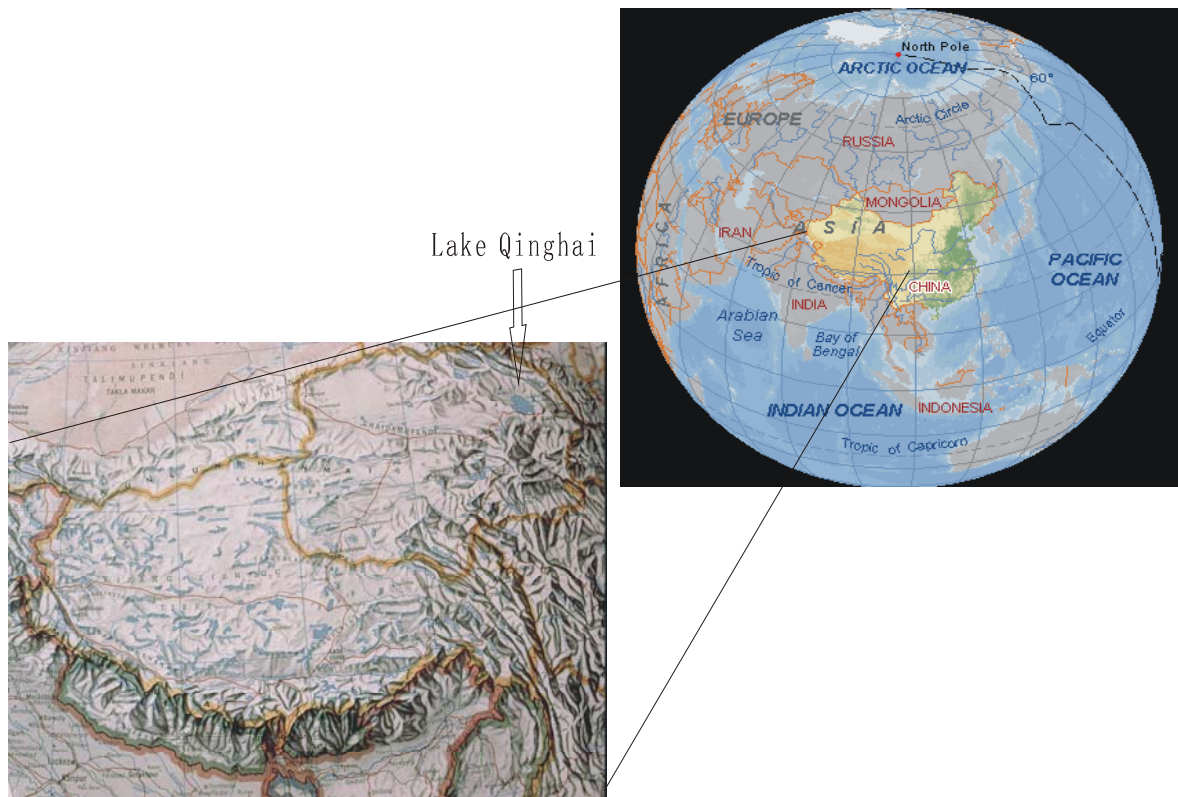
Figure 1.1 The Tibet-Qinghai Plateau, nearly 2 x 10^6 square kilometers in size and an average altitude of over 4000 m above sea level, exerts an important control on the most pronounced monsoon circulation of the globe, including the Indian and East Asian monsoon systems. Lake Qinghai lies on the northeast corner of the Plateau. The Himalayas, the world's highest mountains, are the southern margin of the Plateau.

1.1.2 Sino-Swiss Expedition in 1985

Remarkable progress on the reconstruction and understanding of the past global change was made between 1970 and 1985, but continuous proxy records from lakes in China with century to decadal scale were still too sparse to contribute significantly to the international study. The significance of Lake Qinghai for the study of Asian monsoon circulation has stimulated the formation of a Sino-Swiss joint project on the study of the paleoclimate and paleoenvironment of the high plateau lake, thanks also to China's opening-up policy. The major field investigation took place in the summer of 1985. Seismic profiles and piston cores were recovered from Lake Qinghai by the Sino-Swiss expedition team. The retrieved sediment cores were thereafter investigated and a series of scientific papers were published before 1992 in English (Kelts et al., 1989; Lister et al., 1991; Zhang et al., 1989; Wang and Chen, 1990) and in Chinese (Huang, 1988; Zhang et

al., 1989; Du et al., 1989; Chen et al., 1990; Kong et al., 1990).
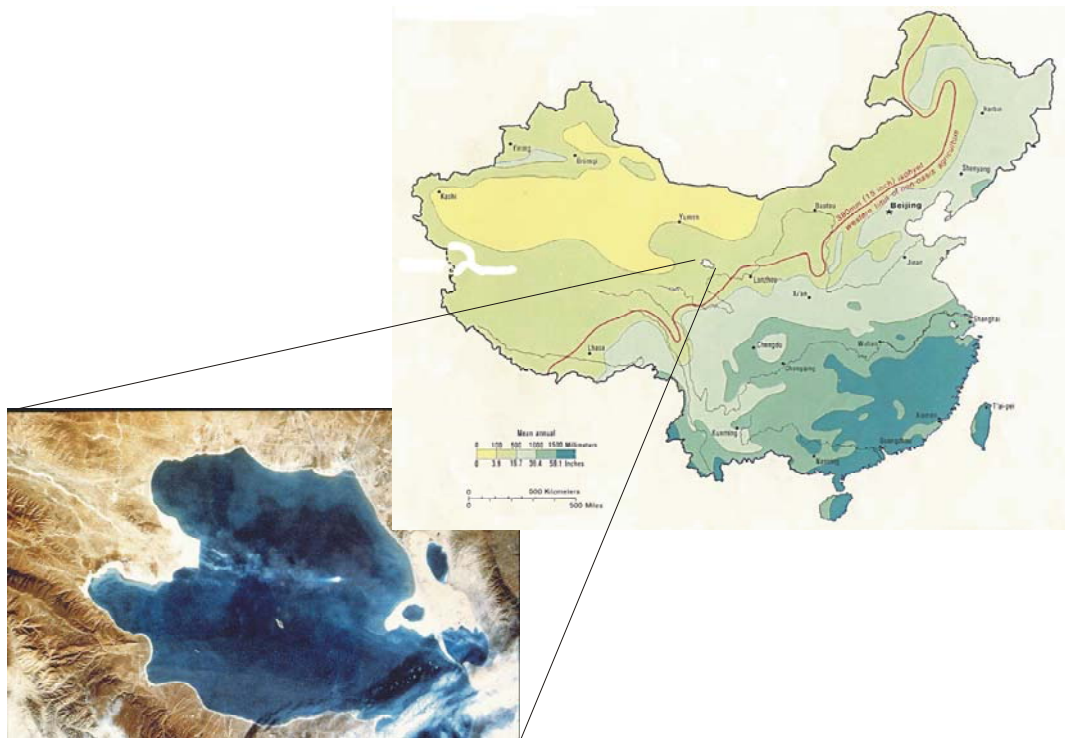
Figure 1.2 The precipitation gradient to the northwest decreasing steadily today from the southeast coast of China towards the site of Lake Qinghai, reflecting the pattern of the East Asian monsoon rainfall. Lake Qinghai is a hydrologically closed-basin lake, the lake-level of which responds sensitively to the changes of precipitation to evaporation balance.

1.1.3 The 1987 drill-core Project

After the initial expedition of 1985 with piston cores recovered from three subbasin centers, a new core with deeper penetration to recover the sediment sequence below the Q-reflector of seismic profiles was required in order to examine the basinal environmental conditions during the last Ice Age, and in particular to test the hypothesis of a unified ice cover on the N. E. Tibet-Qinghai Plateau (Kuhle, 1987). The fieldwork took place in the summer of 1987 and a drill core site was chosen at the middle of the eastern subbasin with a water depth of 23 m. A rotary drilling rig was assembled on a 90-ton barge, which was fixed by four anchors. The subbottom sediments down to 26 m were successfully cored by the drilling operation, although considerable difficulties were encountered with storms breaking the casing. The drill core named Q87 remains until now the deepest core taken from the central area of Lake Qinghai.

1.2 The aim of the thesis research

The aim of the thesis is to report new results obtained after 1991 from investigating on two piston cores, Q14B and Q16C, and on the 26 m drill-core from Lake Qinghai with a multidisciplinary approach. The thesis deals with several key paleoclimatic, paleolimnological, and geochemical problems, such as:

1) the pattern of climate change across the late Glacial-to-Holocene transition, including the Younger Dryas,

2) how to use mineralogical and stable isotopic records to track changes in water chemistry and brine evolution of a closed-basin lake associated with precipitation to evaporation balance, and

3) what are the paleoclimate conditions during the Marine Isotopic Stage 3 (MIS 3) and the Last Glacial Maximum on the northeast Tibet-Qinghai Plateau, as recorded in the sediment record of Lake Qinghai.

The thesis evaluates sediment records so far available from Lake Qinghai and other sites selected from the region with respect to a regional reconstruction of the paleoenvironmental and paleoclimate changes since the Stage 3.

1.3 Paleoclimate study of China: a brief review

1.3.1 East Asian monsoon—the modern climate system

A prominent feature of the East Asian monsoon today is the pronounced reversal of the climate system, exhibiting a distinct summer and winter component (Figure 1.3 A and B), that is, cold and dry in winter and hot and humid in summer. During the East Asian winter monsoon, strong northerly winds are prevailing and cover the entire region of the central and northern China and the South China Sea. This circulation pattern is controlled in general by a huge anticyclone over the Siberia-Mongolia, as shown by H (high-pressure cell) in Figure 1.3A. This is different from Indian monsoon in that the winter monsoon of India is not known to be present to any significant extent (Lau and Li, 1984). Although the summer monsoon has complex space and time structure, it generally induces rain belts by drawn moist air from the southern oceans, which stretch northwards for many thousands of kilometers (Chang, 2004). The difference in heat capacity between land and oceans is a basic physical mechanism causing the prevailing southerly winds in summer months. The huge elevated landmass of the Tibet-Qinghai Plateau provides an important and direct influence of the thermal and dynamic forcing on the circulation of East Asia. Heat flux over the Plateau and latent heat release contribute to a strong tropospheric heat source, which maintains the large scale Asian monsoon circulation (eg. Flohn, 1968; Hahn and Manabe, 1975; Lau and Li, 1984).

The study of the East Asian monsoon is important because monsoon related droughts and floods have enormous social and economic impacts on nearly one third of the world population. It also impacts on the global climate system including effects on the climate change (Chang, 2004). Some anomalies, such as those of sea surface temperature and snow cover over the Tibet-Qinghai Plateau, correlate well with the anomalies of the monsoon rainfall. More work has to be done for the improvement of long-range prediction of the

monsoons.

1.3.2 East Asian paleomonsoon

The circulation pattern of the East Asian monsoon system in the past differed greatly from that of today when large-scale climate forcing and boundary conditions were enormously different from today. Factors affecting the circulation include changes in solar radiation induced by orbital changes, orographic change of the Tibet-Qinghai Plateau due to tectonic development, changes in glacial climate and cryospheric conditions, and internal feedbacks within the climate system. These factors act simultaneously and over different time scales to amplify or lessen the seasonal development of continental heating or cooling, land-sea pressure gradients, latent heat transport, and moisture convergence, all of which control the strength of the monsoon circulation.

1.3.2.1 Loess records

Uplift of the Tibet-Qinghai Plateau was considered to be the most prominent orographic impact on the initiation, intensification, and long-term (10^6 years) evolution of the Asian monsoon circulation (Ruddiman, 1997; An et al., 2001). Model studies suggest that the plateau must be at least half its present elevation to induce a strong monsoon circulation (Prell and Kutzbach, 1992). High-resolution aeolian sequence preserved in the Loess Plateau (see Figure 1.4 for location) of China reveal that the East Asian monsoon may have commenced at least 7.2 Ma ago and the pulsed uplift of the Tibet-Qinghai Plateau at about 3.4 and 7.2 Ma may have played an important role in inducing climate change (An et al., 2001; An, 2004). The study of the aeolian deposits of Qinan in the western Loess Plateau (Figure 1.4) provided evidence indicating that large source areas of aeolian dust and energetic winter monsoon winds to transport the material must have existed in the interior of Asia by the early Miocene epoch (Guo et al., 2002), some 14 million years earlier than previously thought. The initial desertification in the Asian interior and changes in aridity and circulation thereafter in Asia are associated partially with the regional tectonic changes.

During the Quaternary Period, the windblown loess deposit developed extensively in northern China, forming a large Loess Plateau with an area of about 640,000 km^2 and an average thickness of ~150 m (Liu, 1985). The formation of the loess deposits in the past 2.5 Ma represents an intensified drier and windier climate if compared with the late Miocene and Pliocene climate, largely in accordance with the Quaternary glaciation of the Northern Hemisphere (Shackleton et al., 1984; Liu et al., 1985; Kukla and An, 1989). Changes in Siberia High, which were associated with continental ice-sheets and sea-ice cover, may have played an important role in controlling the winter monsoon intensity (Ding et al., 1992). A number of loess-paleosol sections were intensely investigated particularly in the past two decades as it has been recognized as one of the important and continuous terrestrial proxy records for the study of the past global changes. Chronology of the Quaternary loess deposits is mainly based on paleomagnetic stratigraphy (Heller and Liu, 1982; Liu et al., 1988; Kukla and An, 1989). Magnetic susceptibility and grain-size profiles of loess-paleosol sequences from the Loess Plateau were used as the main proxy records for the reconstruction of the East Asian monsoon fluctuations in the past 2.5 Ma. In general, paleosol layers, particularly those of well-developed paleosol layers, show higher values in magnetic susceptibility and lower percentage in coarser particle fraction than in

loess layers. They are formed during warm and wet period, representing events of strengthened summer monsoon. Loess layers involve higher fraction of fine sand and have lower values of magnetic susceptibility. The >63μm particle content in a loess-paleosol sequence is employed as a proxy indicating wet-dry variations of paleoclimate or as a dust-storm indicator when a high content occurs. Quartz particle size was also considered to be an ideal index because the quartz particles resist pedogenic alteration (An and Porter, 1997). This index was used for tracing winter monsoon conditions at the Loess Plateau and six events relating to strengthened winter monsoon between 110 and 70 ka correlate well with those cold events (C19-C24) identified by the *N. pachyderma* (s.) records from North Atlantic during the last interglacial period (McManus et al., 1994; An, 2000). The quartz particle-size data from the Luochuan loess section show good correlation with the *N. pachyderma* (s.) record of the past 80 ka (Bond et al., 1993), suggesting that the Heinrich Events may have had fingerprints in the Chinese loess (Porter and An, 1995).
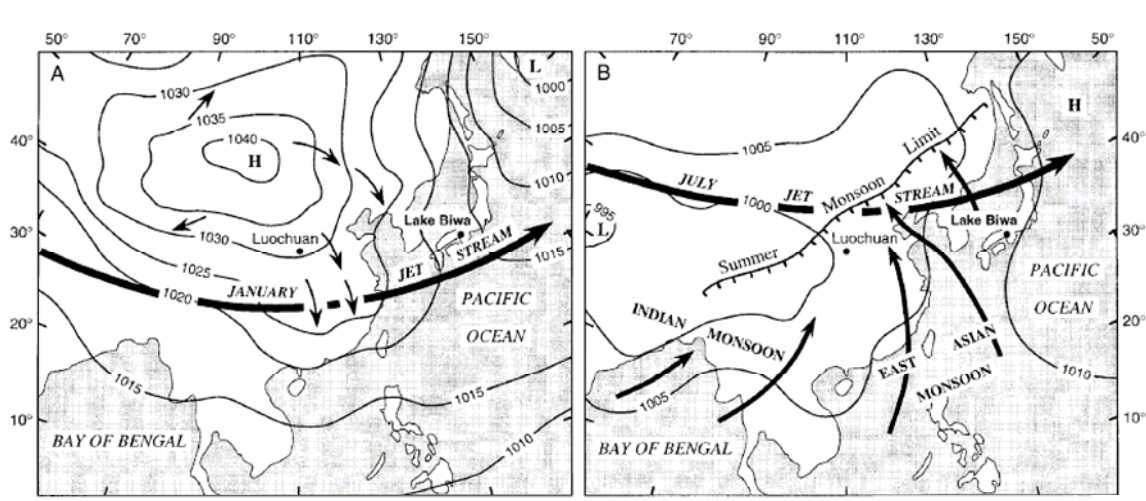
Figure 1.3 The East Asian monsoon system characterized by a distinct seasonal reversal of the pressure gradient. In winter (A) the Siberia-Mongolia High pushes the westerly jet stream southwards, and cold and dry northerly winds are prevailing. During summer months (B), moist airs from the southern low-latitude oceans are driven northwards by the summer monsoon and large areas over East Asia are overall hot and humid (After Xiao et al., 1997; Zhang and Lin, 1992; Chinese Academy of Sciences, 1984).

The characteristics of the East-Asian winter monsoon variability in terms of the Milankovitch periodicities of climate change over the past 2.5 Ma were examined by the study of the Baoji loess-paleosol section based on grain-size data (Ding et al., 1994) and a comparison of the proxy-record with a DSDP (Site 607, N. Atlantic) $\delta^{18}O$ record (Liu et al., 1999). The results indicate that an abrupt transition of winter monsoon variability from various periodicities to dominant 41-ka cycles occurred at 1.7-1.6 Ma as one of the two major shifts in climate modes. Another major shift at 0.8-0.5 Ma is characterized by a relatively gradual transition from constant 41-ka cycles to predominant 100-ka climatic oscillations. This 0.8-0.5 Ma shift matches that registered in deep-sea $\delta^{18}O$ records, whereas the 1.7-1.6 Ma shift is absent in global ice volume changes. However, the strong 41-cycles shown in the Baoji loess record are episodically missing in the proxy records of Luochuan and Xifeng loess-paleosol sections in the central Loess Plateau (refer to Figure

1.4 for location), which is attributed to the relatively low time-resolution of the paleosol units or the unstable depositional process of the dust (Lu et al., 2004). Rather, the longer cycles of approximately 400 ka and 100 ka relating to eccentricity frequencies of the solar irradiance are well recorded. In addition, other non-orbital cycles of 66-, 56-, 33- and 27-ka show quite strong intensity in the loess record, which has been attributed to unstable dust deposition processes and pedogenic processes in the paleosol units.

Figure 1.4 The Loess Plateau of China, and the locations of several
well-studied loess-paleosol sections (after Guo et al., 2002).

1.3.2.2 Marine records

Oceanic conditions of the Western Pacific, which is one active component of the climate system, impact on the East Asian monsoon circulation at present, as well as in the past. The Western Pacific Warm Pool (WPWP), the largest expanse of warm water today

with average annual temperature exceeding 28°C, provides strong latent heat export. Thus it plays a leading role in driving atmospheric circulation (Webster, 1994; 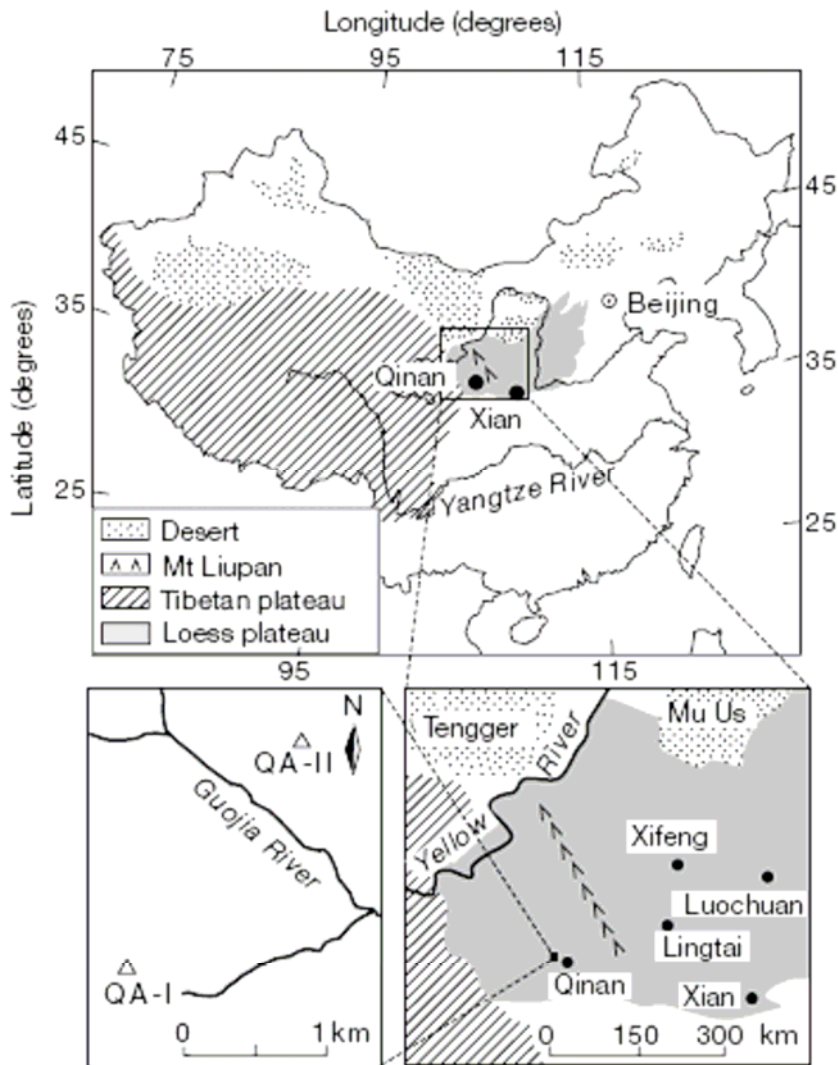Gagen et al., 2004). It is also the major source of atmospheric moisture. According to Dodson et al. (2004), the switch on and off of this moisture source through sea-level variation would have both regional and global implications, for example, in controlling the vigor of ENSO. Cyclones originating in tropical and subtropical regions in the south may affect the climate of southern China and adjacent islands from spring to autumn, while in summer they may extend as far north as the southern coasts of Japan and Korea, bringing intense storms. The January and July monsoon circulation is illustrated by the seasonal reversal of wind patterns and an enormous change from winter to summer precipitation pattern (refer to Figure 1 in Clemens et al., 2003). It may also be illustrated by the marked difference of average temperature patterns between January and July for both hemispheres in the PEP II region (see Figure 2 in Dodson et al., 2004).

Sea surface temperature (SST) reconstructions from foraminiferal Mg/Ca, alkenone, and revised coral Sr/Ca palaeothermometry agree that SSTs in the Indo-Pacific Warm Pool (IPWP) during the LGM were ~3 ^{o}C cooler than at present (Gagen et al., 2004). This reconstructed temperature supports the inference that tropical sea-surface temperatures (SSTs) were lower than the previous estimates (CLIMAP members, 1981; Thunell et al., 1994), implying a weaker hydrological cycle and enhanced aridity on continents during glacial periods. Marginal seas along Asian continent on the Western Pacific had prominent climatic and environmental impact on the region during the late Quaternary glacial cycles because large eustatic sea-level fluctuations resulted in major landward and seaward migrations of the coastline, as well as the closure or opening of the marginal seas via strait gateways to the ocean, which had significant impact on the paleoceanographic circulation (Wang, 1999). The South China Sea (SCS), a marginal sea intensely studied recently, turned to be semi-closed due to an about 100-m (or more) decrease in sea level during the LGM; winter temperature was 6-10 ^{o}C colder with a seasonality much stronger than it is today (Wang and Sun, 1994). As such, much information on the history and variability of the Asian paleomonsoon associated with Quaternary glacial-interglacial cycles can be deciphered from the marine proxy records of the Western Pacific. A number of proxy records obtained by multiple approaches of isotopes, micropaleontology, sedimentology and geochemistry have been applied to investigate some major unknowns of monsoonal paleoclimate at SCS, which include continental aridity and moisture, wind strength, temperature, salinity, and productivity near the sea surface (L. Wang et al., 1999). Briefly, the oxygen isotopic approach was applied to study SST, sea surface salinity (SSS), upwelling, monsoon wind intensity, and the implied global ice volume. The stable carbon isotopic records were used to indicate changes in surface water nutrient level, wind intensity and upwelling. The combined records of silt modal grain-size are useful for tracing fluvial input relating to summer monsoon precipitation and aeolian dust associated with winter monsoon wind. The alkenon biomarker U$^k_{37}$ index and planktonic foraminiferal (PF) census data were used to estimate SST and SSS. In the most recent review, Wang et al. (2005) has evaluated marine proxies, pointing out that some of them were well studied such as census counts of the planktonic foraminifera *Globigerina bulloides*, whereas there were also potential deficiencies in the interpretation of individual proxies. In the significantly weaker upwelling regions of the South and East China Seas, *G. bulloides* is however not as dominant as *N. Dutertrei*, and therefore the later was applied as an upwelling indicator (Jian et al., 2001). Table 1 in the review paper provided a summary

with more information regarding the proxy data and related publications for paleomonsoon reconstructions.

Orbital-scale variability of summer and winter monsoon intensities was examined based on marine proxy records from the SCS. The pollen data of a core at the ODP Site 1144 provided a paleomonsoon proxy-record for the past 1 Ma, using tree-pollen influx to indicate winter-monsoon strength and fern spore proportions to reflect summer-monsoon strength. The spectrum analyses of the pollen percentages of pine and herbs show the presence of 100-ka, 41-ka and 21-ka Milankovitch cyclicities and the tropical-specific 10-ka semi-precession cycles (Sun et al., 2003). The relative intensity of summer and winter monsoons over the past 2 Ma was also assessed by the proxy record of clay mineral assemblage from a core at the ODP Site 1146 (Liu et al., 2003). In general, strengthened summer-monsoon winds during interglacial periods were represented by higher smectites/(illite+chlorite) ratios, and conversely, the lower ratios indicate strongly intensified winter monsoon during glacial periods. Seasonality may have been enhanced between 1.2 and 0.4 Ma, as suggested by the higher mean values of the ratios. Orbital-scale cyclicity can be observed by means of spectral analysis of the ratio data, and the 41-ka cycles are particularly prominent between 2 and 1.2 Ma. Wehausen and Brumsack (2002) employed K/Si ratios from the high-precision element records of Pliocene core intervals from the ODP Site 1145 as a proxy of reconstructing the history of chemical weathering associated with summer monsoon precipitation. The high correlation of the K/Si record with the Northern Hemisphere summer insolation reflects the astronomical forcing (precession of equinoxes) of summer monsoon at 3.2-2.5 Ma.

The high-resolution proxy records from the SCS deep-sea cores provided important contribution to the understanding of climate change since the marine isotopic stage 3 (MIS 3) in association with the East Asian monsoon evolution. Based on the study of 10 sediment cores and 40 core-top samples from the SCS, the following conclusions were drawn in regard to the paleoclimate of the last 40 ka (L. Wang et al., 1999). Heinrich Event 4 probably corresponded to an arid and cool phase in South China. Major events of freshwater flooding associated with summer monsoon rain occurred also in the late Stage 3, as evidenced by short lasting SSS minima in the southern and western SCS. The summer monsoon-driven fluvial runoff and sediment supply intensified right after the LGM insolation minimum, parallel to the early start of Antarctic ice melt and about 3500 years prior to the δ^{18}O signal of post-glacial sea-level rise. The Younger Dryas did not induce a cooling but an arid episode. Cold spells occurred roughly every 3000 years during the Holocene.

The SST of the LGM, as generally agreed by all interpretations from various proxy records, indicates a colder climate with winter monsoon much intensified in the northern SCS than it is today (Wang and Wang, 1990; P. Wang et al., 1995; Huang et al., 1997; Chen et al., 1999). This is accordant with geological evidence from various environmental archives at nearly all reported sites from different regions over the northern Hemisphere. It is not surprising to have such a good accordance primarily because the cause of the LGM cold episode is the insolation minimum at that time. While the cause of the Younger Dryas, the well-established phenomenon of northern Europe, is debated since at least 20 years ago, a positive excursion of foraminiferal δ^{18}O from Sulu Sea record was interpreted as a YD equivalent (Linsley and Thunell, 1990; Kudrass et al., 1991). However, considerable

debate exists on whether the heavier $\delta^{18}O$ values during this time interval are indeed a reflection of decreased SSTs or of other environmental processes (Steinke et al., 2001). The authors thus measured other proxy records for the SST reconstruction, with a particular attempt of detecting a possible YD climate setback in the tropical SCS. The reconstructed SSTs estimated from three different foraminiferal transfer functions did not indicate any consistent cooling. The $U^{k'}_{37}$ SST estimates however show a cooling of ca. 0.2-0.6°C compared to the Bølling-Allerød period. Apparently, more efforts are still needed in order to provide a confirmation of the YD impact on this region (Maloney, 1996).

As clearly stated and recommended by Wang et al. (2005), in order to improve our understanding of the monsoon variability on decadal to millennial time scales from marine records, we first need to improve our knowledge of monsoon proxies by means of a systematic collection of long-term series of sediment trap data along with numbers of carefully calibrated core-top data sets, as well as the satellite data of coeval meteorological observations. This approach and outcomes will surely help to evaluate a dozen proxies reported and to determine how much of their variability is uniquely associated with monsoon dynamics (Clemens et al., 2003). It is equally important to have a substantial improvement on dating of marine sediment archives in terms of methodology and accuracy. For a better understanding of monsoon variability on the sub-orbital time scales, continuous, undisturbed cores in large diameter from sites with high deposition rate and best of all varved marine sediments are needed.

1.3.2.3 Ice core records

Two ice caps on the Tibet-Qinghai Plateau were drilled since 1987 for ice-core proxy records of climate change. Three ice cores of up to 139.8 m long were recovered to bedrock from the Dunde ice cap summit (Thompson et al., 1989). The ice cap is about 200 km west of Lake Qinghai. Counting the annual $\delta^{18}O$ and microparticle concentration peaks to 70 m and the visible dust layers below 70 m indicates that the ice at 117 m depth was deposited about 4550 years ago. The age at the prominent stratigraphic transition at 129.2 m depth in the D-1 core is calculated to be about 11,950 years ago. The investigators estimated the age near the bottom of the D-1 core being potentially more than 100,000 years old. $\delta^{18}O$ ratios, used as a temperature proxy as in all Greenland and polar ice cores, show more negative values in the lower 10 m of D-1. This, in conjunction with the evidence of increased dust content decreased soluble aerosol concentrations, suggests that the late glacial stage was apparently colder, wetter, and dustier than Holocene conditions. All proxy records of the core show abrupt change at ~10,000 years BP. The striking feature of the stable isotopic record, showing extreme less negative values of the last 60 years, may document a greenhouse warming.

In 1992, a 308 m core was recovered to bedrock from the Guliya ice cap located in the far western Mt. Kunlun on the Tibet-Qinghai Plateau (Thompson et al., 1997). It provided more detailed information about the glacial stage in comparison with the Dunde ice-core record in which the pre-Holocene ice was confined to the bottom 10 m of the core. The deepest 20 m of the ice-core may be more than 500 ka based on ^{36}Cl data. Partly because counting layers is usually precluded below 120 m in ice cores due to substaintial thinning, the Guliya time scale for the past 110 ka was established using the apparent correlation between atmospheric CH_4 levels and stadial and interstadial events inferred from values in

polar cores. Most of the interstadial peaks and stadial valleys of the GISP2 CH_4 record are reasonably reproduced in the Guliya $\delta^{18}O$ record. The time scale construction in this manner precluded the periods before 132 ka because MIS 6 ice is not clearly indicated in the Guliya isotopic record.

A sequence of stadial and interstadial events, as suggested by the Guliya $\delta^{18}O$ record, punctuated the last glacial stage (~10 to 110 ka). The precessional forcing of 23 ka was apparently stronger than the obliquitous forcing of 41 ka. This is expected in the mid-latitudes of the Northern Hemisphere either directly from caloric summer insolation or from a moisture feedback amplification of the 23-ka cycle. The ice core record showed approximately 100 $\delta^{18}O$ oscillations between 15 and 33 ka with amplitudes from ~2 to 21 ‰ and an average period of 200 years. Possibly, these short-term variations were resulted from 200-year cycles in sunspot activity. A $\delta^{18}O$ reversal event between 146.5 and 149.5 m following a step rising in $\delta^{18}O$ was interpreted as the Younger Dryas. The $\delta^{18}O$ values of the early-Holocene ice interval between 100 and 130 m were however more depleted in the Guliya record. The large $\delta^{18}O$ oscillations cannot be accounted for solely by temperature variations, including the high $\delta^{18}O$ values of the MIS 3 ice.

1.3.2.4 Lacustrine records

Proxy records from lacustrine basins

Two lacustrine basins in China, the Zoige and Heqing basins, were selected as drill-core sites in 1990s for investigating paleoclimate records of East Asia in the past 1 Ma in order to reconstruct the Asian monsoon evolution in conjunction with China's loess and marine records. **Zoige Basin** is located in the northeastern part of the Tibet-Qinghai Plateau at the elevation of about 3400 m above sea level (a.s.l). The total area of the Zoige basin is about 19600 km^2, which is mainly covered by highland steppe vegetation today with a partial coverage of wetland vegetation. Two sediment cores, named RH and RM, were drilled down to 120.4 m and 310.5 m, respectively. The sediments of the RH core are distinguished as lacustrine sediments intercalated with fluvial deposits, representing an 826 ka depositional history of the Zoige basin; chronology of the core is based on ^{14}C measurements and magnetostratigraphy (Liu et al., 1994). The core RM, located at the terrace of the Heihe River, comprises silty clay, muddy silt, and silt with intercalated thin layers of peat and fine sand; the bottom of the 310.5-m-long core is dated at 900 ka (Xue et al., 1999). Data from geochemical analysis for the sediments of the top 31 m of the RM core indicates that 1) carbonate content is mostly below 5%, 2) TOC is mostly lower than 1%, and hydrogen index (HI) is lower than 160, fluctuating around the value of 100. These stratigraphic variables are thought to reflect 1) effective humidity, 2) organic productivity of the paleo-lake, terrestrial input of organic debris, and OM preservation, and 3) composition of OM, namely, charcoal or coal-related materials if the HI is below 200. The $\delta^{18}O$ variations of the carbonate were considered to reflect a positive correlation with temperature variations, because $\delta^{18}O$ is negatively correlated with $\delta^{13}C$.

It is interesting to learn that authigenic calcite could be separated from the sediment samples mixed with detrital calcite, particularly under the circumstances that most of the samples contain less than 5% in carbonate content (Wu et al., 1997; Wu et al., 2000). Stable isotope measurements of such carbonate samples from the 0-30 m section of core

RM gave rise to a $\delta^{18}O$ curve that was used for indicating paleotemperature variations in the past 140 ka. Chronology of the section is based on 6 radiocarbon dates, including the youngest date of 3,324±145 a BP at 2.6 m and the oldest date of 33,140±2350 a BP at 8.2 m, and the Black event (110,000 a BP) at 25 m. Low values in the $\delta^{18}O$ curve are thought to represent cold and dry periods, some of which were correlated with 4 Heinich events H6, H5, H4 and H3. Some high values were thought to reflect the periods of warm climate correlative with IS20, IS19, IS17, IS14 and IS8 in the GRIP ice core record.

Pollen analysis was carried out for the 120.4-32 m section of core RH. Pollen grains are overall poorly preserved in the sediments. The 88.4-m-long section was divided into 11 zones relatively rich in pollen grains and 8 zones with almost no pollen grains (Liu et al., 1994). One warm stage (interglacial) at 480-298 ka BP and two cold stages (glacial) at 710-529 ka BP and 298-128 ka BP, respectively, were interpreted based mainly on the pollen record. More attention should be paid to the following aspects. Facies analysis for the cored sedimentary sequence should be elaborately done in order to distinguish lacustrine, alluvial, or possibly fluvial deposits, as well as subfacies deposits. Core correlation between RH and RM is apparently needed in order to clarify why the ages at the bottom of the two cores RM (310.5-m-long) and RH (120.4-m-long) are nearly the same. Prior to the stable isotopic analyses for carbonate sediments, mineralogical analysis is fundamental in order to avoid unnecessary stable isotope analysis if the dominant carbonate minerals are detrital in origin.

Heqing basin is a fault-controlled tectonic depression in the Dianxi Plateau of Yunnan province. The Dianxi Plateau is a transitional zone between the Tibetan Plateau and Yun-Gui Plateau. High mountains alongside with "V-shape deep valleys" cut by several main rivers all flowing from north to south, characterize the topographic feature of the western part of the Dianxi Plateau. Earthquakes occur relatively frequent due to active neotectonic movements in the areas. Heqing basin has a total area of about 184 km2. Granite and limestone are the main outcrops in the drainage basin. The regional climate is warm and wet in summer due to the influence of moist air from the Bengal Bay, while in winter the climate is controlled mainly by the southern branch of the westerly jet (Yang et al., 2000). At present, the snowline is at the elevation of about 5000 m a.s.l., and tree lines for the upper reach of conifer forest at 3900 and for fir and spruce forest at 3100-3810 m. Coniferous forest mixed with broad-leaf trees exist between 2800 and 3200 m a.s.l. and dominant trees include *Picea, Tsuga, Querus pannosa, Q. rehderiana*. *Pinus* forest exists only at the elevation blow 2800 m a.s.l. Supplied by numbers of rivers from the surrounding mountains, Yanggong River today is the main river system flowing from the south to north across the basin into Lijiang River.

A 168 m core HQ was drill at the site on the line with widest across between Yanggon River and the basin edges. Three polarity transitions were observed: the Jaramillo upper boundary at 167.0 m, the Brunhes/Matuyama boundary at 141.5 m, and the Black event at 17 m (Hu et al., 2005). This magnetic polarity time scale, together with an AMS ^{14}C age of 51.62 ka BP (+2.42/-1.85 ka) at the 7.3 m and cyclostratigraphy, established a chronological framework for the cored sequence formed in the past 1 Ma. Carbonate content was determined by the method of weight loss following the treatment of adding dilute HCl, provided that it represents the total percentage of carbonate in the samples. The carbonate is mainly detrital in origin as the surrounding rocks are mainly limestone.

Down-core variations in carbonate content therefore represent the influx of detrital carbonate. The highs and lows of magnetic susceptibility (χ) are related to warm and cold periods. The χ values are reversely correlated with carbonate contents though positive correlation exists for some intervals of the core. Alterations between temperate-arid and cold-humid climate conditions are indicated by the pollen data of the core, representing a typical regional paleoclimatic pattern. Highs in *Picea+Tsuga* represent colder and more humid climate conditions and lows in *Pinus* reflect more temperate arid conditions. Pollen assemblages and corresponding climatic conditions could not be consistently interpreted for different environmental stages (Yang et al., 2000). Spectral analysis for the down-core variation records of carbonate, susceptibility and Anhysteretic Remanent Magnetization (ARM) shows clear Milankovitch cyclicities (95 ka), but not for the records of *Pinus* and *Picea+Tsuga*. The answer is yet inconclusive regarding why carbonate content, TOC and C/N ratio all peaked at the sediment interval formed during the LGM (Jiang et al., 1999). Investigation to a new core of more than 500 m long, drilled at the site close to core HQ with improved coring technology is ongoing, and the outcome will expectably shed more light on the regional paleoclimate history.

Sediment records from modern lakes

Numbers of field trips to lakes located in different geographic sites and diverse geomorphological and climatic setting in China started around 1985, focused mainly on paleoclimate and paleoenvironmental studies. Sediment cores were recovered from those modern lakes, including lakes in the Tibet-Qinghai Plateau: Lake Qinghai (Kelts et al., 1989; Lister et al., 1991; Yu and Kelts, 2002), Lake Sumxi (Gasse et al., 1991), Lake Siling-co (Kashiwaya et al., 1991; Kashiwaya et al., 1995), Lake Bangong (Gasse et al., 1996), Lake Luanhaizi (Mischke et al., 2005; Herzschuh et al., 2005); lakes in the Yunnan-Guizhou Plateau: Lakes Xingyun and Qilu (Hodell et al., 1999), Lake Erhai (Shen et al., 2005); lakes in Taiwan: Lake Chitsoui (Liew and Huang, 1994; Liew et al., 1998); Maar lakes: the Huguang maar lake (Mingram et al., 2005; Liu et al., 2000), Lake Shihailongwan (Mingram et al., 2004); closed-basin lakes in Inner Mongolia: Lake Daihai (Xiao et al., 2005), Lake Huangqihai (Yu et al., 2003; Li and Yu, 2002). Refer to these papers as listed in the references of this thesis for detailed information on the paleoclimate and paleoenvironmental history of each lake site. Correlation of proxy records from these lakes with the Lake Qinghai record will be discussed in Chapters 5 and 7.

2 Geographic, geological and limnological setting of Lake Qinghai

Lake Qinghai, the Blue Lake in Chinese, was named during the Northern Wei Dynasty. Koko Nor is the Mongolia name of the lake, also meaning Blue Lake. There are extensive grazing lands around the lake that make the area home to nomadic Tibetans. Bird Island is the breeding ground and migration route from China to India and southeastern Asia for a variety of birds (Liu et al., 2005), though the island has become a peninsula since the 1970s. An endemic fish living in the high-altitude oligotrophic lake is a scale-less carp that sharply decreased in number in the past two decades due to unsustainable catching. The natural beauties of Lake Qinghai have been attracting large numbers of tourists from all over the world. The geographic significance of Lake Qinghai may be marked by its size and volume—the largest water body in China, and by its high altitude location at 3,195 m above sea level (a.s.l) on the northeastern corner of the Tibet-Qinghai Plateau (Figures 1.1 and 1.2).

2.1 Geological setting

Lake Qinghai, a closed-basin lake with an area of 4437 km^2, lies in an intermountain basin between Qilian Mountain range and Mt. Qinghai Nanshan. The lake basin was formed between late Tertiary and Pleistocene as a consequence of fault-controlled tectonic depression at a triple junction of tectonic units (Geological Survey of QHP, 1991). Two groups of faults are thought to have played an important role in controlling the formation of the lake. One involves faults striking WNW, which are parallel to the axial plane of the regional folds, as well as to the strike of the thrust fault along the northern margin of Qilian Mountain range (Molnar and Tapponnier, 1975). Another set includes faults with NNW strike, which were probably shear faults formed under the main tectonic compression stress of the region. A representative of such faults is the right-lateral fault roughly parallel to the northeastern shoreline of the lake, along which the uplifting of the mountains, such as Mt. Riyue Shan, resulted in Lake Qinghai to become a topographically closed-basin lake.

According to the special report of the regional geology of Qinghai Province, rock strata distributed in the Buha River catchment include:

1) Lower Silurian sandstones, mainly graywacke and arkose, interbedded with slate,

2) Permian siltstone interbedded with sandstones, shales and limestones,

3) Triassic limestones and interbeds of arkose, siltstone and shales. Triassic rock strata occupy about half of the catchment area. Granite masses intruded into the Paleozoic strata during the Caledonian cycle are mainly present on the northern catchment of the lake, bounded roughly by the Haergai River. Lower Proterozoic metamorphic rocks, mainly schists and phyllites, crop out in the northeastern to eastern catchment, along with the intrusive rocks of granite and quartz diorite.

Outcrops in the southern catchment area, i.e. Mt. Qinghai Nanshan, include 1) Lower Triassic Rongwohe Gr. consisting mainly of mudstone, sandstone and slate, and intercalated beds of lime mudstone, siltstone and limestone, 2) Intrusive masses of

granodiorite and granite, and 3) Lower Paleozoic graywacke and arkose, interbedded with slate.

Quaternary deposits around the lakeshore areas were revealed by sediment cores drilled at four sites (Lanzhou Institute of Geology, 1978). QING5 is a 210 m long core, the deepest core of the four cores at the Erlangjian site. From 210 m to 95 m depth, loess deposits with intercalated beds of sand and gravels were encountered, that were identified as the Lower to Middle Pleistocene deposits. They have similar sediment character to the loess deposited in the adjacent Gonghe Basin. The sediment interval of 76-3.5 m comprises mainly silty clay and clayey silt with intercalated layers of sand and gravels, which was assigned to the Middle to Upper Pleistocene deposits. Based on the data of ostracoda, the dominant facies of the deposits is lacustrine.

2.2 Geomorphological setting

Lake Qinghai is surrounded by Mt. Datong Shan, Mt. Qinghai Nanshan and Mt. Riyue Shan. It has a large drainage basin with an area of 29,660 km^2, about seven times larger

Figure 2.1 Lake Qinghai bathymetry, and its main river inlets and peripheral lakes
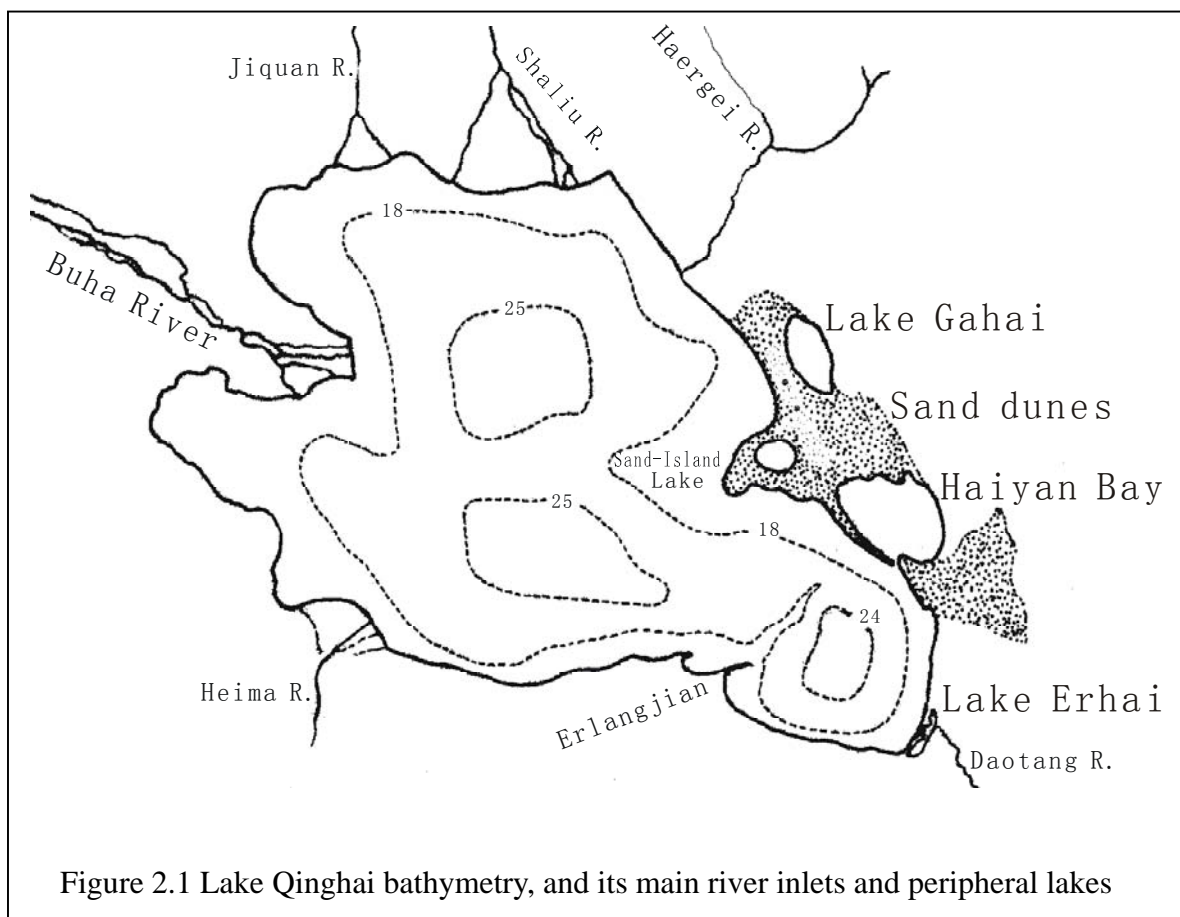
than the size of the lake. Surface runoff is drained into the hydrologically closed-basin lake by river systems unevenly distributed on the western and northern catchment areas of the lake. Large deltas and alluvial fans developed on the western and northern lakeshore

(Figure 2.1). These are the prominent geomorphological features, which to a large extent were brought about by the abrupt transition from mountainous terrain to the lakeshore plain (Plate 2.1). The mountains east of the lake retard the prevailing westerly strong winds so that wind-blown sands are deposited on the northeastern lakeshore and large dune fields were formed there. The deposition of wind-blown sand has been rather rapid, as evidenced by the development and formation of the sand peninsula, which in fact was only a sand island with a size of 11 km^2 in 1961. A sand bar formed between Haiyan Bay and the main lake within about 50 years, which provides another example showing how fast the wind-blown sands are deposited in the area. Moreover, it is reasonable to assume that Lake Gahai was once a part of Lake Qinghai and the segmentation occurred as a result of a conjunctive development of the alluvial fan of Haergai and the sand-dune field (Plate 2.1).

Plate 2.1 Satellite picture of Lake Qinghai, showing abrupt transition from mountainous terrain to the lakeshore plain, river delta and alluvial fans, and sand-dune fields in the proximity of Lake Gahai, Haiyan Bay and newly formed Sand-Island Lake.

A series of stranded terraces are preserved on the lakeshore areas, particularly those within 900 m from the lake today. These paleoshorelines are as yet undated because they lack adequate dating materials. The stranded terrace on the northwest shore, as shown on Plate 2.2, is about 200 m away from the lake and less than three meters above the present

lake level. This terrace most likely represents the lake shoreline during the late 1950s, and since then the lake level has decreased about 2.8 m, as gauged at the Shatuosi Hydrological Station.

2.3 Geographic setting

2.3.1 Climate

Plate 2.2 A stranded terrace at Hadatan, the paleoshoreline of Lake Qinghai several decades ago formed along the northwest lakeshore (photographed by J.Q. Yu).

The Qinghai Plateau has an alpine, continental climate with intense sunshine and a short frost-free season. Qaidam Basin, to the west of Lake Qinghai, is a large playa desert (121,000 km^2) with a number of subbasins where saline lakes and windswept salt crusts are formed under arid conditions with an extremely low precipitation (< 50 mm per year) and a precipitation/evaporation ratio around 1:100). Annual precipitation at Lake Qinghai is 310-390 mm on average according to the records of meteorological stations around the lake. The lowermost and highest annual precipitation records are 270 mm in 1973 and 561 mm in 1989, respectively. About 65% of the precipitation falls in summer from June to September, during which peak river flows occur correspondingly. Annual evaporation is 1460 mm, about 3.7-4.7 times higher than precipitation. The average annual temperature ranges from 0.9-2.7^{o}C. The highest temperature is about 28°C recorded in July with a monthly average temperature of 12.4^{o}C. January is the coldest month with a monthly

average temperature of -12.7° C and a lowermost record of -31° C. Ice-cover usually starts from November and extends until the end of March next year. The thickness of the ice cover usually is 10-15 cm, but a thickness up to 50 cm was once recorded under an especially severe cold winter. Strong northwesterly winds are common. They provide prevailing impact on wave actions of the lake and on the formation of sand dune field on the northeastern shore area.

2.3.2 Vegetation

Under the cold and semi-arid climate, highland herbaceous vegetation covers about 75% of the catchment basins of Lake Qinghai. Shrubs occur in relatively moist places such as on the shaded sides of mountainous areas. The catchment basins are almost treeless except for the hillsides south to the village Shinaihai. There the Qilian cypress (*Sabina przewalskii*) forms open stands. Furthermore, Qinghai spruce (*Picea crassifolia*) is sparsely distributed in the areas of Mt. Tuanbao Shan.

2.3.3 Rivers in the catchment basins

Buha River, the largest river of the seven main rivers in the drainage basin, contributes more than 60% of the total runoff into the lake from the western drainage basin. It is about 300 km in length and 22 m wide at its lower reaches. The drainage area of Buha River covers nearly half of the total catchment area. The annual discharge of 10.64×10^8 m^3 water has developed a large delta extending for at least 20 km into the lake on its western side. Four other larger rivers flow directly into the lake. In order of annual runoff, they are Shaliu River, Haergei River, Jiquan River and Heima River (Figure 2.1). Each has built a well-developed alluvial fan 5-15 km wide. Two other rivers, Daotang R. and Ganzi R., flow into Erhai Lake and unnamed ponds, respectively.

2.4 Limnological setting

2.4.1 Water chemistry

Water chemistry of the lake is shown in Table 2.1. The water of Lake Qinghai is brackish and alkaline with a total dissolved solid concentration of 14.1 g/l and a pH of 9.2. Chloride, sodium and sulphate are dominant ions. Magnesium is abundant and the weight ratio of Mg/Ca ranges from 82 to 61. Aragonite is now the main carbonate mineral precipitated directly from the lake water. The total dissolved solids (TDS) have increased irregularly from 12.5 g/l measured in 1961-62 to 14.1 g/l in 1985. It has however decreased to 12.5 g/l, following high runoff events induced by excess precipitation in the summer of 1989.

The waters of Lake Qinghai, Lake Erhai and Lake Gahai are all supersaturated with respect to aragonite, calcite and dolomite as indicated by the saturation indices (Table 2.2), calculated with PHREEQC (Plummer, 1988). These saturation indices of Lake Qinghai are overall lower than those of Lake Van, the largest soda lake on Earth with a pH of 9.7-9.8 and a salinity of 21.7 (Kempe et al., 1991).

2.4.2 Physical characteristics

The bottom topography of the lake is extremely flat. Most of its area is deeper than 16 m and the deepest point is 26.5 m (measured in the summer of 1985). The water column becomes stratified sometimes in winter after an ice-cover has formed. In January of 1962, the temperature was 0-1°C in the epilimnion and up to 4°C in the hypolimnion when

Table 2.1 Chemical compositions of Lake Qinghai, Lake Gahai and Lake Erhai waters. Composition of South China Sea water is given for comparison.

		Lake Qinghai		Lake Erhai	Lake Gahai	S China Sea#
Year of sampling		1961*	1985**	1961*	1961*	
pH		9.1-9.4	9.2	9.0	9.4	7.5
TDS (mg/l)		12480	14370	1120	24900	33900
Na$^+$	(mg/l)	3260	3970	268	6720	10240
	(meq/l)	144.3	172.6	11.7	292.2	445.2
K$^+$	(mg/l)	147	157	19	309	399
	(meq/l)	3.8	4	0.5	7.9	10.2
Mg^{2+}	(mg/l)	822	797	86	1470	1160
	(meq/l)	67.7	65.6	7.1	121	47.7
Ca^{2+}	(mg/l)	10	13	12	15	399
	(meq/l)	0.5	0.66	0.6	0.8	20
Mg/Ca	(mg/l)	82	61	7.2	98	2.9
	(meq/l)	135	99	11.8	151	2.4
Cl$^-$	(mg/l)	5270	5850	292	10700	18850
	(meq/l)	148.5	164.8	8.2	301.4	531
SO$_4^{2-}$	(mg/l)	2030	2380	208	4590	2670
	(meq/l)	42.3	49.6	4.4	95.6	55.6
HCO$_3^-$	(mg/l)	525	679	87	520	153
	(meq/l)	8.6	11.1	1.4	8.5	2.5
CO$_3^{2-}$	(mg/l)	419	522	148	573	
	(meq/l)	14	17.4	5	19.1	

*Data from Lanzhou Institute of Geology, 1974; **Data from Qinghai Institute of Salt Lakes, CAS; #Data from Li, Y.W. and Han, W.T., China University of Geology, Beijing; Mg/Ca ratios are all in weight ratio.

salinity was 12.5% in TDS. Persistent thermal stratification in the dimictic lake usually does not occur until July and the position of the thermocline and its thickness is different from place to place. Strong, mainly northwesterly winds are common and act to prevent the

development of a shallow thermocline. Measurements in October 1961 and in May 1962 indicate that the depth profile of the temperature is almost uniform (Lanzhou Institute of Geology et al., 1979). Epilimnion temperatures in high summer are 12-16°C with a hypolimnion of 6-7°C.

Table 2.2 Saturation indices of Lake Qinghai, Lake Gahai and Lake Erhai waters with respect to aragonite, calcite and dolomite calculated with PHREEQC.

	Year of sampling	T (°C)	$SI_{aragonite}$	$SI_{calcite}$	$SI_{dolomite}$	pCO_2 (ppmv)
Lake Qinghai (pH 9.2)	1961	20	0.65	0.79	3.83	229
		4	0.53	0.69	3.34	251
	1985	20	0.83	0.98	4.08	295
		4	0.72	0.88	3.60	324
Lake Gahai (pH 9.4)	1961	20	0.77	0.91	4.15	95.5
		4	0.70	0.86	3.78	120
Lake Erhai (pH 9.0)	1961	20	0.35	0.50	2.15	112
		4	0.14	0.31	1.48	100
SI: Saturation Index = log IAP – log Ksp IAP: ion activity product; Ksp: solubility product at a given temperature						

2.4.3 Biological characteristics

Planktonic algae of 35 genera are found in Lake Qinghai. Nine genera occur year-around, including *Cyclotella, Amphora, Navicula, Nitzschia, Cocconcis, Chroomonas, Oocystis, Cladophora,* and *Trachelomonas* (Lanzhou Institute of Geology et al., 1979). The lake contains 18 diatom genera and the dominant diatom genus is *Cyclotella*. Diatoms are abundant in the lake, particularly in summer, with an abundance rate of 32 to 88.9% relative to the total amount of phytoplankton.

Principal zooplankton genera include 1) six genera of protozoan *Vorticella, Strombidium, Strobilidium, Arcella, Difflugia, Didinium*, 2) five genera of rotifers *Brachionus, Pedalia (Hexarthra), Colurella, Mytilina, Notholca*, 3) four genera of copepod *Arctodiaptomus, Eucylops, Bryocamptus, Nauplius*, and 4) three genera of coladoceran *Moina, Chydorus, Daphnia*. Protozoans are the dominant zooplankton genera by number. They account for 99% of all zooplankton in winter, according to the survey of 1961-62.

Plankton appears to be more abundant in pelagic areas with muddy bottom than in the

sandy bottom areas. Plankton populations are denser in the upper 14 m of waters than in the lower water column.

In summer, sessile *Cladophora* forms abundant covers on almost the entire lake bottom up to at least 24 m depth. It persists as a benthic species in winter and spring. The benthic biomass of *Cladophora* usually exceeds 50 g/m^2 (wet weight) and becomes less in the areas > 10 km away from shore. The highest algal biomass in the littoral zone was 2360 g/m^2 recorded in 1962. Large quantities of the algal mats may be gathered by winds and waves to form long rows along shores, such as those reported as "Green Banks" 100 m long, 1 m wide and 0.5 m thick (Li, 1959).

Other macrophytes are overall rare in the lake today, but *Chara*, *Ruppia* and *Potamogeton* are occasionally found in fringing swamps.

Chironomids are the most important representatives of the benthic fauna in Lake Qinghai, accounting for more than 80% in both population density and biomass of the total benthic fauna. Benthos includes 19 genera identified in the 1961-62 survey, exclusive of ostracoda and nematoda. The juveniles of *Tendipes gr. Reductus* are the dominant taxa of the chironomids in the lake. There exist abundant ostracods in the near bottom waters and their valves are well preserved in the lake sediments, in which *Eucypris inflata* and *Limnocythere inopinata* are the main species identified.

The scale-less carp, *Gymnocypris przewalskii*, is the dominant fish living in the high-altitude mesosaline water of Lake Qinghai that supports commercial fisheries. These fish make annual spawning migrations into freshwater rivers (Wang et al., 2003). This endemic species may represent a relict fauna indicative of a long-term isolation of the lake, perhaps since the Quaternary (Chao et al, 1981). The naked carp is closely related to *G. eckloni* of the Yellow River (Wu, 1984). In addition, there are minor quantities of four species of loach: *Triplophysa alticeps, T. microps, T. scleropterus and T. stoliczkae* (Walker, et al, 1996).

2.5 Peripheral lakes

The main peripheral lakes are Lake Gahai and Lake Erhai on the northeastern and eastern coast of Lake Qinghai. A newly formed lake on the sand peninsula has yet no formal name. In addition, a bay near Haiyan County, named Haiyan Bay, was completely open in 1960s but now is cut off by a sand bar.

2.5.1 Lake Erhai

Lake Erhai is a fresh water lake (TDS 1.15-1.22 g/l) with a size of 4-5 km^2 and located to the east of Lake Qinghai. It has no direct surface connection with the main lake and receives an annual discharge of 15.8 x 10^6 m^3 through the Daotang River (Figure 2.1; Plate 2.3). Water depth of Lake Erhai range from 2 to 5 m. The fresh water lake has high pH values of 9.0 to 9.4 and a Mg/Ca ratio of around 13 (Table 2.1). Diatoms are the dominant phytoplankton in number and *Trachelomonas* seems to be more flourishing than in Lake Qinghai. The 1961-62 investigations reported that the phytoplankton and zooplankton by number are respectively 89 and 3 times more than those in Lake Qinghai.

Plate 2.3 Lake Erhai, one of the peripheral lakes on the east shoreside of Lake Qinghai. Daotang River flows into the lake from the eastern catchment.

2.5.2 Lake Gahai

Lake Gahai lies on the northeastern side of the main lake (Figure 2.1; Plate 2.1). It had a size of 47.5 km^2 and a maximum depth of 11 m in the summer of 1990. Sand dunes have been developing between Lake Qinghai and Lake Gahai and numerous small ponds are distributed among the dunes. The total dissolved solids of Lake Gahai are 25.3 g/l, being nearly double of the TDS of Lake Qinghai (Table 2.1). The weight ratio of Mg/Ca is as high as 97, similar or slightly higher than that of Lake Qinghai. There is no direct river flow into the lake. Groundwater is the main source of water supply, either as spring-supplied streams or groundwater discharge directly into the lake. In addition, it is uncertain whether or not there are any types of underground water connection between Lake Gahai and Lake Qinghai. The pH value of the lake is 9.4, similar or slightly higher than that of Lake Qinghai.

Diatoms are as abundant in Lake Gahai as in Lake Qinghai, whereas *Trachelomonas* was not found in the 1961-62 survey. Phytoplankton in Lake Gahai is 2.5 times more and zooplankton is slightly less abundant than in Lake Qinghai.

2.5.3 Haiyan Bay

Haiyan Bay today is a lagoon-like lake, as it is nearly cut off by a sand bar (Plate 2.1). It has a size of about 110 km^2 and a maximum depth of 13 m. The TDS of its water is 18 g/l with a pH of 9.0 and a Mg/Ca ratio close to 100:1 (weight ratio). Salinity is much lower than that of Lake Gahai but the deposition of hydromagnesite, an authigenic carbonate mineral not found in the main lake, is found in the near-shore shallow waters of the eastern

shore of Haiyan Bay. This characterizes the water chemistry of Haiyan Bay as distinct from that in the main lake and in all other peripheral lakes.

2.5.4 Sand-Island Lake

Sand-Island Lake is a newly formed lake (Figure 2.1; Plate 2.1). As the name implies, Sand-Island Lake was a part of Lake Qinghai in the 1960s between a small, isolated island and the sand-dune fields. It became a peripheral lake around 1980s, as a result of rapid expansion of sand-dune fields. Located on the newly-formed sand peninsula near Lake Gahai and Haiyan Bay, the Sand-Island Lake has a size of about 16 km^2. Its water depth and chemistry are not measured and reported yet.

3. Methods

3.1 Introduction

Sediment records recovered from lakes often contain continuous and high-resolution information on paleoenvironmental changes. Much of the information is of regional significance. To obtain an environmental history from just one lake site, however, requires large amount of work, beginning with a field campaign and followed by several years of detailed laboratory work.

Seismic investigations provide useful information on the sub-bottom sedimentary structures of a lake. This is important not only for reconstructing changes in sedimentological conditions but also for the selection of coring sites in order to assure continuity and representativity of sedimentary environments.

Next, it is essential to get sediment cores of high quality for paleoenvironmental and paleoclimatic studies. Although lakes are diverse with large differences in size and depth, one can now choose coring or drilling equipment suitable for taking cores from different types of lakes, thanks to the tremendous efforts of many colleagues since the 1960s.

A multi-proxy approach, though time-consuming, is often applied in laboratory investigation on sediment cores. This allows to collect as much information and evidence as possible for the reconstruction of paleoclimate and paleoenvironmental changes with cross-checked reliability. Apparently, multidisciplinary knowledge and experience on core studies are required in decoding various environmental signals.

Closed-basin lakes are subject to sensitive and large fluctuations in lake level in response to climate changes in the past (e.g. Street-Perrott and Harrison, 1995). Consequent shifts in water chemistry, limnological and sedimentological conditions are often readily detectable using geochemical, mineralogical, isotopic or biological methods, as well as other sedimentological analyses and geophysical logging techniques.

3.2 Field investigation

The field work of 1985 includes seismic profiling, and piston and trigger coring as described below. The Sino-Swiss Expedition team, including the author of the dissertation as a member of the team, operated the field investigation with device mainly from the Institute of Geology, ETH-Z.

3.2.1 Seismic profiling

About 500 km of seismic data were collected in the 1985 Expedition to Lake Qinghai using the ETH-Geology 3.5 kHz ORE seismic profiler with an EPC 1600 digital recorder. Transmitted sound pulses were set at one-second intervals with a ship speed of about 10 km per hour. Seismic profiles show that penetration reaches 25-30 m in depth with a high resolution of ca. 15 cm.

3.2.2 Coring

3.2.2.1 Kullenberg corer

A modified Kullenberg-type corer (Kelts et al., 1986) was used to take sediment cores from subbasinal centers of Lake Qinghai by the Sino-Swiss expedition team in the summer of 1985. This piston-operated free-fall gravity corer proved to be the most convenient coring equipment for extracting sediment columns from Lake Qinghai. The operation diagram of the Kullenberg corer is shown in Figure 3.1.
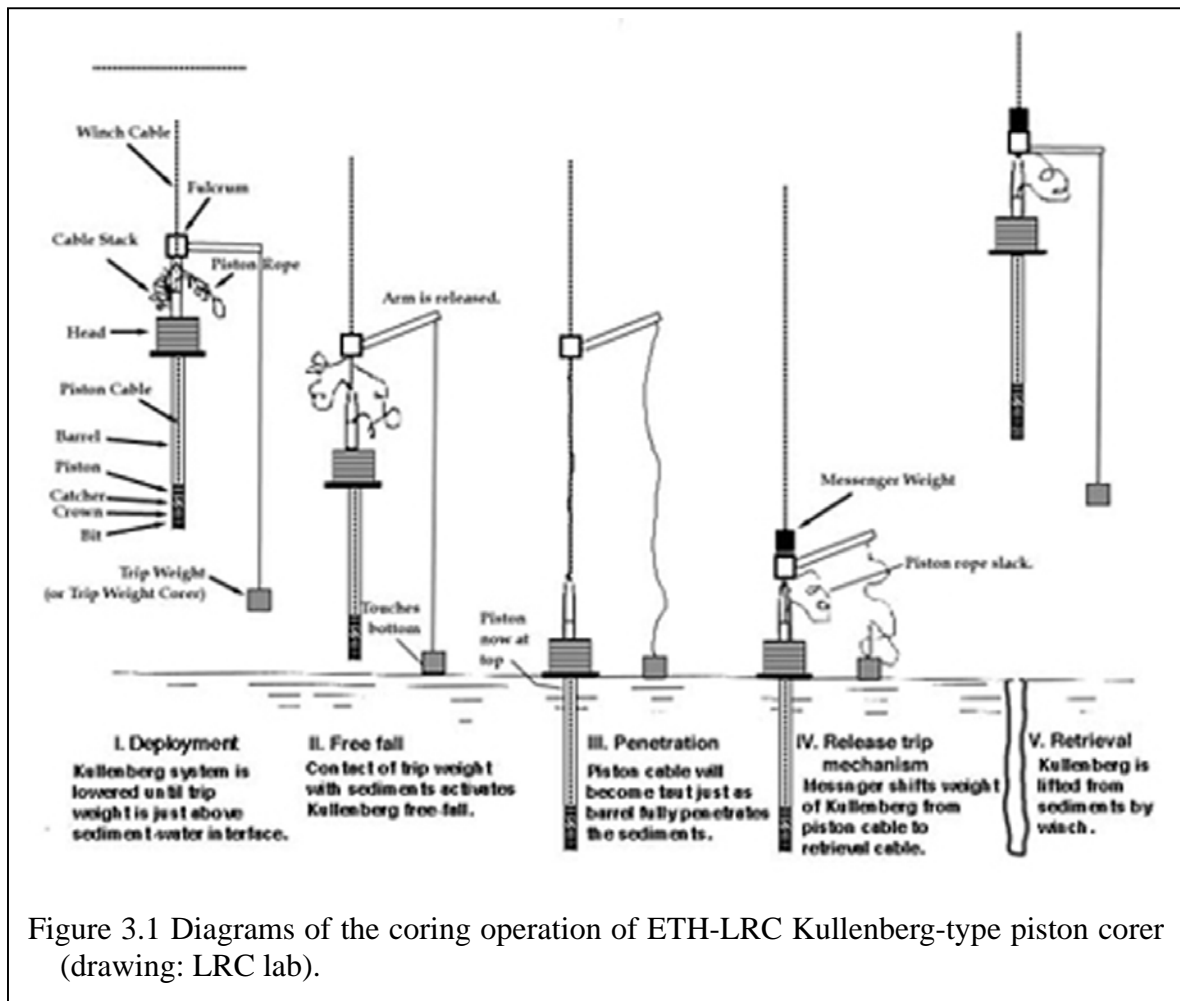

Figure 3.1 Diagrams of the coring operation of ETH-LRC Kullenberg-type piston corer (drawing: LRC lab).

To operate the system, a coring tower is fixed on one side of a 30-ton ship and used for mounting the Kullenberg corer (Plate 3.1). The winch system of the ship was employed for laying down the corer and, following its penetration into the subbottom sediments, for lifting the corer holding retrieved sediments in plastic liners. The depth of each coring penetration, as well as the length of the cored sediments, depends on the sediment character. The maximum penetration of the Kullenberg corer into the sub-bottom sediments of Lake Qinghai was 5.6 m. Further penetration of the coring was retarded mainly because the basal sediments become denser and harder than the sediments of the upper sections of the

Plate 3.1 ETH Kullenberg-type corer and coring tower mounted on one side of a 30-ton ship, used for retrieving the sub-bottom sediment cores of Lake Qinghai.

sediment column.

Sediment cores were then cut into 1-m sections in the field and carefully sealed with plastic caps for transport.

3.2.2.2 Trigger corer

A trigger corer was used to retrieve undisturbed samples of the top 1-1.5 m sediments, either in conjunction with a Kullenberg piston corer or as an independent corer on a small cable or rope. A transparent PVC liner with 6 cm diameter is attached to the head of the trigger corer containing valve seals that hold the retrieved sediments. A careful removal of the water on top of the liner is demanded in order to prevent the loss of the materials from the sediment-water interface.

3.3 Laboratory investigation

Sediment cores taken from Lake Qinghai were stored in a cool room of 4° C. Prior to core splitting, whole-core magnetic susceptibility (MS) was measured at a resolution of 1-2 cm with a model MS2 Magnetic Susceptibility Meter. Core sections of one meter long were split and immediately photographed. Visual descriptions of a core were followed by sampling of the core materials based on a well coordinated plan with carefully considered processes such as sampling priorities, quantity and density for each specific analysis, multi-stage sampling procedures etc. In this thesis study the author has applied the following methods to the study of the sediment cores.

3.3.1 Radiometric dating

3.3.1.1 AMS radiocarbon dating methods

Radiocarbon (^{14}C) dating has been the mainstay of the radiometric chronology for lake sediments as paleoclimate and paleoenvironmental archives. The development of AMS ^{14}C dating method have made it possible to date small samples collected from sediment cores. Terrestrial organic fragments are the best dating materials, if not redeposited, but seldom found in a core retrieved at a large lake center. Reliability and accuracy of dating other carbon fractions, such as biogenic carbonate, depend on adequate evaluation of possible deviations introduced, like the reservoir effect. Possible contaminations caused naturally or artificially must be avoided during collection and processing of samples.

Organic fragments were hand-picked or sieved from Lake Qinghai sediments for radiocarbon dating. They are macrofossil seed cases and stalks of the aquatic plant *Ruppia* or algal filaments of *Cladophora fracta*. The seeds were cleaned of adhering sediments by sonic vibration followed by a series of distilled water baths. They were inspected under a binocular microscope, and then soaked in a 10% HCl solution to remove carbonates possibly sticked within seed cases. Rinsed with distilled water for several times, the seeds were washed with a 1% NaOH solution to leach out humic acid. The pretreatment of the macrofossil stalks and algal filaments is similar to that of seed cases.

The dried dating material of about 10 mg was sealed in a 4 mm Pt capsule and graphitized in a pyrex-graphite-talc assembly (Lister et al, 1984). Graphitized samples,

which yield the highest and stable negative carbon currents in the ion source of the ETH facility, were mounted on copper target discs and measured with the accelerator mass spectrometry (AMS) at the Mittelenergiephysik Institut, ETH-Hoeggerberg, Zurich (Woelfli, 1983). The measured ^{14}C dates are calibrated for being expressed as calendar years, using INTCAL radiocarbon age calibration (Stuiver et al., 1998).

3.3.1.2 ^{210}Pb dating method

Lead-210, a short-lived natural radionuclide with a half-life of 22.3 years is used as one of the best methods to establish a high-resolution chronology for the past 100-150 years (Krishnaswami, 1971), though model-dependent in many cases (Appleby and Oldfield, 1992). The dating range of ^{210}Pb method complements that of radiocarbon, which is of little use for samples younger than 150 years (Roberts, 1989).

^{210}Pb in lake sediments is mainly of atmospheric production through the decay chain of ^{226}Ra released from bedrock as ^{222}Rn, which decays via a series of short-lived isotopes to form ^{210}Pb. This is defined as excess or unsupported ^{210}Pb, which enters a lake as rainfall or as dry fallout and decays in sediments with time. Dates are derived from the down-core decline in unsupported ^{210}Pb. A minor portion of ^{210}Pb in the sediments is so-called supported ^{210}Pb that is derived from in situ decay of radium-226 obtained from catchment erosion. Although the ^{226}Ra-supported ^{210}Pb activity can be measured by separate analyses, it is often estimated from the "tail" of a ^{210}Pb profile, where unsupported ^{210}Pb become undetectable and assumed to be approximately constant.

In this study, the determination of the ^{210}Pb content relies on the detection of ^{210}Po, the ground-daughter of ^{210}Pb, using alpha spectroscopy. Polonium-210 is assumed to be in equilibrium with lead-210 in the sediment samples.

A dried sediment sample of 1-3 g was leached by 8 N HNO_3 and 30% H_2O_2, after being spiked with ^{210}Po as tracer. By adding HN_3OH of 25% into the solution, polonium-210 was co-precipitated with $Fe(OH)_3$, and NO_2 was driven out by heating. The 1.5 N HCl was added to dissolve ^{210}Po in the residue and ^{210}Po in the solution is self-plated on a silver disc at 80°C in a bath. Note that 1 g ascorbic acid was added into the solution for masking Fe^{3+} and Cr^{3+} and 0.5 g sodium citrate was added to facilitate the plating. The ^{210}Po alpha-activity was determined using a multi-channel α spectrometer. The counting error was in general less than 1%.

3.3.2 Magnetic susceptibility: core logging

The whole-core logging of magnetic susceptibility is a non-destructive and cost effective method of obtaining a high-resolution down-core variation profile in volume susceptibility, which is related to the concentration of iron-bearing minerals in the cored sediments. The Fe-bearing substances in the sediments, mainly ferromagnetic and paramagnetic minerals, become magnetized when the whole-core is exposed to an artificial magnetic field. Sediment sections relatively rich in magnetizable minerals yield higher values in magnetic susceptibility (MS) than other sections poorer in magnetizable minerals.

A whole core is moved incrementally in 2 cm steps to pass through a Bartington Instrument MS2C loop sensor for down-core logs of MS. The MS2C device is zeroed at

the beginning of each run, and a possible instrument drift can be corrected by a zero-background measurement at the end of a core section log. In addition to coil calibration, measured MS values need to be corrected for mass difference. A particular attention should be paid to the correction of MS values near the ends of each core sections. The instrument has a precision of 2 x 10^{-6} cgs, and accuracy of the measurements is about 5%.

It has been proved by many case studies that magnetic susceptibility is an indication of sediment provenance and style of deposition (Andrews and Jennings, 1987; Peck et al., 1994; Yu and Kelts, 2002) and provides a valuable tool for core-to-core correlation, and is therefore recommended as a "should-be-done" measurement in almost all cases (Colman, 1996).

3.3.3 Total organic carbon and total nitrogen, and C/N ratio

Total organic carbon and total nitrogen contents in the sediments of closed-basin lakes proved to be valuable proxies indicating the lake's paleoproductivity under the precondition that organic matter in the sediments originates predominantly from the lake itself, and that both preservation conditions and sedimentation rate in the past can be well evaluated (Yu and Kelts, 2002). The source of organic matter in the lake sediments is commonly indicated by the ratio of carbon to nitrogen (Stein, 1991; Yu et al., 2001).

A dried sediment sample of 5-10 mg is weighed on the scale of SARTORIUS 4503 Micro and analyzed for total nitrogen and total carbon contents with a CNS Analyzer (NA 1500, Carlo Erba) at EAWAG, Duebendorf. Detection limit of the Analyzer is about 10 ppm. The measurements of a 25-sample batch start with three standards of sulfanilamide and end with two plus one blank sample. Reproducibility is better than $\pm 0.1\%$ absolute value. Total organic carbon content is from subtraction of total carbon by total inorganic carbon, for which the sample duplicate is measured with a Coulometer.

3.3.4 Macrofossil indicator

Macrofossils from plants and animals preserved in lake sediments, such as seeds, leaves, wood, conifer needles, fish bones, mollusks, insects and other remains, may be hand-picked or sieved from the sediments and identified to species level. Critical paleolimnological and -ecological information thus may be obtained from macrofossil evidence not from all but probably just one or two species, depending on the ecological and environmental conditions of each lake.

Ruppia, a rooted aquatic plant, is widely distributed in lagoons and in brackish lakes. It grows in the littoral zone with a water depth usually ranging from 0.2-2.5 m but not more than 4.5 m for some species under specific circumstances (Verhoeven, 1979). Low-energy shallow water areas with a regular periodicity of freshwater inflow and low turbidity are favourable conditions for *Ruppia* plant to grow and flourish. It cannot survive long period of desiccation. In winter, abundant seeds of up to 20,000 per square meter are annually deposited and buried together with stalks of the aquatic plants (Hammer, 1988).

Ruppia is found to grow in a protected bay of Lake Qinghai today, where the water is less than 0.5 m deep and not turbid with inflowing fresh water. The seeds of *Ruppia* are

found in the bottom sediments, indicating that they were dropped from the aquatic plant and buried in situ. The seeds of this species are collected from the sediment core Q14B, recovered from the central southern subbasin, where water depth was 26.5 m in 1985. There are at least nine layers containing *Ruppia* seeds in a 127 cm section of the core. The annual production rate of the seed is estimated in number at 180-500 per square meters, based on counting the number of seeds collected and average sedimentation rate of 0.5 mm per year. Such a lot of seeds are unlikely transported from the nearshore area over a large and extremely flat lake bottom. The presence of the seeds and stalks from the rooted aquatic plant *Ruppia* at the today's pelagic area of the lake is recognized, in conjunction with sedimentological evidence, as the original deposition when the lake was as shallow as only a few meters in water depth (Yu and Kelts, 2002; Liu and Yu, 2005).

3.3.5 Total inorganic carbon and carbonate content

A number of closed-basin lakes are brackish and alkaline due to evaporative concentration in arid or semi-arid climate. Carbonates from chemical precipitation are the important composition of the lake's deposits, and the changes in carbonate production of the lake are related to shifts in total carbonate content (TCC). Therefore, TCC is the "must-be-obtained" stratigraphic record for this type of lake, and it is particularly useful for the reconstruction of the climate-induced changes in water chemistry and lake level when the TCC record is used in conjunction with the record of carbonate composition (Yu and Kelts, 2002).

In this study, the method of carbon coulometry is applied to measure total inorganic carbon (TIC) that can be converted to TCC by multiplying TIC results by a factor 8.333 for calcium carbonate and by a factor of 7.8 for a dolomite with 60% $CaCO_3$. TIC is measured with a Carbon Dioxide Coulometer at the EAWAG, Duebendorf. Dried sediment samples were sufficiently ground and 10-20 mg (containing 1-3 mg C) were used for analysis. Prior to the sample analyses, a blank sample analysis is run by using an empty container and followed by the analysis of one standard sample at least. The coulometric measurement requires small amount of sample and is an easy-to-run, precise and fast method.

3.3.6 X-ray diffraction and scanning electron microscopy (SEM)

Sediments from large lakes contain fine-grained mixtures of both allochthonous and autochthonous minerals. The instrumental technique of X-ray powder diffraction (XRD) provides a fast and reliable tool for the routine mineral identification and for the determination of the proportion of the different minerals present. XRD method can also be used for other specific mineralogical studies including the degree of crystallinity of the minerals present, possible deviations of the minerals from their ideal compositions, and evaluating the mol percentage of MgO in dolomite and magnesium calcite. XRD analysis is particularly useful for identifying very fine-grained minerals present in the sediments that are too small to be identified by optical light microscopy.

In this study, the proportion of aragonite, calcite and dolomite relative to total carbonate content in the sediment samples was determined with Philips X-ray diffraction units. Consistent setting is held for all runs, and each run allows analyzing 10 samples by using an automatic slide changer. Dried sediment samples are ground to a fine powder of less than 63 micron in an agate mortar with pestle in ethanol.

Table 3.1 Summary of paleoenvironmental parameters and fieldwork reported in the thesis study

Parameters	Laboratory	Analyzer	Processing
^{14}C	ETH-Höngerberg	G. Bonani (Pre-treatment by J.Q. Yu)	Kelts/Lister/Yu
^{210}Pb	EAWAG	J.Q. Yu	J.Q. Yu
Magnetic susceptibility	ETH-Z	J.Q. Yu	J.Q. Yu
TOC, TN and C/N ratio*	EAWAG	M. Langmeier (Pre-treatment and weighing by J.Q. Yu)	J.Q. Yu
Macrofossil indicator	EAWAG/ETH-Z	J.Q. Yu	J.Q. Yu
TIC/TC/TCC**	EAWAG	J.Q. Yu	Kelts/Lister/Yu
SEM for carbonates	ETH-Z	J.Q. Yu	J.Q. Yu
^{18}O and ^{13}C	ETH-Z	J.Q. Yu	J.Q. Yu
Fieldwork			
Seismic profiling	ETH-Z Limnogeology	Sino-Swiss expedition team	Kelts/Lister/Yu
Coring	Inst. Salt Lakes (Drill corer)		J.Q. Yu
	ETH-Z (Kullenberg corer)	Sino-Swiss expedition team	Kelts/Lister/Yu
	ETH-Z (Trigger corer)		J.Q. Yu
*TOC: Total organic carbon; TN: Total nitrogen. **TIC: Total inorganic carbon; TC: Total carbonate; TCC: Total carbonate content.			

The mol percentage of magnesium in Mg-calcite is calculated using the d (104) value (Goldsmith, 1961). Mineralogical examinations of carbonate minerals on micrographic scales were carried out with a Scanning Electron Microscopy (SEM) coupled with an energy dispersive X-ray (EDAX).

3.3.7 Oxygen and carbon stable isotopes

3.3.7.1 Carbonate mineral samples for stable isotope analysis

The carbonate minerals, common and abundant in sediments of alkaline and mesosaline lakes, are measured for their stable isotope ratios. Their ratios are affected by both stable isotope composition and temperature of the lake's surface water or upper water column during carbonate-mineral nucleation. In hydrologically closed lakes, evaporative- and residence-related effects play a predominant role in controlling isotope composition of the lake, whereas temperature effects are of secondary importance (Gonfiantini, 1986; Talbot, 1990).

Bulk carbonate samples were first examined under binoculars to remove most ostracode shells and then pre-cleaned in a sodium hypochlorite solution for 24 hours to oxidize organic matter and then washed repeatedly with distilled water. $CaCO_3$ samples were reacted directly with 100% phosphoric acid at $50^o C$ for approximately 20 minutes. For dolomite rich samples, the reaction proceeded at $25^o C$ for 72 hours. Oxygen and carbon isotopic compositions of carbonate minerals were determined with a VG Micromass 903 mass spectrometer at the Geologisches Institut, ETH-Zürich. The isotopic compositions are reported as the per mil (‰) with respect to PDB isotopic standard. The mean standard deviations for the working standard are 0.19‰ for oxygen and 0.23‰ for carbon.

4. Seismic investigation, lithologic study of sediment cores and radiometric dating

4.1 Introduction

Piston cores recovered from the depo-centers of the lake today have been used as the continuously archived proxy records for the post-glacial paleoclimate and paleoenvironmental reconstruction (Kelts et al., 1989; Lister et al., 1991; Yu et al., 2000; Yu and Kelts, 2002). This chapter reports the results of lithology, radiometric dating of cored sediment sequence, and seismic investigations for sub-bottom sediment structures. This is to provide basic information on the post-glacial sedimentary history of the lake. Other proxy data will be provided in the followed chapters dealing with specific problems with regard to paleoclimate, paleolimnology and paleoenvironments of the lake.

4.2 Sub-bottom profiles from the 3.5 kHz seismic investigations

Seismic profiles No. 1, 5 and 10 are shown in Figure 4.1. The profiles indicate that central plains of the lake are broad and flat with narrow, abrupt littoral zones. This charact-
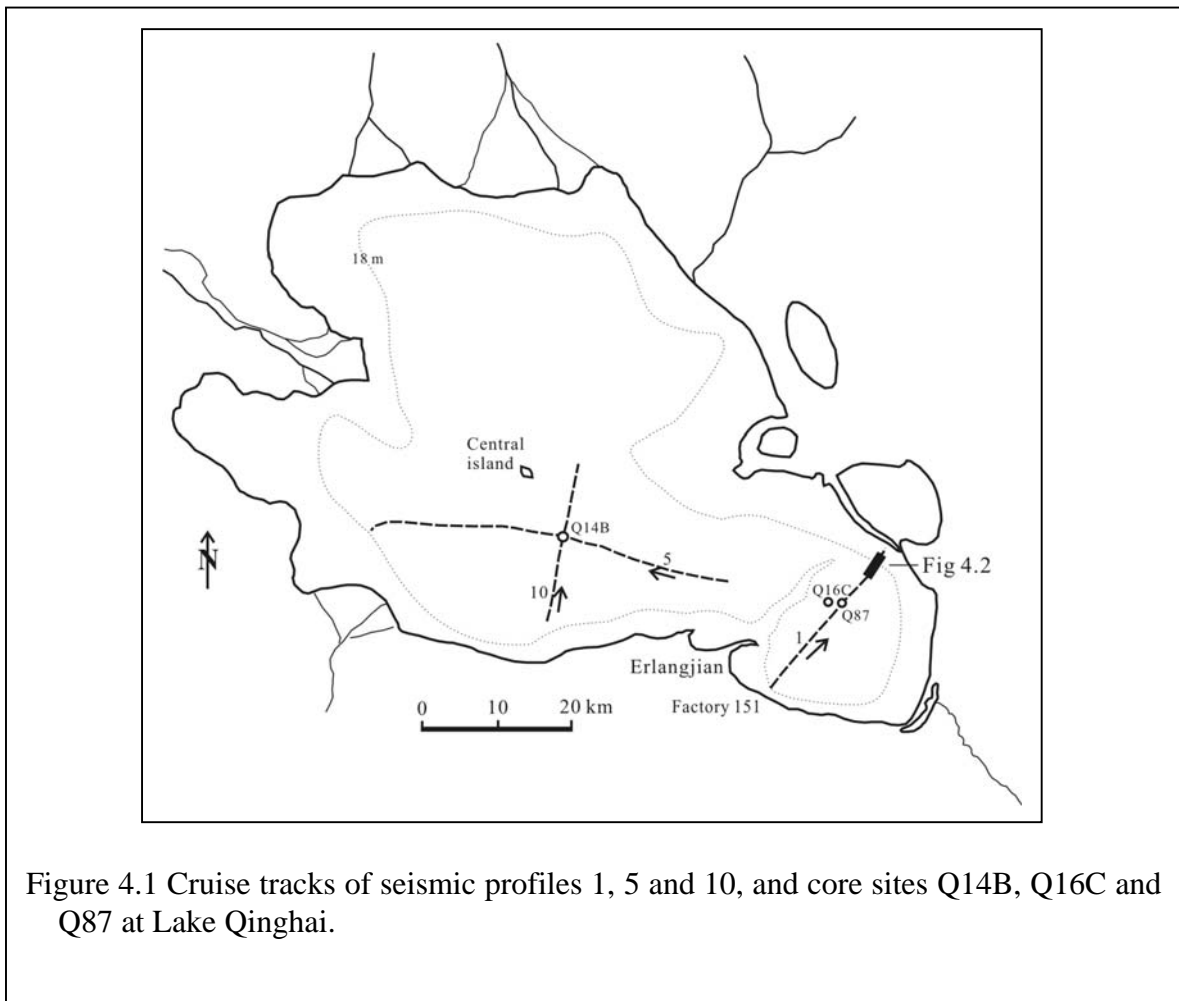
Figure 4.1 Cruise tracks of seismic profiles 1, 5 and 10, and core sites Q14B, Q16C and Q87 at Lake Qinghai.

-erizes the topography of the lake bottom. A submerged ridge covered by calcareous tufa extends from Erlangjan Peninsular and lies between the southern and the eastern basins of the lake. The tufa ridge is about 14 m below the lake surface in 1985.

The sub-bottom profiles of the 3.5 kHz seismic surveys show a series of reflectors. The most notable reflector is the one named Q-reflector (Kelts et al., 1989; Figure 4.2). It shows a strong reflection and a planar and ubiquitous distribution. The sub-bottom profiles below the Q-reflector display two identifiable reflectors, named Q-1 and Q-2 (Figure 4.3).
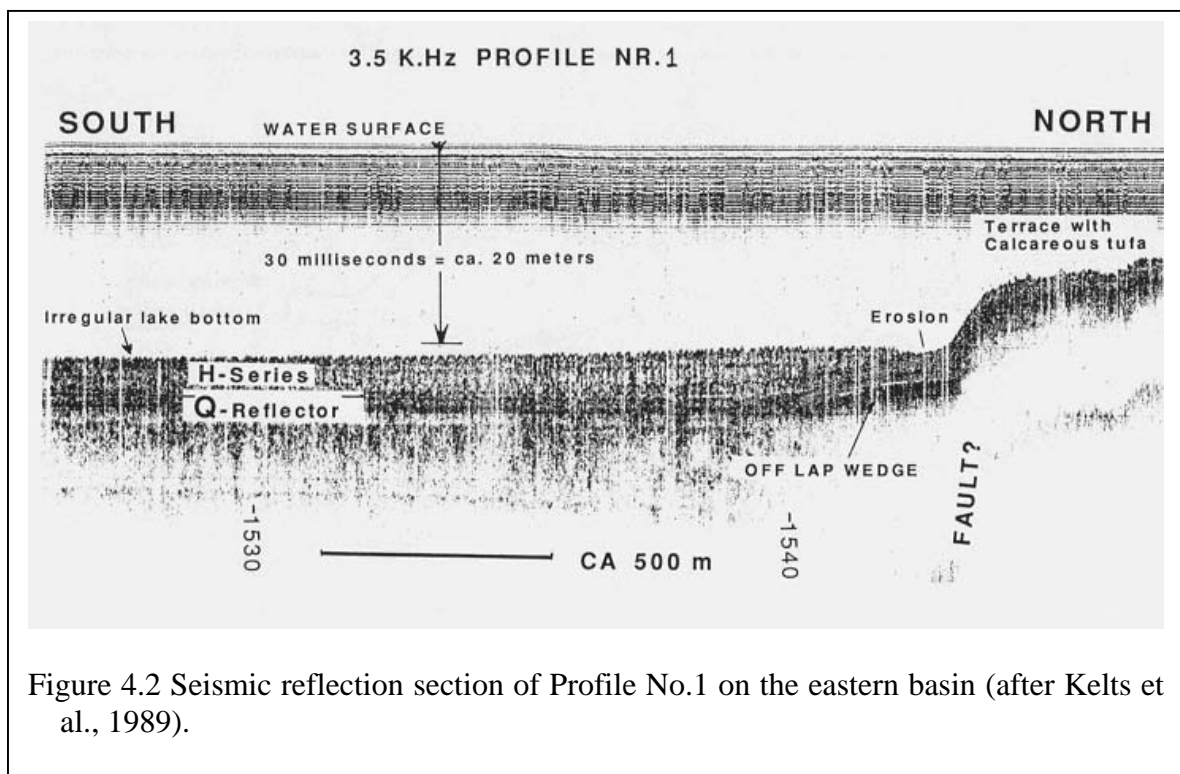
Figure 4.2 Seismic reflection section of Profile No.1 on the eastern basin (after Kelts et al., 1989).

The pattern of reflectors Q-1 and Q-2 indicates an offlap sequence of deposits, typical for a lake shrinking in size (Lister et al., 1991). Above the Q-reflector the seismic stratigraphic features are indicated by parallel, closely-spaced reflectors (H-series), representing a 3.8-6.5 m sequence of the post-glacial deposits. The widespread distribution of the deposits above the Q-reflector and commonly unconformable contact with the underlying deposits indicates a rapid and permanent expansion of the lake from much smaller or nearly desiccated lakes on a wind-swept basin plain.

4.3 Radiometric dating

4.3.1 Radiocarbon dating and sedimentation rates

Five organic samples were hand-picked or sieved from the sediments of core Q14B (see Figure 4.1 for location) for AMS ^{14}C dating. They include four samples of macrofossil
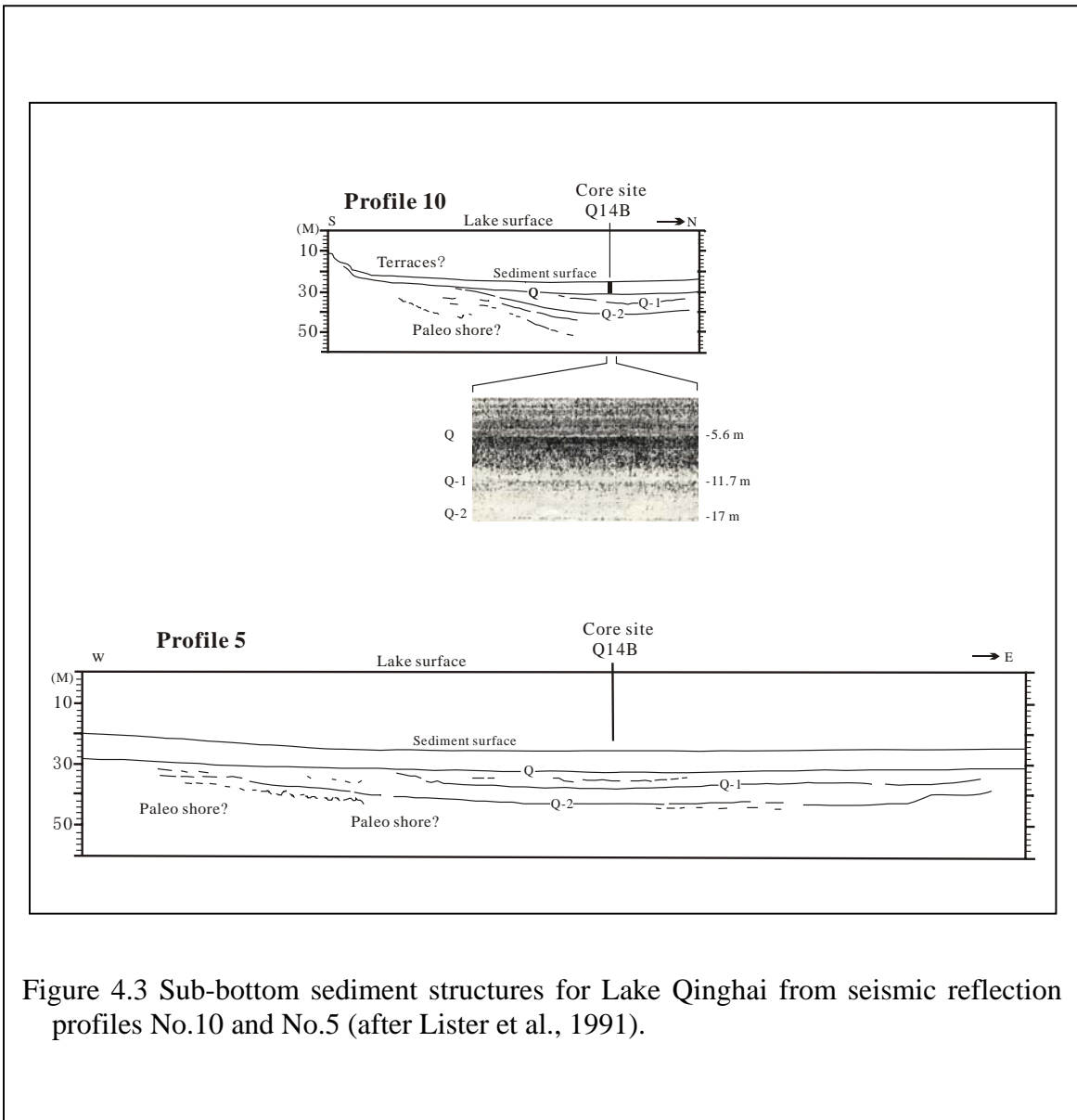
Figure 4.3 Sub-bottom sediment structures for Lake Qinghai from seismic reflection profiles No.10 and No.5 (after Lister et al., 1991).

seeds and stalks from the aquatic plant *Ruppia* and one from algal filament of *Cladophora fracta* remains. For methods see Chapter 3.3.1. Result of radiocarbon dating of the selected organic samples is given in Table 4.1. The radiocarbon chronology of core Q14B is shown in Figure 4.4, and ages at the boundaries between each pair of lithological units are based on extrapolations from those five AMS ^{14}C dates. Sedimentation rates calculated for each lithological unit are also shown in Figure 4.4. Ages older than 10,900 years B.P. are extrapolated with uncertainty.

4.3.2 ^{210}Pb dating and sediment accumulation rates in the past 150 years

Three short cores were selected for ^{210}Pb dating of the sediments deposited in the last 150 years or so. They are QH85-7, QH85-12 and QH85-2, taken respectively from the three subbasins of Lake Qinghai, where water depths are deeper than 25 m. The coring
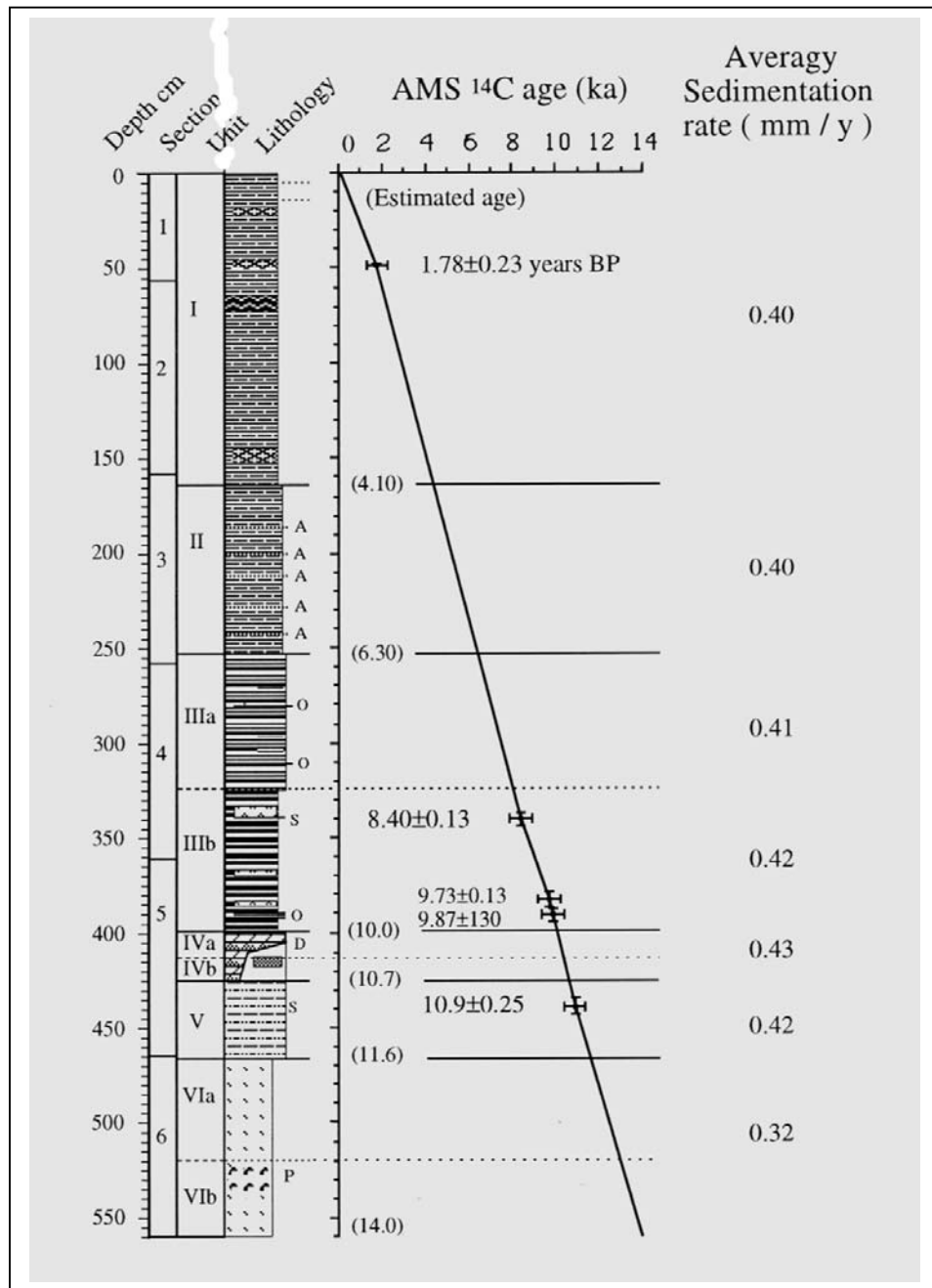
Figure 4.4 AMS ^{14}C chronology of core Q14B and sedimentation rates.

sites of the three short cores are shown in Figure 4.5. For methods see Chapter 3.3.1.2.

Table 4.1 Radiocarbon ages from core Q14B measured by ETH-AMS facility.

Lab No.	Section/cm	Core depth interval in cm	Mean depth in cm	Material	[14]C age in years BP	Calibrated ^{14}C age (2σ) (cal yr BP)
QH-1	1/47.5-49	47.5-49	48.3	Algal	1,780±20	1687-1741
QH-2	4/81.5-83	339.5-341	340.3	Seeds	8,400±130	9597-9030
QH-3	5/21-22.5	382-383.5	382.8	Seeds	9,730±130	11,545-10,692
QH-4	5/26-34	387-395	391.0	Seeds	9,870±170	12,088-10,748
QH-5	5/77-79	438-440	439.0	Seeds	10,900±250	13,432-12,191
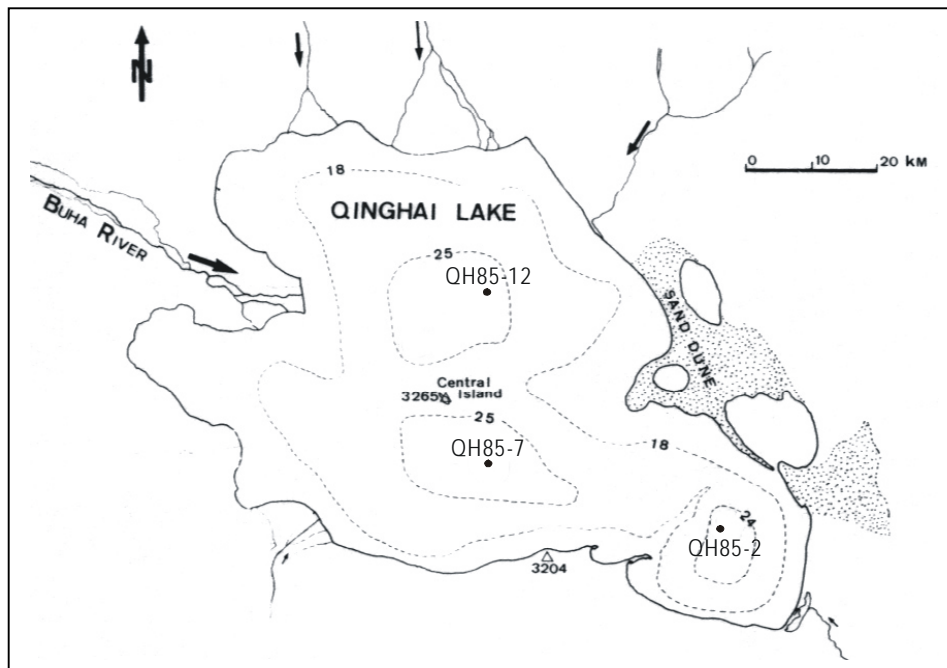
Figure 4.5 Sites of three short-cores selected for ^{210}Pb dating of the sediments deposited in the last 150 years.

The data of total ^{210}Pb activity versus mass depth are shown in Figure 4.6. The three plots all show that the total ^{210}Pb activity decreases exponentially with mass depth, though the curve pattern differs from each other. Supported ^{210}Pb activity is clearly indicated by the 'tail' activities of ^{210}Pb with a narrow range from 2.14-1.55 dpm/g for core QH85-7 and from 1.94-1.41 dpm/g for core QH85-12. For core QH85-7, the 'tail' activity of about 2.2 dpm/g shows at the mass depth below 11 g/cm^2 (equivalent to the sediment depth of 20 cm).

The data of the unsupported ^{210}Pb activity on a logarithmic scale against mass depth of the three cores are shown in Figure 4.7. The data plot exhibits three straight lines that diverge from an approximately common initial activity in unsupported ^{210}Pb on top of the three short cores. The linear distribution of ^{210}Pb concentration versus mass depth on the plot suggests a 'simple model' that can be used for calculating the sediment accumulation rate at the core site. The mathematic expression of the simple model, that is, a constant sedimentation rate and a constant ^{210}Pb flux model (Krishnaswamy, 1971; Robbins, 1978), is shown in Equation (1):

$$A = A_0 \, e^{\,-lm/R} \qquad (1)$$

Where A is the unsupported ^{210}Pb concentration in situ, A_0 is the initial concentration of the unsupported ^{210}Pb at the water-sediment interface, l is the decay constant of [210]Pb (0.03114 y^{-1}), R is the dry sediment accumulation rate, and m is the cumulative dry-mass depth (g/cm^2) as expressed in Equation (2):

$$m = \int r_s \, [1\text{-}\Phi(z)]dz \qquad (2)$$

where r_s is the effective density of the solid phase (2.49±0.05 g/cm^3), Φ (z) is the corresponding sediment porosity. The equation (3) shown below is a converted form of the equation (1) and the sediment accumulation rate R can be calculated by the simple regression of the ^{210}Pb concentration of each sample via cumulative mass depth.

$$Ln \, A = Ln \, A_0 + (\text{-l/R}) \, m \qquad (3)$$

The dry sediment accumulation rates, calculated based on the 'simple model' as described above, are 30.4±3.7 mg/cm^2/year for core QH85-7 site and 55.9±6.7 mg/cm^2/year for core QH85-2 site.

Figure 4.6 shows the non-linear distribution of ^{210}Pb concentration versus mass depth, which implicates the presence of a top-mixing layer of [210]Pb. Equation (4) thus is introduced as follows:

$$A = A_0 \, e^{\,-l\,(m\text{-}z')\,/\,R} \qquad (4)$$

where z' is the mass depth of the mixing layer. The sediment accumulation rate for the core QH85-12 site, calculated based on Equation (4), is 18.3±4 mg/cm^2/year.

The dry sediment accumulation rates determined based on ^{210}Pb dating of three sediment cores range from 18.3 to 55.9 mg/cm^2/year. The sediment accumulation rates are thought to represent the rate range of sediment accumulation in the pelagic areas of Lake
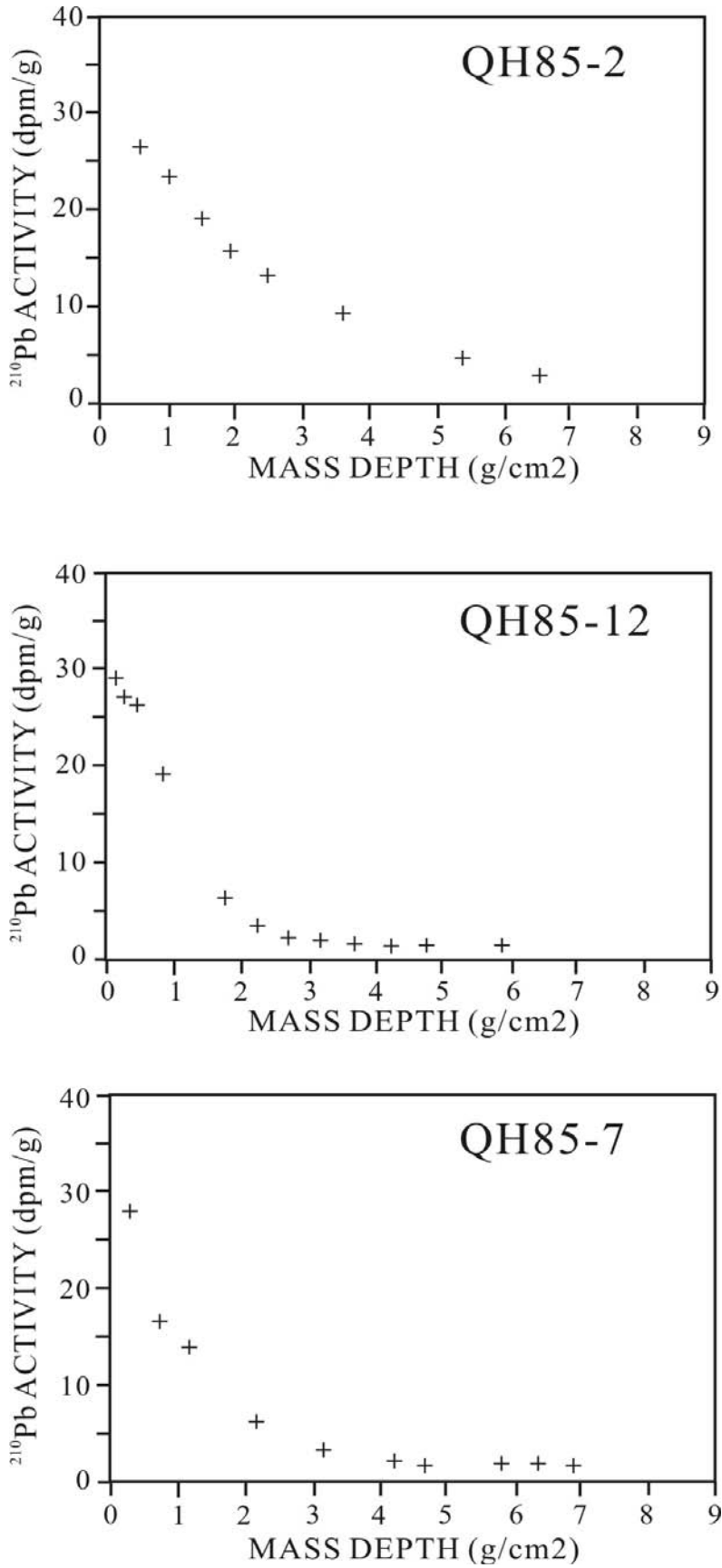
Figure 4.6 Lead-210 plots of the short-cores QH85-7 (A), QH85-12 (B), and QH85-2 (C), showing exponential flareout of ^{210}Pb activity with dry mass depth.

Qinghai. The accumulation rate of the three sites on average is 34.8 mg/cm^2/year, which is close to the rate of 30.4±3.7 mg/cm^2/year for core QH85-7 site at the central southern subbasin. The highest sedimentation rate occurs at the core site of the eastern basin
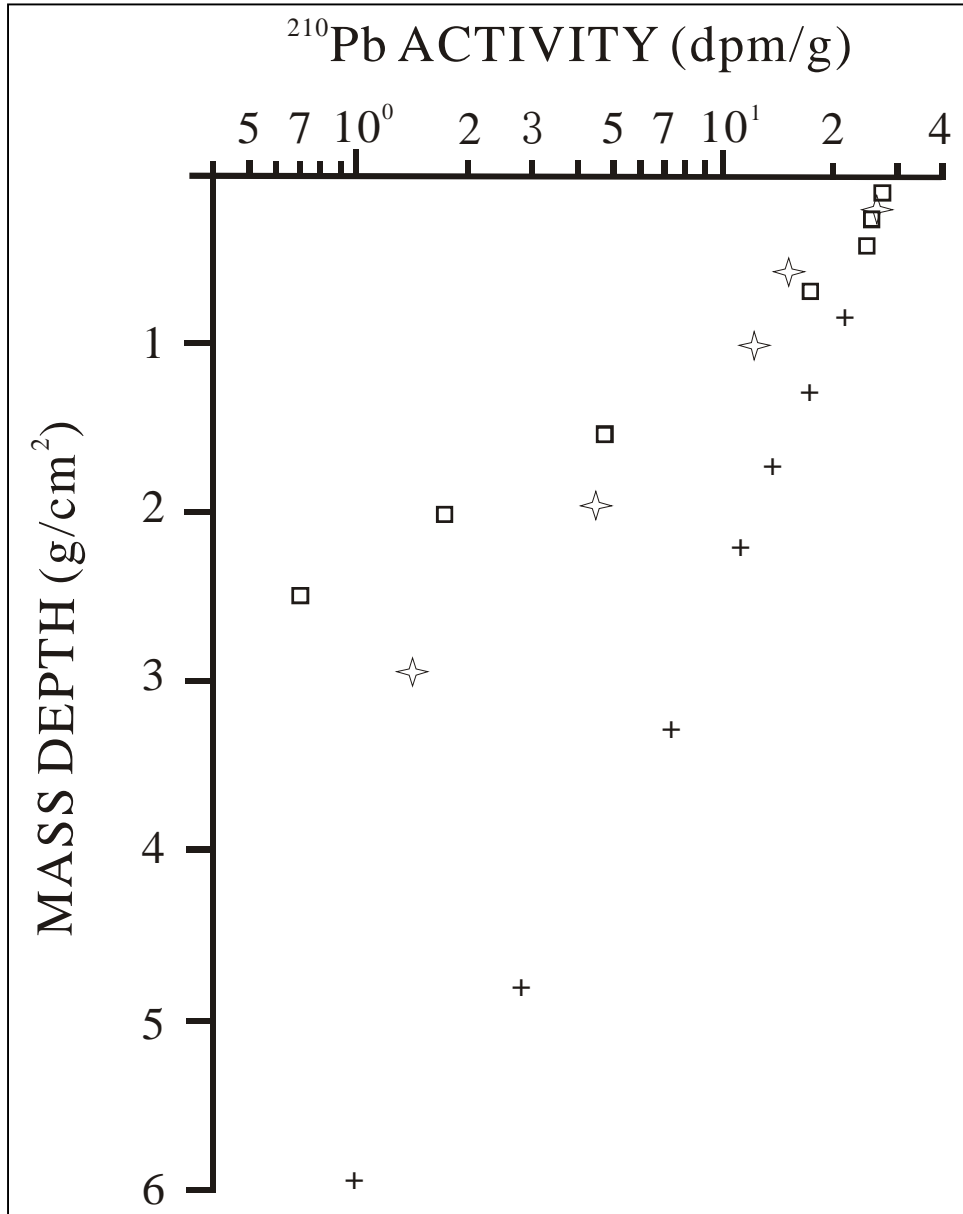

Figure 4.7 Unsupported ^{210}Pb concentrations on logarithmic scale versus sediment mass depths in the cores of QH85-7 (✦), QH85-12 (□), and QH85-2 (+). The ^{210}Pb$_{unsupported}$ concentrations of the topmost samples in the three cores are almost identical. The sediment accumulation rate at the QH85-7 site is close to the average sedimentation rate of the three cores.

although there is no direct river input. This is because somewhat more sediments were carried by return flow in the eastern basin where high winds pile up waters (Yu et al., 1987).

4.4 Lithologic units

Lithologic units of piston cores are assigned primarily on the basis of sediment character such as colour, mineralogical composition, grain size, or sediment structure. Other stratigraphic variables that have been taken into account for the designation of lithologic units and sub-units include carbonate content and carbonate mineral composition, total organic carbon and nitrogen, and magnetic susceptibility characteristics.

4.4.1 Lithologic units of core Q14B

Core Q14B was taken from the central area of the southern basin at a site where water depth is 26.5 m (Figure 4.1). Plate 4.1 shows the colour photograph of the 560 cm long core Q14B in six sections with top section left and bottom section right. Six lithologic units, Unit I to Unit VI, were distinguished (Figure 4.8), which modify those of Kelts et al., 1989 and Lister et al., 1991. The sediment character of each lithologic unit is described upward from Unit VI, the basal unit of core Q14B, to Unit I, the most recent unit.

Unit VI (corresponding to depth interval: 560-466.5 cm) is the basal sediment unit of core Q14B. It is characterized by massive light-gray muddy silts with relatively low carbonate (21.2-38.1%) and total organic carbon ($< 0.1\%$) contents. Small ostracode valves, mainly *Limnocythere inopinata*, are sparsely present in the sediments. The sediments of Sub-unit VIb (550-520 cm) are weakly structured with irregular flecks as a result of the presence of pyrite. The age of sediment deposition at the base of the unit is estimated at 14,000 years BP on the basis of an extrapolation of four AMS ^{14}C dates in the upper units.

Unit V (466.5-429 cm) shows light gray clastic laminations. *Ruppia* seeds and *Eucypris inflata* valves are scattered in four thin layers. A 2 cm thick sandy layer with darker colour rests on the top of Unit VI, followed by clastic laminations more irregular and coarser than those in the upper Unit V. Total carbonate content (TCC) varies from 25%-35%, on average about 8% less than that of the Unit VI sediments. The deposition of the detrital laminations started at about 11,600 ^{14}C years BP and terminated at about 10,700 ^{14}C years BP.

Unit IV (429-399 cm) is composed of five bands: (1) a 5 cm thick band with *Ruppia* seeds and *Eucypris inflata* valves, which rests on top of the detrital laminations of Unit V, (2) a massive light gray calcitic mud in which TCC increases from 25% to 35%, (3) a 4 cm thick, relatively dark band rich in organic matter and TOC, (4) a 8 cm thick massive dolomitic and dolomite mud in which dolomite content increases from 32% to 77%, and (5) a 5 cm thick dolomite nodular band on top of Unit IV. The dolomite deposition terminated at ~10,000 ^{14}C years BP. Dolomite content and organic matter are used as the criteria for defining subunits. The boundary between Unit IVb and Unit IVa is assigned between the band (3) and band (4), as described above.
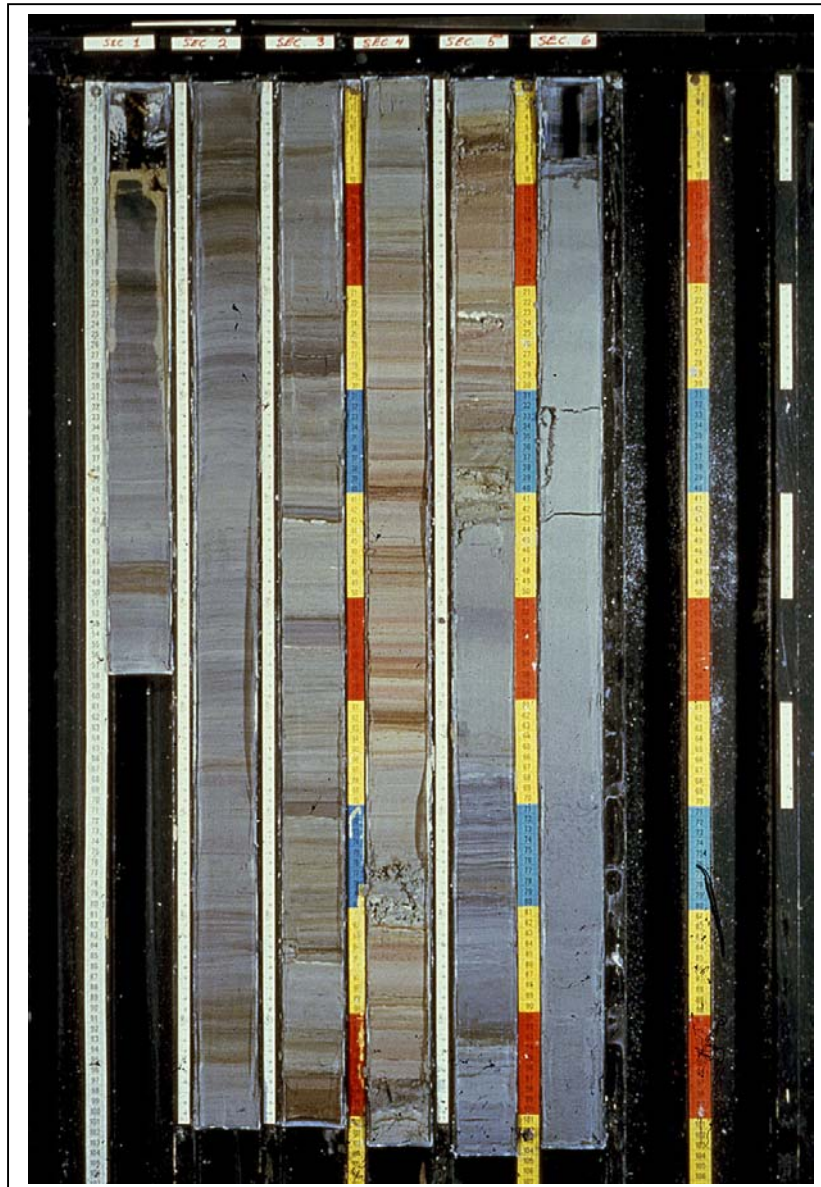
Plate 4.1 Colour photograph of core Q14B. The 560 cm long piston
core, taken from the central southern basin, was cut into 6 sections
with top Section 1 left and bottom Sect. 6 right.

Unit III (399-253 cm) is characterized by a reddish coloured, aragonite dominated
calcareous mud, and abundant ostracode valves. Two subunits, Unit IIIb and Unit IIIa, are
distinguished.

Unit IIIb (399-321 cm) is characterized by reddish-gray aragonitic mud with bands and
couplets of algal remains and aragonite laminae. The presence of five aragonite-nodular
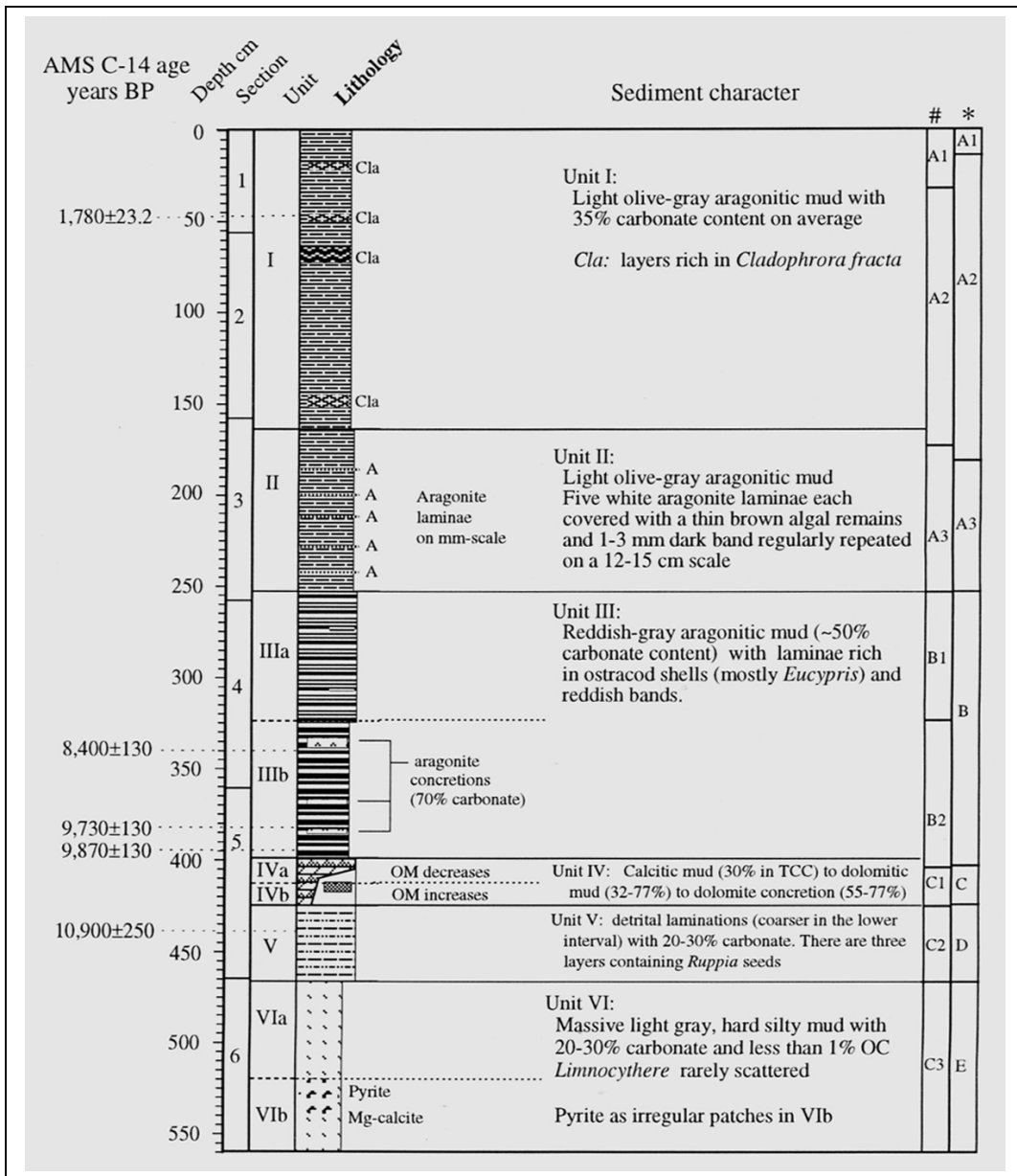
Figure 4.8 Summary of core description for Q14B, radiocarbon ages, and lithologic units. The distinguished six lithologic units modify those of Kelts et al., 1989* and Lister et al., 1991#.

layer on cm scales is a unique feature of Unit IIIb. Several mm-thin layers rich in dolomite

are intercalated in those aragonite layers. Abundant ostracode valves present in the sediments of Unit IIIb with several laminae being composed of ostracode valves. Macrofossils from aquatic plant are relatively rich, which coincides with a higher TOC content in the sediments of Unit IIIb. TCC decreases sharply in a 6 cm layer at the base of Unit IIIb, coincident with a sharp increase in TOC.

Unit IIIa (321-253 cm) has a more regular lamination, and shows bands and thin beds grouped on a decimeter scale. Fine carbonate couplets are preserved such as in Section 4/39-42 cm. Sedimentation takes on a cyclic appearance and ostracode bivalve layers diminished upwards in abundance with an exception of a reddish layer at the uppermost contact. Aragonite content remains stable at about 30% in the sediments, whereas dolomite thin layers are absent in this subunit. The termination of the Unit III deposition is dated at ~6300 years BP based on an extrapolation of the AMS ^{14}C dates.

Unit II (253-164 cm) is characterized by a light olive-gray aragonitic mud with six sedimentation cycles marked by regularly repeated bands of 1 to 3 cm thick dark layers with a mm-thin, white aragonite lamina at the base. The sediments contain about 50% carbonate minerals in which the aragonite component is about 30% on average. TOC varies from 1.5 to 2.5%. The age of the Unit II deposition is estimated at ~6300-4100 years BP based on an extrapolation from four AMS ^{14}C ages.

Unit I (164-0 cm) comprises light olive-gray aragonitic mud deposited in the last 4100 ^{14}C years. The sediment character appears overall uniform though faint cyclic banding on decimeter scale persists. Total carbonate content is about 35% on average, about 10% less than that of Unit II. There are a number of bands rich in algal filaments, among which a dark gray interval at the core depth from 64-75 cm consists of three darker layers that coincide with lower TCCs.

4.4.2 Lithologic units of core Q16C

The piston core Q16C was taken from a site of 25 m water depth in the middle of the eastern basin. The colour photograph of Plate 4.2 shows the six sections of the 555 cm long core Q16C with top section left and bottom section right. Six lithologic units, Unit I to Unit VI, were distinguished and the sediment character of each lithologic unit is described upward from Unit VI, the basal unit of core Q16C, to Unit I, the most recent unit.

Unit VI (555-461 cm) includes two sediment intervals. The lower interval of Unit VI (555-507 cm) comprises massive light gray silty mud with faint structures of irregular flecks due to the presence of pyrite. The upper interval (507-461 cm) basically has the same sediment composition as that in the lower interval but shows distinct post-depositional structures of folding and tilting. TCC ranges from 20-30% and is lower (around 20%) in the deformed upper interval.

Unit V (461-426 cm) is characterized by light gray clastic laminations that rest unconformably on top of the deformed sediments of Unit VI. Erosion marks and irregular laminations are common. A 2 cm thick layer rich in *Ruppia* seeds and stalks is present in Section 5 at 85-87 cm. TCC ranges from 20 to 30%.
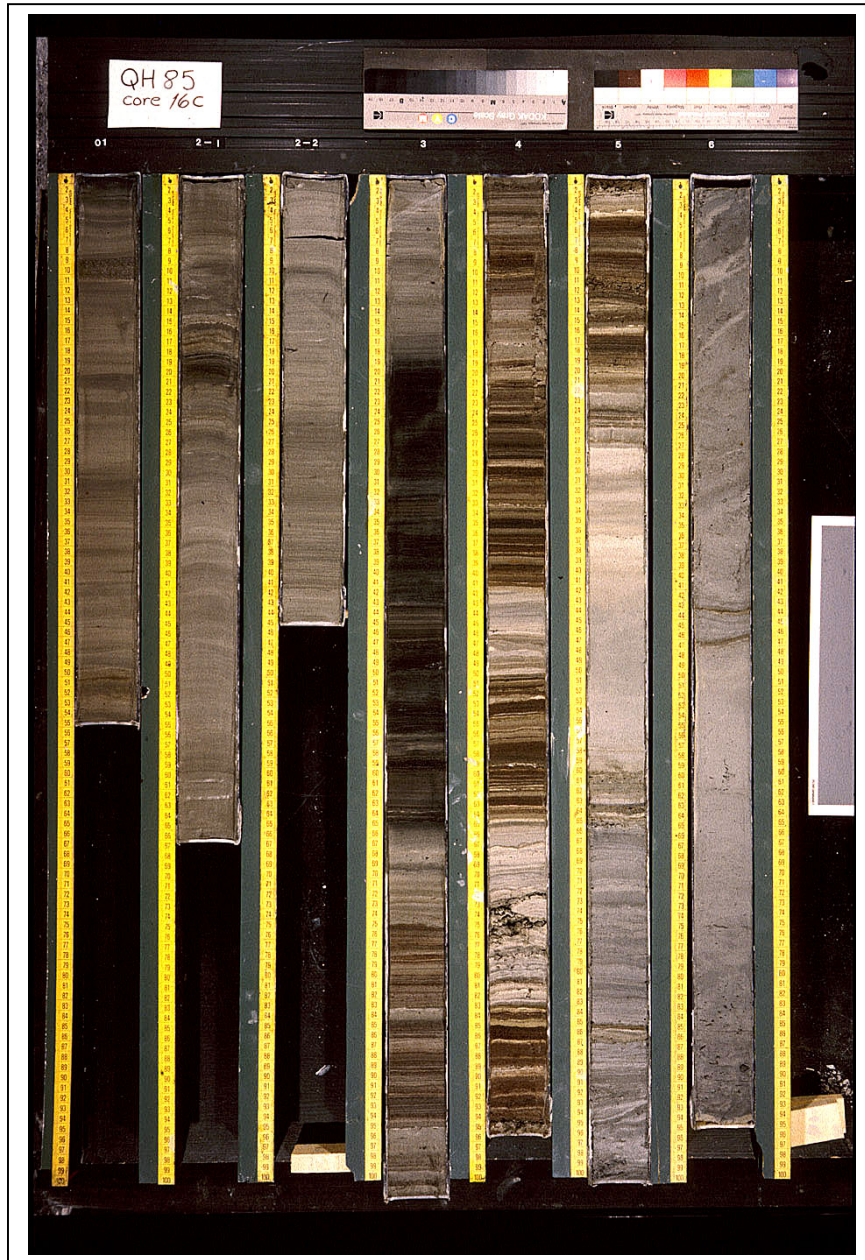
Plate 4.2 Colour photograph of core Q16C. Six sections of the 555 cm long piston core, taken from the central eastern basin, are numbered 1 (top section left) to 6 (bottom section right).

Unit IV (426-388.4 cm) consists of six bands that include (1) a 6 cm thick laminated layer rich in *Ruppia* seeds and stalks as the basal band of Unit IV, (2) a 7 cm thick massive muddy silt with 30-40% TCC, (3) a 9 cm thick relatively dark band and rich in algal remains, (4) a 7 cm thick faintly structured aragonitic muddy silt in which aragonite

Table 4.2 Core correlation between Q14B and Q16C, and a correlation of the stratigraphic record with European chronozones.

Unit	Core Q14B	Core Q16C	Time period	^{14}C years BP	European chronozone
I	Core depth: 0-164 cm Light olive-gray aragonitic mud with 35% TC on average and 1.5-2.5% TOC	Core depth: 0-172 cm Medium gray, finely laminated mud.	Holocene		Holocene
II	164-253 cm Light olive-gray aragonitic mud with 45-55% TC and 1.5-2.5% TOC.	172-259 cm Light brownish-gray well-laminated aragonitic mud		4100	
III	253-399 cm Reddish-gray, laminated aragonitic mud with 45-78% TC and 1.2-4% TOC, rich in ostracod shell.	259-388.4 cm Reddish-brown, laminated aragonitic mud.		6300	Preboreal?
IV	399-429 cm Dolomite nodular layer/dolomitic mud/massive calcitic mud	388.4-426 cm Dolomite layer/weakly laminated band (38-48% TC)/massive calcitic to aragonitic mud (30-40% TC)	Late Pleistocene	10,000	Younger Dryas
V	429-466.5- cm Light gray clastic laminations with 25-35% TC and 0.5-1% TOC.	426-461 cm Light gray clastic laminations.		10,700	Allerød
VI	466.5-560 cm Massive light-gray muddy silt with 21-38% carbonate.	461-555 cm Massive light-gray muddy silt. Post-depositional deformation present in the upper section.		11,600 ~14,000	Older Dryas Bølling?

content increases up to 40%, (5) a 7 cm thick weakly and irregularly laminated band with 38-48% TCC, and (6) a 2 cm thick white dolomite layer with 65% TCC as the top band of Unit IV.

Unit III (388.4-259 cm) is characterized by a reddish-brown colour, aragonite dominated calcareous muddy silt with abundant ostracode shells. The sediment is overall well laminated. Aragonite nodular layers are present along with the more frequent presence of white aragonite laminae in the lower interval between 388.4 and 330.5 cm. The thickness of the carbonate nodular layers ranges from 2 to 6 cm. *Ruppia* seeds are present either on top or at the base of the nodular layers. Erosion scour marks are occasionally present in Unit III.

Unit II (259-172 cm) comprises well-laminated aragonitic sediments with TCC ranging from 35-44%. The sediment interval of 229-182 cm shows a dark gray FeS cast, representing more reduced conditions. Rhythmic sedimentation of 2 cm thick finely laminated layer occurs on a decimeter scale in the dark-gray interval.

Unit I (172-0 cm) is characterized by medium gray, finely laminated muddy silts. Some 1 to 3 cm thick bands rich in algal filaments are present in Unit I, among which the dark gray interval at 66-78.5 cm with the pattern correlative to that at 64-75 cm in core Q14B.

4.4.3 Core correlation and boundary description

Table 4.2 gives a brief summary on core correlation between Q14B and Q16C. The boundary of Unit III /Unit IV is designated as the division of the Holocene and Pleistocene based on 1) AMS radiocarbon dating, which gives an extrapolated ^{14}C age of 10 ka BP, and 2) a major change in sediment character from clastic deposits to laminated calcareous sediments. Unit IV was deposited between 10.7 and 10 ka ^{14}C BP, coeval with the European Younger Dryas. The sediments of Unit IV also show the characteristics of transitional sedimentation from more detrital deposition of the Late Pleistocene to more carbonate precipitation of the Holocene. The boundary of Unit V/Unit VI marks a lithologic shift from massive sediments to clastic laminations, indicating an abrupt change in sedimentation regime of the lake. The timing of the change was at ~ 11.6 ka ^{14}C BP, closely matching that between the Older Dryas and Allerød in Northern Europe, although both the timing of the chronozones and related paleoclimate conditions in the Late Pleistocene may differ from each other, to some extent, between the two continents.

5. Abrupt changes in climatic conditions across the Late-Glacial/ Holocene transition on the N. E. Tibet-Qinghai Plateau

5.1 Introduction

The AMS ^{14}C dated lithostratigraphy (Figures 4.4, 4.8) indicates that the sediment interval of the top 164 cm show little change in sediment character, suggesting relatively steady conditions of the lake in the last 4.1 ka (^{14}C years). By contrast, lake conditions from about 12 to 9.8 ka ^{14}C BP, were rather unstable, as indicated by marked shifts in sediment composition, colour and structure in the interval of 470-380 cm. One of the main foci of the thesis study is placed on the pattern of climate change across the Late-Glacial/Holocene transition on the N. E. Tibet-Qinghai Plateau based on a high-resolution, multi-proxy investigation of the two piston cores, Q14B and Q16C.

Proxy records from many sites all over the world have manifested the instability of climate systems across the Late Glacial to Holocene transition. Younger Dryas (YD) is one of the time windows included in the transition, which is a well-established phenomenon of climate setback to cold and dry conditions in northern Europe in the general warming trend of the last deglaciation. Yet, questions remain elusive regarding what are the causes of the YD event (Broecker, 1988; Berger, 1990; Broecker, 2000) and whether or not the geographic extent of the event is on the global scale (Wright, 1989; Singer, 1998; Gasse et al., 1991; Rind et al., 1986; Kudrass et al., 1991; Peteet, 1992; An et al., 1993; Maloney, 1996; Bennett et al., 2000). The significance of this study on the continuous and intact sediment record from Lake Qinghai is to provide key-site evidence of climate change pattern across the Late-Glacial/Holocene transition on the N. E. Tibet-Qinghai Plateau. The results of this study may also give some contribution to a better understanding on how various components of the atmosphere, cryosphere, biosphere and ocean interact on short time scales.

5.2 Results from a multi-proxy investigation on cores Q14B and Q16C

5.2.1 Distinct lithostratigraphic units

The chronology of the lacustrine sequence deposited across the Late-Glacial/Holocene transition is framed by four AMS radiocarbon dates on macrofossil seeds from core Q14B (Figure 5.1a, b). Four lithostratigraphic units are defined on the basis of sediment structure, texture, and mineralogy, characteristic colour as well as marked contacts between each pair of units. These four distinct stratigraphic units correlate well with those in core Q16C (Figure 5.2), even though the two cores are about 40 km apart and in different basins. The radiocarbon ages for the unit contacts in core Q14B are therefore extrapolated to similar features in Q16C.

Unit VI, the basal sediment unit in both cores, is characterized by massive, light-gray silts with much lower TCC and TN contents than those in the early-Holocene sediments of Unit IIIb. The homogeneity of the Unit VI sediments of core Q14B suggests relatively steady conditions at the central southern subbasin between ~14 and 11.6 ka ^{14}C BP. The lower parts of Unit VI in both cores Q14B and Q16C show nearly identical sediment character, with pyrite patches and Mg-calcite present. Sediment from the upper part (45 cm

thick) of the unit in Q16C shows deformation structures, including tilting and folding (Figure 5.2). The deformed sediment is present between the underlying massive sediment and overlying clastic laminations that show no deformation structure. The whole core was collected in one coring penetration with a Kullenberg device. The deformation structures present in the upper part of Unit VI are therefore not a coring artifact. Because the lake bottom both at present and in the past is extremely flat, as revealed by seismic reflection profiles and core correlation, those post-deposional structures are unlikely caused by a slump process.
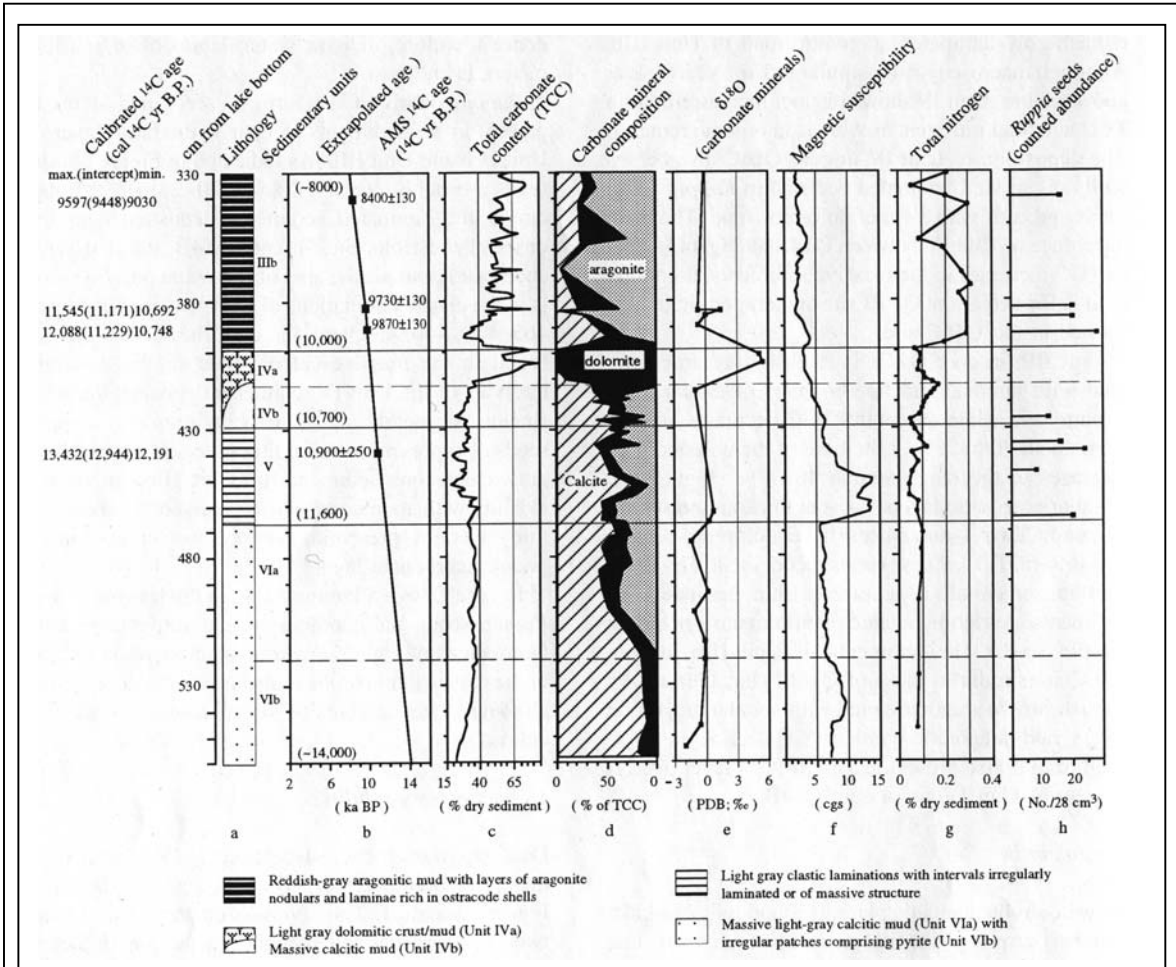
Figure 5.1 Multiple proxy records obtained from sediment core Q14B. Chronology is framed by four AMS ^{14}C ages for aquatic macrofossil seeds (b). Calibrated ^{14}C ages and 2 sigma ranges are obtained according to the methods by Stuiver et al. (1998). The Late-Glacial sediments have lower total carbonate content (c), lower total nitrogen (g), and higher magnetic susceptibility (f) compared with the early-Holocene sediments. Magnetic susceptibility peaks coincide with the sediments with coarser detrital materials (a). Ostracod shells are much more abundant in Unit IIIb than in Unit VI. TCC increase in Unit VIb is due to an increase in Mg-calcite. Dolomite deposition (d) is accompanied by increases in TCC and $\delta^{18}O$ (e). Total nitrogen (g) and aragonite contents (d) increased markedly in the early-Holocene sediments. Seeds from the rooted aquatic plant, *Ruppia*, are present mainly in the laminated sediments of Unit V and Unit IIIb (h).

Light-gray detrital laminations, with the presence of scattered *Ruppia* seeds and *Eucypris* ostracod shells, characterize Unit V, which is 38 cm thick in Q14B and 36 cm thick in Q16C. The enhanced detrital content to both southern and eastern central basins throughout Unit V is accompanied by an increase in the MS values and by a TCC decrease.

In core Q14B, Unit IV begins with a 5 cm bed rich in *Ruppia* fossils and concludes with a dolomite layer that includes 11 cm of dolomitic mud capped by 5 cm of dolomitic nodules. The missing texture and light-gray colour of the main part of the unit are visually distinct from either the underlying clastic laminations of Unit V or overlying reddish-gray laminated aragonitic mud of Unit IIIb. Although macroscopically similar to Unit VI in colour and structure, Unit IV shows distinct increases both in TCC and total nitrogen, as well as in organic remains. The deposition of Unit IV in core Q16C also begins with a 5-cm well-laminated bed rich in *Ruppia* fossil seeds and ends with 3 centimeters of dolomitic mud. The main difference of Unit IV between Q14B and Q16C is that as TCC increases in the massive sediments, dolomitic mud is formed at the Q14B site and aragonitic mud is formed at the Q16C site. This suggests a separation of the paleo-lake into individual basins at the time.

Unit IIIb in core Q14B is composed of a reddish-gray aragonitic mud with laminae and fine couplets of darker algal remains and white aragonite. TCC decreases sharply from about 70% to 28% at the base of the unit and then increases to 40-77% (Figure 5.1c). Nodular aragonitic layers 1 cm to 5 cm thick are present in the unit. Two 1 mm slices have a dolomite content of 40 to 46% of TCC. *Eucypris* ostracod shells are abundant in some 0.5 cm thin laminae. The sediments are rich in aquatic plant remains, including *Ruppia* seeds. The sediments of Unit IIIb in core Q16C are similar to those of Q14B, characterized by reddish-brown aragonitic mud with nodular aragonitic layers and aragonitic laminae. A decline in TCC (Figure 5.2) is also present in a 4 cm thick layer, which overlies on top of Unit IV, as in core Q14B.

5.2.2 Paleobotanic evidence

Seeds and stalks from *Ruppia* sp. are present in the sediments of Unit V, the basal layer of Unit IVb and Unit IIIb. As indicated in Figure 5.1h, the seeds are richly preserved with about 1/cm^3 in the laminated sediments deposited near the onset of the Holocene. In core Q14B, the first presence of *Ruppia* seeds, also of the ostracode *Eucypris* is in the clastic laminations of Unit V at core depths of 465 cm, 447 cm, 440 cm, 436 cm, and 426 cm. The seeds were not found in the massive calcitic mud or the dolomite intervals of the Unit IV sediments deposited in a shallow or nearly desiccated environment. *Ruppia* seeds are also present in some thin layers of the reddish-gray calcareous sediments of Unit IIIb, either co-existing with abundant *Eucypris* ostracode valves in a thin layer, or being present at the base or on top of the nodular carbonate layers.

In core Q16C, abundant *Ruppia* seeds and stalks are present in a laminated 6 cm thick layer right above the detrital laminations of Unit V. An equivalent layer, although it contains fewer *Ruppia* seeds and stalks is present in core Q14B as well.

Ruppia sp is still growing in the low-energy, near-shore areas today, where water depth is less than 2 m in the proximity of a fresh water inflow. A question regarding whether the presence of *Ruppia* seeds preserved in the sediment intervals of cores taken from the sites
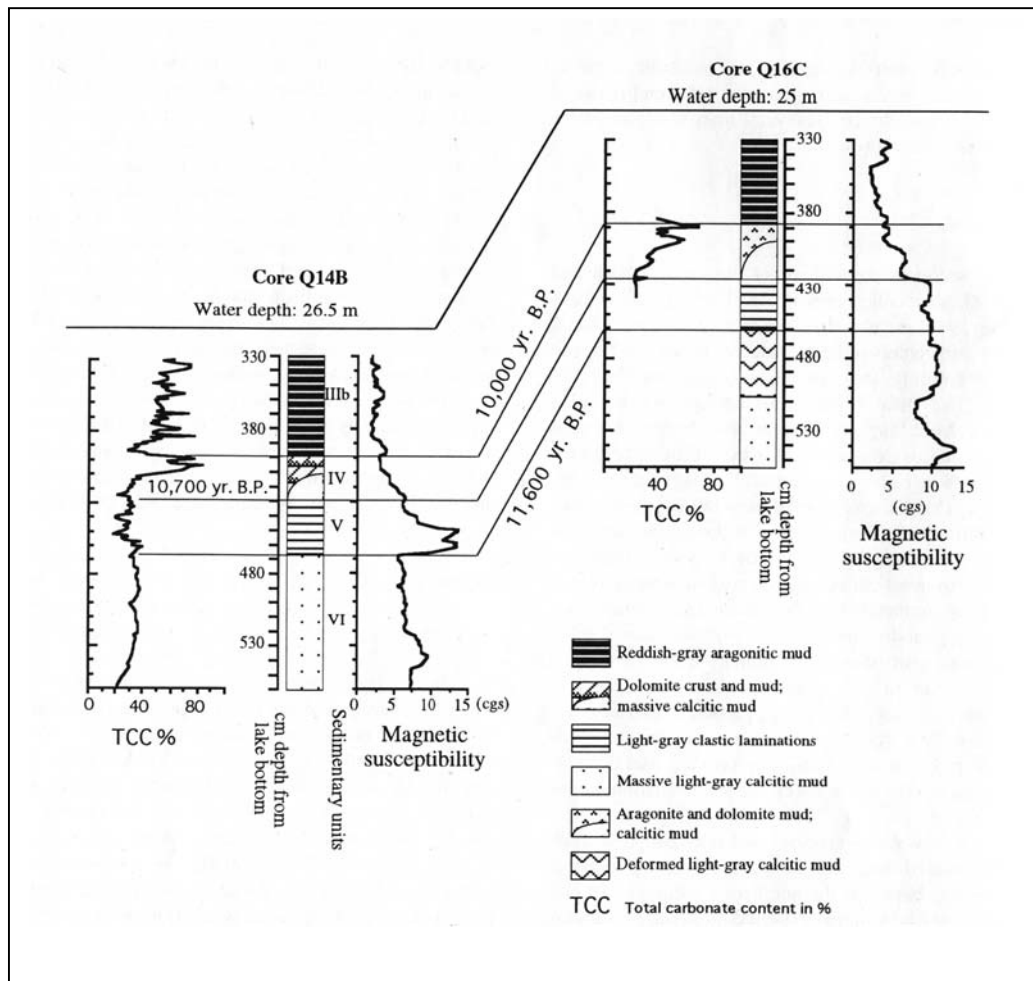
Figure 5.2 Correlation of the late-glacial/Holocene transition between two cores, Q14B and Q16C recovered respectively from the central southern subbasin and the central eastern subbasin. Ages between lithologic units are uncalibrated ^{14}C ages based on an extrapolation of four measured AMS radiocarbon ages from core Q14B. Correlation between Q14B and Q16C are based on distinct lithologic feature, magnetic susceptibility, and carbonate mineralogy. Offset in vertical position represents differences in water depth.

with the water depth today more than 25 m can be used as a shallow water indicator depends on whether the seeds are in situ dropped and buried or transported from the littoral zone of the lake. The fact that the frequent presence of *Ruppia* seeds with abundant amounts in the laminated sediment intervals and shallow-water subfacies does not favour the possibility of a long-distance transportation of the *Ruppia* seeds over the very flat lake bottom.

5.2.3 Core logs of MS

Data from MS measurements for both cores Q14B and Q16C are shown in Figure 5.1f and Figure 5.2. The common characteristic of the two curves is that MS is higher in the pre-Holocene sediments of Unit VI and Unit V, decreases in Unit IV, and is low in the early-Holocene sediments of Unit IIIb. Positive excursions in MS in the pre-Holocene sediments correspond with sediment intervals rich in coarser detrital minerals. The variations of MS value with depth appear to be controlled by detrital influx to the core sites. A positive excursion in MS occurs in both cores in the lower part of Unit VI, where the sediments show nearly identical mineralogy. This coherence indicates a very similar sedimentation regime in both central subbasins. From the upper part of Unit VI to Unit V, the MS pattern of the two cores diverges. MS values in core Q14B remain approximately constant in the massive sediments of the upper part of Unit VI, whereas in core Q16C MS values increase and remain high in the deformed sediments of the upper part of Unit VI. This pattern suggests that the influx of detrital material to the Q16C core site in the central eastern basin was higher than at the Q14B site. During the later deposition of the lower part of Unit V, MS values peak in core Q14B. This MS peak probably reflects increased inflow of sediment laden waters from the Buha River, which today carries about 67% of the annual inflow from the western catchment (Figure 4.1). The difference between the two cores in MS curve pattern for Unit VI and V may indicate that the two central basins were supplied by different river systems at the time when the lake was very shallow.

The cessation of clastic laminations in Unit V is followed at both core sites by a decrease in MS. Core Q14B displays gradually decreasing values, whereas core Q16C shows a step decrease within a 5 cm thick layer. The decrease in MS value in the Unit IVb sediment of Q14B correlates with an increase in both nitrogen content (Figure 5.1g) and organic matter.

MS values in the early-Holocene sediments of Unit IIIb are lowest in both cores. In core Q14B a small peak in MS is present at the base of Unit IIIb. Assuming that the paleo-lake levels during the early Holocene were similar to those during Unit V deposition (see lake-level reconstruction below), the lowest MS values in the early-Holocene sediments may be attributed to increased vegetation cover in the catchment, resulting in a substantial decrease in detrital influx to the core site.

5.2.4 Carbonate content and mineralogical record

Total carbonate content (TCC) in the sediments of Lake Qinghai ranges from 18.3% to 83.6% in weight percentage (Figure 5.1c). Carbonate minerals in the sediments include aragonite, calcite and dolomite (Figure 5.1d). Mineralogical examinations for these carbonate minerals from both sediment cores and traps (see Chapter 6) indicate that they are autochthonously formed in the lake. TCC in the pre-Holocene sediments of Unit VI, Unit V, and Unit IVb ranges from about 18.3% to 39.1%. It increases from the base of Unit IVa and quickly reaches 77% in a 7 cm interval as a result of increasing dolomite content. A negative excursion of TCC is present at the base of Unit IIIb. Following an increase of aragonite content, TCC is constantly higher ranging between 44.7% and 77.8% in the early Holocene sediments of Unit IIIb.

A gradual increase in TCC from 21% to 37% in Unit VIb is followed by a marked mineralogical change at the boundary between Unit VIb and Unit VIa, from which high-Mg-calcite gives way to aragonite. This implies a threshold shift of Mg/Ca ratio of the paleo-lake. As aragonite is only 15-44% of TCC in Unit VIb, Unit V and Unit IVb, low Mg-calcite 38-63% of TCC represents the main carbonate phase in these sediment Units. About 5% occurs as dolomite in the pre-Holocene sediments except in Unit IVa where dolomite is the dominant phase (21-77 wt.% of the bulk sediments). Both TCC and dolomite increase progressively in Unit IVb, following an abrupt cessation of the clastic laminations (Unit V), and then increase sharply in Unit IVa, forming a dolomitic layer at the central southern subbasin (core Q14B). The dolomite phase ceased abruptly around 10 ka ^{14}C BP., as also indicated by a negative excursion in TCC at the base of Unit IIIb. Aragonite increases from the base of Unit IIIb and within a 7 cm interval it becomes the dominant carbonate phase with aragonite content 59-74% of TCC in the early Holocene sediments. At least two mm-thin layers higher in dolomite content (about 40-46% of TCC) are present in Unit IIIb.

Four distinct carbonate subfacies are distinguished for the sediment sequence spanning the Late-Glacial/Holocene transition, based on both TCC and relative abundance of calcite, dolomite, and aragonite, as shown in Figure 5.1d. The carbonate subfacies changes from Mg-calcite-dominated in Unit VIb to calcite- and aragonite-dominated in Unit VIa, Unit V, and Unit IVb, and then from dolomite-dominated in Unit IVa to aragonite-dominated in the early Holocene sediments of Unit IIIb.

5.2.5 Oxygen stable-isotopic record

Most of samples selected for oxygen and carbon stable-isotope analyses are bulk sediments from 1 cm core slices representing about 20-year-mean isotopic signals each (Figure 5.1e). One exception is the sample of an aragonite lamina from Unit IIIb, which is yearly or seasonally precipitated from the lake. It shows a δ^{18}O value of 1.47‰, some 1.50‰ to 2.15‰ more positive than those of the underlying and overlying aragonitic sediment samples. This indicates that the surface water isotopic composition could go up substantially due to either strong summer evaporation or a negative P-E balance. Two dolomite samples from Unit IVa have the isotopic composition of 5.1‰ and 5.5‰ in δ^{18}O, about 6‰ higher than the δ^{18}O values of the underlying and overlying calcitic sediments. The higher δ^{18}O values coincide with higher TCC in Unit IVa, suggesting that the dolomite layer was formed under highly negative P-E, provided that the difference of fractionation factors between dolomite and calcite is insignificant compared with the 6‰ shifts. The δ^{18}O values of the calcitic sediments from Unit VI, Unit V, and Unit IVb range from -2.0‰ to 0.3‰. Seven data points for δ^{18}O in Unit VI show the tendency of positive correlation with TCC.

The δ^{18}O value of carbonate minerals precipitated in the surface water should (1) parallel the δ^{18}O value of the water and (2) depend on the ambient water temperature during carbonate-mineral nucleation. The temperature-dependent fractionation factor for δ^{18}O is about 0.29‰/℃ and 0.26‰/℃ during aragonite and calcite precipitation, respectively (Craig, 1965; Grossman and Ku, 1986). For hydrologically open lakes (often freshwater with short residence times), δ^{18}O variations of the lake waters are considered to qualitatively reflect the δ^{18}O variations in precipitation (Siegenthaler et al., 1984) and thus

fluctuations in mean air temperature (Dansgaard et al., 1989). For hydrologically closed lakes, on the other hand, $\delta^{18}O$ variations of the lake waters are mainly controlled by effective moisture (P-E) and residence time, more than air-temperature effects (Talbot, 1990; Talbot and Kelts, 1990; Lister et al., 1991). Therefore, the $\delta^{18}O$ ratios of authigenic carbonates in the sediment sequences of closed-basin lakes indicate both long- and short-term variations in P-E.

5.2.6 Total nitrogen content

The total nitrogen (TN) content (Figure 5.1g) of pre-Holocene sediments from Unit VI and Unit V ranges between 0.05 and 0.10%. It increases in Unit IVb up to about 0.18% with an increase in aquatic plant remains. The TN content decreases in Unit IVa as dolomite content increases. The TN abruptly increases from the base of Unit IIIb and reaches 0.3% within a 4 cm interval. The TN contents of the early-Holocene sediments of Unit IIIb mostly range between 0.2% and 0.3%, about 2-3 times higher than those of the pre-Holocene sediments of Unit VI and Unit V, with the exception of two samples having TN less than 0.1% (these two samples were from white laminae that are nearly pure aragonite). Correspondingly, the organic remains of algal filaments and macrophytes are abundant in the early-Holocene sediments of Unit IIIb and rare in the pre-Holocene sediments of Unit VI. Most nitrogen in sediments is bound to organic matter (Bengtsson and Enell, 1986). TN content is about one tenth of total organic carbon content in lake sediments if organic matter is primarily produced within the lake. The TN content is a useful stratigraphic variable indicating the abundance of organic matter in the lake sediments.

The organic matter (OM) originated mostly from the primary production within Lake Qinghai, as its C/N ratios are mostly close to 10, similar to those of autochthonous OM (Yu et al., 2001). The curve for TN might therefore reflect paleo-productivity of Lake Qinghai if factors affecting the down-core variations of OM are evaluated. These factors include (1) change in preservation of OM, and (2) variations in sedimentation rates of clastic and/or carbonate deposition.

Average sedimentation rates for the intervals interpolated between the radiocarbon dates are in the range of 0.35-0.45 mm per year. Within this range, the maximum deviation of total nitrogen resulting from the changing sedimentation rate is about 0.05%, assuming a constant influx rate of total nitrogen. Hence we conclude that the 0.1- 0.25% higher TN content of early-Holocene sediments compared with pre-Holocene sediments is not a result of changing sedimentation rate. In fact, the average sedimentation rate was slightly higher during the early Holocene due most likely to higher carbonate production rate.

5.3 Reconstruction of lake levels and limnological conditions

The elevation of the lake bottom at the Q14B site today is 1.5 m lower than that at the Q16C site (Figure 5.2). Seismic investigation reveals that the lake bottom topography is very flat. The southern and eastern subbasins exchange water if levels today exceed 2-3 meters, creating a large contiguous lake. The elevation differences of the paleo-lake bottom between the two core sites were only 1.56 m at the Unit VI/Unit V contact, 1.53 m at the Unit V/Unit IV and 1.61 m at the Unit IV/Unit IIIb, respectively, i.e. rather similar to that of today.

A few meters deep shallow lake environment is suggested near the termination of Unit VI by the following evidence: (1) in core Q14B, the erosion surface of Unit VI is overlain by coarser detritus of Unit V, and (2) the upper half of Unit VI in core Q16C is deformed likely due to frost-heaving under near desiccation conditions at the central eastern subbasin. As implied by the carbonate mineral record (Figure 5.1c, d) and lithologic correlation between the two cores, the paleo-lake during the deposition of the lower half of Unit VI was less saline and perhaps a few meters deeper than during the deposition of the upper part of Unit VI. While the uniform character of the Unit VI sediments suggests a relatively stable sedimentation regime at the Q14B site from ~14 to 11.6 ka ^{14}C BP, changes in TCC and carbonate-mineral assemblage, as well as isotopic change, indicate minor variations in water chemistry. A change in Mg/Ca ratio, as suggested by a mineralogical change from Mg-calcite to aragonite, occurred between Unit VIb and Unit VIa, following increases in both carbonate alkalinity and [18]O of the water during the Unit VIb deposition. The proxy data of TCC, carbonate mineral assemblage, and TN content, suggest that the carbonate alkalinity, Mg/Ca ratio, and organic productivity of the paleo-lake during ~14 to 11.6 ka ^{14}C BP were much lower than those during the early Holocene.

Between ~14 and 11.6 ka ^{14}C BP during the deposition of Unit V, water chemistry and organic productivity of the lake remained similar to that during the Unit VIa deposition, as suggested by carbonate-mineral assemblage, TCC and TN (Figure 5.1). Slightly lower TN and TCC in Unit V may reflect dilution by an increased detrital influx, as evidenced by sandy sediments coincided with high MS values. The frequent presence of *Ruppia* seeds in the clastic laminations indicates that the lake levels were from about 2 to 6 m deep during Unit V deposition.

Correlation between the two cores of the sediment beds just above the clastic laminations of Unit V provides evidence for defining the water depth. *Ruppia* seeds are richly preserved in the well-laminated, 6-cm thick deposit above the top of the clastic laminations of core Q16C, suggesting that the seeds were deposited in-situ. If so, the water depth then was around 2 m deep for about a century (estimated from average sedimentation rates around 0.40-0.59 mm/year based on radiocarbon ages). This deposit correlates well with a 5-cm deposit at the top of Unit V in core Q14B, although not as well laminated. The rooted *Ruppia* likely colonized the entire central subbasins for about a century following the deposition of clastic laminations. The *Ruppia*-rich deposits at the base and the dolomite layer at the top of Unit IV, along with carbonate mineral records define the water depths ranging from near desiccation to a few meters between ~10.7 and 10 ka ^{14}C BP.

Increases in TN and algal filaments in the sediments of Unit IVb (Figure 5.1g), suggest a progressive increase in organic productivity during the deposition of Unit IVb. A decrease of TN content in Unit IVa is accompanied by a fairly sharp increase in dolomite. This TN decrease is not interpreted as a decrease in organic productivity, for the formation of the lacustrine dolomite might require incorporation of organic matter as indicated by the ^{13}C value of the dolomite 4‰-7‰ more negative than that of calcite and aragonite.

Abrupt termination of the playa lake(s) at ~10 ka ^{14}C BP was followed by negative shifts in TCC and $\delta^{18}O$, which suggest an abrupt increase of water inflow and thus a deepened lake. The water depths at ~10-8 ka ^{14}C BP, however, were unlikely to be more than 8 m. This reconstruction is based on the evidence of the existence of five aragonite nodular layers and the presence of seeds, joints, and stems from *Ruppia* in the

early-Holocene sediments, suggesting that the paleo-lake levels fell occasionally down to a depth of about 2 meters. Organic productivity increased from about 10 ka ^{14}C BP and reached a maximum within about 50 years, as indicated by the TN record. High production rate of authigenic aragonite during the early Holocene indicates that the carbonate alkalinity and presumably the salinity of the lake then were higher than that before 10.7 ka ^{14}C BP.

5.4 Abrupt shifts in hydro-climatic conditions

The water levels of Lake Qinghai, as reconstructed in the above section for the period between ~14 and 8 ka ^{14}C BP, range from near desiccation to about 8 m deep, some 20 m shallower than today. This clearly indicates that the effective moisture during this time was much lower than today. As such, it can be concluded that there was no large meltwater inflow into the closed-basin lake since at least ~14 ka ^{14}C BP. During the overall shallow lake conditions at that time, four distinct lithostratigraphic units were formed, each of which represents a unique sedimentation regime and paleolimnological state. Sharp changes between lithostratigraphic units suggest abrupt shifts in regional hydrological and climatic conditions.

As discussed above, between ~14 and 11.6 ka ^{14}C BP the lake was a few meters shallower than that during the early Holocene, and was also fresher with lower organic productivity. This suggests that both precipitation and evaporation were much lower than during the early Holocene, reflecting a cold and arid climate. A cold climate would have resulted in lower productivity, reduced summer evaporation, as well as a longer period of ice-cover that reduced evaporative losses and maintained a relatively low salinity, despite a shallow lake depth. Most likely, a near glacial high-pressure regime then persisted above the plateau, causing the monsoonal precipitation to be much weaker than at any periods later in the Holocene.

Around 11.6 ka ^{14}C BP seasonal catchment inflow increased abruptly, as indicated by the deposition of clastic laminations with fossil *Ruppia*. As a result, the lake was fresher and deeper, although not deeper than 6 m. The water depths between ~11.6 and 10.7 ka ^{14}C BP were similar to or several meters shallower than those during the early Holocene, but salinity and organic productivity were much lower. Evaporation intensity and summer temperature were lower at ~11.6-10.7 ka ^{14}C BP than those of the early Holocene. The abrupt enhancement of seasonal catchment inflow from ~11.6 ka ^{14}C BP represents a cessation of near-glacial conditions on the Tibet-Qinghai Plateau. The enhanced inflow could have resulted from an increase in either precipitation from monsoon rainfall or meltwater influx from small local glaciers.

Snowline elevations during the Last Glacial Maximum (LGM) are estimated to have been lower by about 800-900 m than at present based on investigations of glacial deposits in areas adjacent to Lake Qinghai (Shi et al., 1992; Shi, 2002). Thus, permanent ice fields during the LGM were limited to cirque glaciers on Mt. Qinghai Nanshan above 3900 m a.s.l., which was the source area supplying distal meltwater to the eastern basin. It is likely that the snowline around 11.6 ka ^{14}C BP had retreated to higher altitudes than during the LGM, and small glaciers no longer existed on Mt. Qinghai Nanshan. In addition, detrital materials forming the clastic laminations were transported by different river systems into the southern and eastern subbasins, and the cessation of clastic laminations occurred

abruptly in both basins. Therefore, the cessation of clastic laminations was unlikely induced by a sudden cut-off of meltwater from rapidly diminishing small glaciers. The sediment evidence appears to favour an abrupt change in precipitation balance. The deposition of clastic laminations between ~11.6 and 10.7 ka ^{14}C BP is interpreted as resulting from enhanced seasonal inflow mainly from precipitation and a low vegetation cover in the lower catchment. The enhanced precipitation might represent an abrupt change of monsoonal circulation.

Catchment inflows decreased abruptly around 10.7 ka ^{14}C BP as implied by the abrupt cessation of clastic laminations and marked decrease in MS in both cores, Q14B and Q16C (Figure 5.2). Thereafter, a negative P-E budget between ~10.7 and 10 ka ^{14}C BP is indicated by TCC increase in both sediment profiles and the development of a playa lake environment. The sharp increase in TCC (mainly aragonite) began at the base of Unit IV (Figure 5.2, core Q16C), indicating high summer evaporation and arid conditions from about 10.7 ka ^{14}C BP. The most negative P-E budget and maximum salinity of the central lake occurred at ~10.3-10 ka ^{14}C BP, as indicated by a sharp increase in dolomite up to 80% and a positive shift in δ^{18}O value from -1‰ to +5.3‰ (Figure 5.1). The sediment evidence suggests that increased aridity at Lake Qinghai at ~10.7-10 ka ^{14}C BP was caused by a decrease in catchment inflow along with an enhancement of summer evaporation.

The beginning of the early-Holocene hydro-climatic regime is marked by the abrupt termination of the carbonate playa lake(s) and the deposition of reddish-gray laminated sediments at ~10 ka ^{14}C BP Enhanced precipitation in the catchment lead to a substantial dilution of the lake, as suggested by negative shifts in TCC and δ^{18}O (Figure 5.1c, e) from the base of Unit IIIb. The fact that the enhanced catchment inflow did not induce a high peak of MS like that at the lower half section of Unit V implies an increase in vegetation cover in the catchment. Precipitation at ~10-8 ka ^{14}C BP is considered to be higher than that during the deposition of Unit V, although the lake depth was similar to or only a few meter deeper than Unit V. This is because summer evaporation was much higher during early Holocene, as suggested by a TCC of over 50%, an aragonite-dominated mineral assemblage, and aragonite laminae. In addition, organic productivity in the early Holocene was distinctly higher than that during pre-Holocene deposition. Evidence from the multi-proxy record all point to warm early-Holocene conditions. Intensified summer evaporation then might have prevented a further increase in lake level, though precipitation was enhanced if compared to the earlier stages from about 14 to 10 ka ^{14}C BP.

5.5 Correlation with other paleoenvironmental records in China

Evidence from the proxy record of Lake Qinghai indicates that on the N.E. Tibet-Qinghai Plateau the climate across the Late-Glacial/Holocene transition was unstable, showing three abrupt shifts in hydro-climatic conditions on time scales of less than a millennium. Correlation with other paleoenvironmental records from Sumxi Lake (Gasse et al., 1991), Guliya ice cap (Thompson et al., 1997), and Baxie loess-paleosol section (An et al., 1993) indicate that short-term variations in climatic conditions on time scales similar to that at Lake Qinghai occurred at all sites studied, and that the onset of a warm and relatively wet early-Holocene climate was synchronous at about 10 ka ^{14}C BP. Late-glacial climatic instability is indeed a regional phenomenon, probably the consequence of increasing seasonality of insolation and changing surface boundary conditions

accompanying regional deglaciation.

During shallow lake conditions across the transition, Lake Qinghai appeared to have sensitively responded to hydro-climatic changes. The sediment record shows four distinct lithologic units, that archived marked shifts in water depth, carbonate alkalinity, Mg/Ca ratio, stable isotopic composition, detrital influx, and organic productivity. The reconstructed hydro-climatic history suggests that within about 1600 years the climate changed from cold and arid conditions before ~11.6 ka ^{14}C BP to a warm and wetter early Holocene with an abrupt onset at ~10 ka ^{14}C BP In between, there were two distinct hydro-climatic regimes. From ~11.6 to 10.7 ka ^{14}C BP, increased seasonal inflow occurred during a relatively cool climate with lower summer evaporation compared with the early Holocene. The other abrupt event at ~10.7-10 ka ^{14}C BP is characterized by arid conditions with enhanced evaporation and reduced catchment inflow, leading to the formation of a carbonate playa environment. This arid event at ~10.7-10 ka ^{14}C BP is chronologically synchronous with the European Younger Dryas (Lister et al., 1991), the climatic setback to cold and arid conditions (Lowe et al., 1980; Dansgaard et al., 1982). It might also be linked to the cold and dry episode at ~11-10 ka ^{14}C BP as interpreted from the Lake Sumxi record from the western Tibet-Qinghai Plateau (Gasse et al., 1991) and to a $\delta^{18}O$ reversal event between 146.5 and 149.5 m of the ice core from the Guliya ice cap (Thompson et al., 1997). The proxy record from Lake Qinghai, however, provides no clear evidence for a return to cold climatic conditions during the Younger Dryas time. The increases of both carbonate production and organic productivity at ~10.7-10 ka ^{14}C BP indicate an intensified summer evaporation, which is distinctly different from the cold and arid period between ~14 and 11.6 ka ^{14}C BP when Lake Qinghai had low carbonate production and low organic productivity. The data suggest an abrupt increase in summer temperature at about 10.7 ka ^{14}C BP. If so, monsoon moist penetration to the N. E. Tibet-Qinghai Plateau then might lag behind the change of inland surface conditions for about seven hundred years. In other words, from about 10.7 ka ^{14}C BP the increased summer temperature, as a result of increased summer insolation and regional deglaciation, brought about the enhancement of summer evaporation and aridification of the lake, but a further enhancement of monsoonal rainfall did not come along until about 10 ka ^{14}C BP. Our results thus suggest a step-wise pattern of climatic change across the Late-Glacial/Holocene transition along with abrupt shifts in effective moisture on the N. E. Tibet-Qinghai Plateau.

5.6 Conclusions

A multi-proxy investigation of two sediment cores from the large closed-basin Lake Qinghai provides evidence of abrupt changes in paleolimnological conditions across the Late-Glacial/Holocene transition. The chronology of the lacustrine sediment sequence is framed by four AMS ^{14}C ages for aquatic-plant macrofossil seeds. Four distinct stratigraphic units are identified on the basis of abrupt shifts in lithology, carbonate composition, $\delta^{18}O$ of authigenic carbonates, magnetic susceptibility characteristics, and total nitrogen content. These units represent four environmental stages that were each initiated by three abrupt changes in hydro-climatic regime at ~11.6, 10.7 and 10 ka ^{14}C BP. Each of the four environmental stages thus represents a characteristic precipitation-to-evaporation balance for the lake catchment. The paleoenvironmental evidence indicates that the lake before 11.6 ka ^{14}C BP was very shallow with carbonate production and organic productivity much lower than in the Holocene, suggesting a much colder and drier

climate than in the Holocene. From ~11.6 to 10.7 ka ^{14}C BP, the presence of clastic laminations and *Ruppia* fossil seeds suggests an increased inflow of sediment-laden waters into the lake. Between ~10.7 and 10 ka ^{14}C BP, the development of a carbonate playa lake indicates that a negative water balance persisted. From ~10 ka ^{14}C BP an abrupt increase in rainfall is suggested by a sudden termination of the playa lake environment and the diluted lake waters, as evidenced by a negative shift in both total carbonate content and $\delta^{18}O$ values of mineral carbonate. However, the lake level during the early Holocene was about 20 m shallower than today, indicating that the effective moisture then was much lower than it is today. The step-wise pattern of climatic change across the Late-Glacial/Holocene transition along with abrupt shifts in P-E balance is characterized by reorganization of the Asian monsoon circulation. Probably this reorganization was determined by increasing summer insolation and changes in surface boundary conditions accompanying regional deglaciation on the N. E. Tibet-Qinghai Plateau. The arid event at ~10.7-10 ka ^{14}C BP is interpreted as a Younger Dryas equivalent, although climatic cooling is not indicated by the evidence at hand.

6 Paleoenvironmental signatures from carbonate minerals and stable isotopic ratios from Lake Qinghai

6.1 Introduction

The lake level and chemistry of hydrologically closed-basin lakes respond sensitively to changes in precipitation or precipitation minus evaporation (P-E) balance in their catchment basins (e.g., Street-Perrotte and Harrison, 1985). Many of such lakes with mesosaline water exist in semi-arid areas of the Tibet-Qinghai Plateau and Northwest China. Authigenic carbonates are common minerals present in the sediments of those lakes with pH over 8.5. Environmental information on past changes in water chemistry, lake level and P-E balance are recorded by carbonate minerals, biogenic carbonates, and their stable isotope ratios from the sedimentary sequence of the lakes (Kelts et al., 1989; Gasse et al., 1991; Lister et al., 1991; Yu et al., 1992; Fontes et al., 1993; Wei and Gasse, 1999; Yu et al., 2000; Yu and Kelts, 2002).

The bottom sediments formed in the profundal areas of Lake Qinghai contain about 30% authigenic carbonates, including aragonite, calcite and small amount of dolomite identified on smear-slides from a number of 1 m long cores (Lanzhou Institute of Geology et al., 1979). Drill cores at the lakeshore sites in the 1961-62 field investigations, however, failed to recover the Holocene calcareous succession of chemical sedimentation. A continuous profile in total carbonate content with 1 cm resolution was obtained from core Q14B, the 5.6 m long piston core recovered from the central southern basin in the 1985 Sino-Swiss Expedition to Lake Qinghai. It provided a sensitive proxy record, which has helped in the interpretation of the lake's chemical state in relation to several major environmental changes and subordinate chemical variations of the paleo-lake (Kelts et al., 1989; Lister et al., 1991). The record of carbonate mineral composition, alongside with that of total carbonate content (TCC) added more paleoenvironmental information such as on shifts in Mg/Ca ratio, carbonate alkalinity and salinity of the paleo-lake for the study of climatic change across the Late-Glacial/Holocene transition (Yu and Kelts, 2002). A study of carbonate mineral stratigraphy of the post-glacial sediment sequence will undoubtedly provide more detailed information on the brine evolution of the closed-basin lake and the corresponding paleoclimate conditions. This becomes one of the research foci of this chapter.

The Mg/Ca ratio of a perennial lake is considered to be one of the critical factors affecting carbonate mineral phase formed in the lake (Müller and Irion, 1972; Eugster and Kelts, 1985; Scoffin, 1987). Initially, Mg/Ca < 2: low-Mg-calcite; Mg/Ca = 2-7: Mg-calcite; Mg/Ca=7-12: Mg-calcite and protodolomite; Mg/Ca > 12: aragonite and possibly magnesite. The evolution of Mg/Ca ratio of the lake will be discussed on the basis of the carbonate mineral records of core Q14B investigated by the author.

Although lake systems are diverse and each may have its own fashion of dominant environmental controls on stable isotopic signals, covariance between $\delta^{13}C$ and $\delta^{18}O$ for primarily precipitated carbonates has been recognized to be an important isotopic characteristic of hydrologically closed-basin lakes (Talbot, 1990; Talbot and Kelts, 1990). Lake Qinghai, the largest waterbody in China with an area of 4437 km^2, has been a hydrologically closed-basin lake since at least the last Ice Age. The post-glacial sequence

revealed by two cores from central areas of the southern and eastern basins is an intact and continuous calcareous succession, from which four types of carbonate minerals are identified (Yu et al., 2000; Yu and Kelts, 2002). As such, carbonates from Lake Qinghai may provide ideal samples for testing the current hypothesis of isotopic covariance as a tool with great potential for paleohydrological analysis of ancient lacustrine basins.

Dolomite formation and dolomitization in sedimentary environments are subjects of long-standing interest (e.g. Last, 1990). The effort in dealing with the "dolomite problem", a centuries-old controversy, has carried over in the 21st century, and new scientific developments on the topic will further improve our understanding on the earth's geochemical cycles (McKenzie, 1991; Frisia, 1999a). Modern and Holocene dolomite occurs in many inland lacustrine settings, and lakes are ideal large-scale laboratories that permit detailed examination of many important aspects of dolomite formation (e.g. Last, 1990; Landmann et. al., 1996). However, among nearly 50 reported occurrences of non-detrital lacustrine dolomite of Quaternary age, only a few of these have been studied in detail, according to the overview by Last (1990), and most of the reported occurrences are located in Australia or North America, only one of which is from China (Chen and Bowler, 1986). Here in this chapter results from the study of non-detrital dolomite presented in both trapped sediments and the cored post-glacial sediment sequence of Lake Qinghai are reported. Geochemical conditions favourable for the formation of the lacustrine dolomite and the relevant environmental conditions of the paleo-lake are discussed.

In the following sections, the modern carbonate environments of Lake Qinghai including precipitation of primary carbonate minerals collected by sediment traps from the lake today will be introduced first. The presentation of carbonate mineralogical data will be followed by a discussion of the Lake Qinghai dolomite. Furthermore, the chemical evolution of the lake and paleoenvironmental implications are discussed based on the detailed mineralogical records from core Q14B. Sediment trap data presented in this chapter serve as modern analogues with salinities from fresh to mesosaline, which helped to improve our understanding of brine evolution drawn from the mineralogical record of the intact post-glacial sediment sequence. The study of stable carbon and oxygen isotopes in this chapter is focused on isotopic covariance and aims to deepen our understanding of the isotopic characteristic of a large closed-basin lake based on stable isotope results from samples with well-defined mineralogy.

6.2 Modern carbonate environments

The alkaline water of Lake Qinghai today with a Mg/Ca ratio of 62 is precipitating carbonate minerals, mostly aragonite. Along the eastern shores, Lake Qinghai has a number of partially or completely enclosed embayment such as Gahai, Haiyan Bay and Erhai. Each is restricted by sand bars, and has different depth ranges. Gahai and Erhai now are cut off from the main lake, but have once been joined. Each has different chemistry and precipitates of diverse carbonate minerals, including aragonite, calcite and dolomite. Hydromagnesite is found on the surface of the near-shore beach and shallow water sediments of Haiyan Bay, a bay almost cut-off in the eastern part of the lake. These peripheral lakes related to Lake Qinghai may provide potential reference systems to help in interpreting past states of the lake chemistry, levels and environments from the carbonate sequences formed since the post-glacial time. The margins of the modern lake do not have

evidence of coquinas or molluscan fauna remains in the littoral zone. Cobbles marking former shoreline commonly have crystal aragonite minerals on their surface, and beach rocks (Plate 6.1) have been forming along the western shore side of Erlangjian caped ridge, which are composed of sands cemented by aragonite. Calcareous tufas were dredged from various submerged ridges or rises, but their age of formation is uncertain.

Plate 6.1 Newly formed beach rocks are composed of well-rounded sands cemented by crystal aragonite needles.

Mineral carbonate precipitates were collected by sediment traps set at the depths of 6 m, 5 m and 1.2 m below the lake surface, respectively, in Lake Qinghai, Lake Gahai and Lake Erhai for three months from July-October in 1989 (Table 6.1). Total carbonate content of the trapped sediments is 20.8% from Lake Erhai, which is a fresh water lake with TDS 1.22 g/l, 53.9% from Lake Qinghai (TDS 14.39 g/l), and 63.6% from Lake Gahai (TDS 32.64 g/l). This indicates that the higher the water salinity among the three lakes, the more carbonate precipitates will be formed. A mixed carbonate mineral composition is identified by means of X-ray diffraction analysis with three or four types of carbonate minerals, namely aragonite, calcite, dolomite and hydromagnesite. For Lake Qinghai and Lake Gahai, aragonite is the main carbonate mineral precipitated from the water with the Mg/Ca ratios of 83-137. For Lake Erhai, the aragonite content in the trapped sediments is about 1.4 times more than calcite precipitated from the fresh water with a weight Mg/Ca ratio of 13 in the summer of 1989. More calcite than aragonite could be precipitated from the water of Lake Erhai when the weight Mg/Ca ratio is lower than 7, such as in 1963 (Lanzhou Institute of Geology et al., 1979). Small amounts of dolomite

were detected by X-ray diffraction analysis from the trapped sediments with 4.9% from Lake Qinghai and 8.9% from Lake Erhai, respectively. In comparison with Lake Qinghai and Lake Erhai, a relatively higher portion of primary dolomite was trapped from Lake Gahai with higher salinity (TDS 32.64 g/l) and Mg/Ca ratio (137), along with some hydromagnesite (12.1% relative to the TCC).

Table 6.1 Carbonate content and composition of trapped sediments from Lake Qinghai and two peripheral lakes (Lake Gahai and Lake Erhai)*

Lake	Depth of sediment trap (m)	Carbonate content (%)	Carbonate composition and contents relative to total carbonate content (%)				Water chemistry		
			Aragonite	Calcite	Dolomite	Hydro-magnesite	pH	TDS (g/l)	Mg/Ca#
Qinghai	6	53.9	66.2	28.9	4.9	0	9.11	14.39	98
Gahai	5	63.6	56.0	17	14.9	12.1	9.01	32.64	137
Erhai	1.2	20.8	52.5	38.6	8.9	0	9.46	1.22	13

*Data by courtesy of Prof. Gao, Salt Lake Institute, CAS.
#Weight ratio

6.3 Carbonate minerals in the sediment cores

In the sediments of Lake Qinghai, aragonite is the main carbonate mineral, 56% on average relative to TCC. Calcite averages about 25% and dolomite about 9% relative to TCC. Note that the ratio of aragonite:calcite:dolomite of the Holocene sediments is similar to that of the trapped sediments of today.

Light-colour laminae, present in the Holocene and more frequently in the early-Holocene sediments, are often made up mostly with chemically precipitated aragonite. The SEM photomicrograph of a carbonate lamina collected from core Q14B at Sect. 5/22.8-23 cm shows that needle-shaped aragonite crystals are 5-12 µm in length and 1-2 µm in width (Plate 6.2). These aragonite crystals are, by comparison, not as well crystallized as the aragonite needles (Plate 6.3) present as cement of the newly formed beach rocks. Low-Mg-calcite with 1-3 mol % $MgCO_3$ is present occasionally in the Holocene sediments of Lake Qinghai. High-Mg-calcite with 8-15 mol % $MgCO_3$ occurs only in the basal sediment interval of core Q14B, in which Mg-calcite accounts for more than 80% relative to the total carbonate content of about 30%.

Plate 6.2 SEM photomicrograph showing the needle-like aragonite
crystals of a carbonate lamina in the early-Holocene sediments.
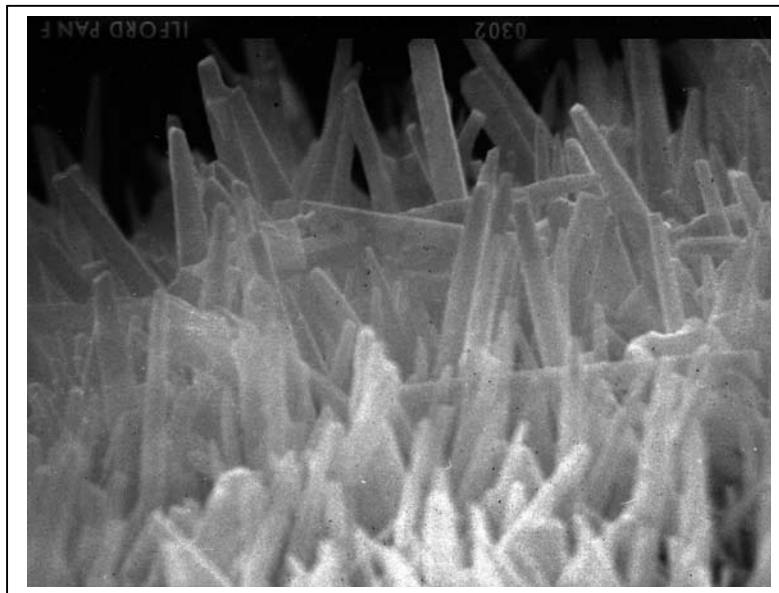
Plate 6.3 Crystal aragonite needles, SEM photomicrograph, present
on the surface of a sand grain from beach rocks (refer to Plate 6.1).
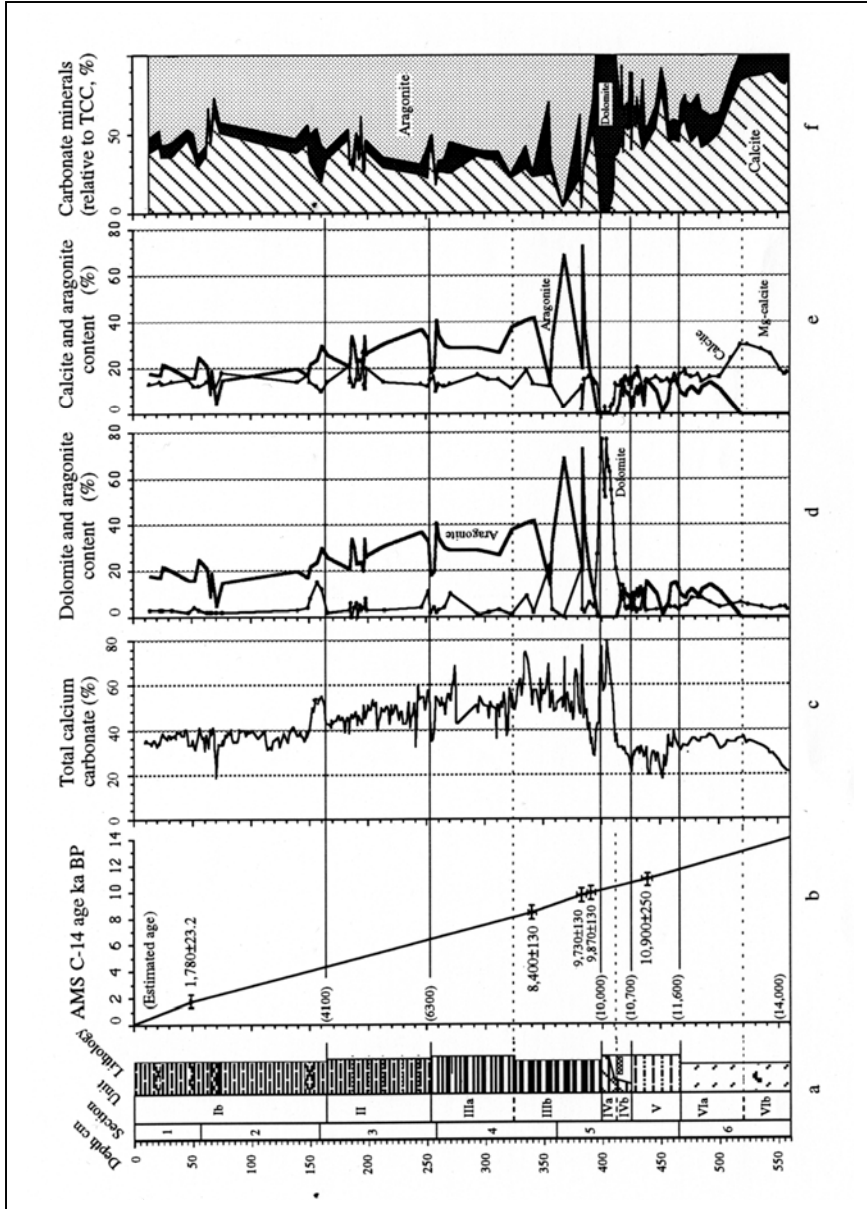
Figure 6.1 AMS ^{14}C dated carbonate mineral stratigraphy of core Q14B. Authigenic carbonate minerals in the post-glacial sediment sequence including aragonite, calcite and dolomite, which dominate the variations of total carbonate content (TCC) in the sediment profile. The pre-Holocene sediments of Units VI-IVb are characterized by calcite-dominated carbonate composition with lower TCC (20-40%), followed by a 13-cm dolomite layer (Unit IVa). Aragonite forms the dominant carbonate since the early Holocene, and TCC variations are determined by aragonite content.

6.3.1 Carbonate content and composition of core Q14B

Total carbonate content (TCC) ranges from 18-78% in the post-glacial sediments deposited in Lake Qinghai. The results of total carbonate content (TCC) and carbonate

mineral composition from core Q14B are shown in Figure 6.1. Unit VI, the basal sediment section of Q14B, is characterized by relatively low TCC (from 20% to 36%) dominated by calcite. High-Mg-calcite is the main carbonate composition in the subunit VIb. As TCC increases from 17% to 36%, a marked mineralogical change occurs at the boundary between Unit VIb and Unit VIa, from which high-Mg-calcite gives way to aragonite, though low-Mg-calcite is the dominant carbonate mineral in the subunit VIa through Unit V.

As coarser detrital material increases in Unit V, TCC decreases by about 11% in comparison with those in Unit VI. Three negative TCC excursions coincide with thin layers richer in detritus. Unit IV is characterized by light gray sediment with a massive texture, which differs from the underlying sediments with clastic laminations. An increase in TCC from 21-34% in the subunit IVb is followed by dolomite deposition in the subunit IVa (see Section 6.4.1).

A marked mineralogical change at the boundary between Unit IV and Unit III is shown by an abrupt cessation of dolomite deposition around 10 ^{14}C ka BP and a negative excursion of TCC at the base of the reddish-gray laminated sediments of the Holocene. The negative excursion of TCC within a cm sediment interval is followed by a sharp increase in aragonite composition from 9-69% in weight percentage. Both aragonite content and TCC are higher on average in Unit IIIb than in the sediment units above. Two thin layers with higher dolomite and lower aragonite content are present in the early-Holocene sediments of Unit IIIb. Five layers with carbonate concretions composed mainly of aragonite are present in the sediments of Unit IIIb.

6.4 Lake Qinghai dolomite and the related environmental conditions

6.4.1 Lithologic features, mineralogy, organic carbon and nitrogen, and isotopic composition

A dolomite layer 13 cm thick (Unit IVa) was deposited in the central southern basin at ~10.3-10 ^{14}C ka BP (Figure 6.2). It includes two bands. The lower band comprises massive, light-gray dolomitic mud in which the dolomite content increases upward from 21% to 77%. The upper band is a dolomite nodular layer 5-cm thick with 52-77% dolomite. The lithologic evidence indicates in-situ deposition of the dolomite layer.

X-ray diffraction analysis shows that stoichiometric dolomite has a d(104) value of 2.884 Å. The dolomite concretions of Lake Qinghai have a d(104) value of 2.901 Å, indicating that they are nonstoichiometric dolomite, containing excess calcium. The SEM photomicrograph of the dolomite concretion (core Q14B at Sect.5/39-40 cm, Plate 6.4) shows that the dolomite is euhedral and present as spherical aggregates, 3-5 μm in diameter. The dolomite aggregate includes fine rhombohedral crystals of less than 1 μm, which differ completely from other carbonate mineral forms such as needle-shaped aragonite.

Prior to the deposition of the dolomite layer, the total organic carbon (TOC) and total nitrogen (TN) increase gradually in the sediments of Unit IVb and reach a high content in a dark band on top of Unit IVb (Figure 6.2). The TOC and TN content then turned to decrease as dolomite content began to increase. The δ^{18}O values of the dolomite samples increase along with an increase in dolomite content, whereas δ^{13}C values of the dolomite

turn to be more negative. Note that the stable isotopic ratios of aragonite samples from Unit IIIb clearly show positive correlation between $\delta^{13}C$ and $\delta^{18}O$.

6.4.2 Geochemical and paleoenvironmental conditions of dolomite formation

A relatively small portion of dolomite, usually 2-9% along with other carbonate
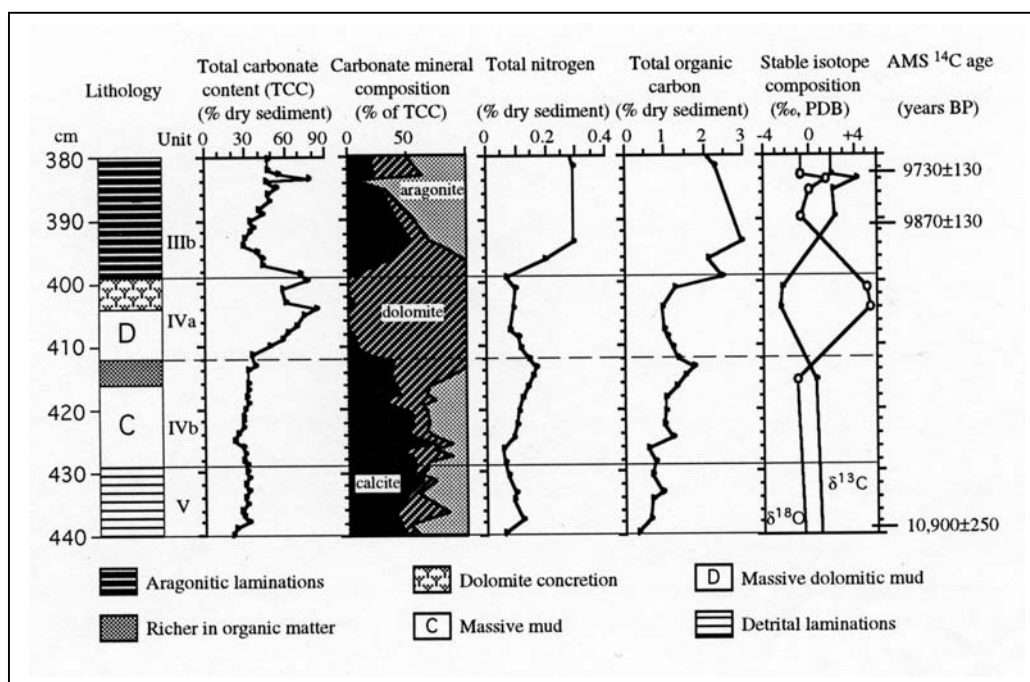
Figure 6.2 Lithological, mineralogical, geochemical and stable isotopic records for dolomite section in core Q14B. The dolomite deposition was preceded with a substantial increase in TOC and TN. The increase of dolomite content was accompanied by a decrease in TOC and TN. The dolomite has distinctly negative $\delta^{13}C$ values as an isotopic characteristic distinguishable from other authigenic carbonate minerals.
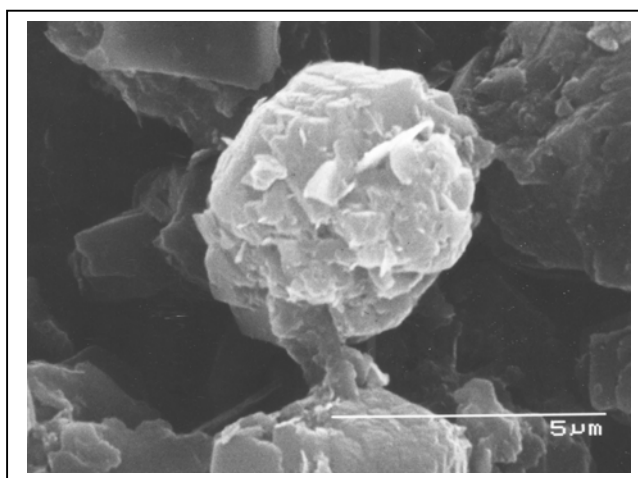
Plate 6.4 SEM photomicrograph of a spherical aggregate of the Lake Qinghai dolomite, which includes euhedral rhombohedra-like crystals.

minerals, is present in the trapped sediments of Lake Qinghai as well as in the post-glacial sediments. As shown in Table 6.1, the dolomite precipitation today occurs also in Lake Gahai from which the amount of dolomite formed is three times higher than that of Lake Qinghai. Note that there is no river inflow into the higher salinity waters of Lake Gahai. Evidently, the 2-8% dolomite in the post-glacial sediments was formed directly from the paleo-lake at various salinities.

Lake Qinghai and its peripheral lakes, however, provide no modern analogue for the dolomite deposition of Unit IVa in core Q14B. Based on the results afore-presented, the following factors appear to be important in promoting the dolomite deposition in the paleo-lake: 1) high evaporative concentration of the brine, 2) increased organic productivity and anoxic conditions, 3) suitable Mg/Ca ratios, usually 7-12, and 4) a very shallow to nearly desiccated lake environment.

The distinctly negative values of $\delta^{13}C$ of the dolomite, unlike those of the aragonite that are positively correlated with $\delta^{18}O$, provide isotopic evidence of a partial incorporation of ^{13}C-depleted carbon from decomposition of organic matter into the dolomite. In the case of Lake Qinghai, this process requires increasing organic productivity for the source of organic matter and anoxic conditions for OM decomposition. A substantial increase in organic productivity before the deposition of the dolomite layer is evidenced by marked increase in both TOC and TN as C/N ratio is around 10 (Figure 6.2). The fact that the increase of dolomite content corresponds with the decrease of TOC and TN reflects the existence of the decomposition of organic matter.

Before the dolomite deposition, Lake Qinghai was only a few meters deep (refer to Chapter 5.3). A negative water balance and evaporative concentration led to a gradual increase in TCC in Unit IVb and a sharp increase in dolomite content in Unit IVa. Apparently, sharply increased alkalinity and highly supersaturated brine provided a fundamental cause of the dolomite deposition in a very shallow lake. Under the circumstances, two other factors are decisive of promoting dolomite deposition rather than forming other carbonate minerals. One is the increase of organic productivity and the development of anoxic conditions. Another is the Mg/Ca ratio of the paleo-lake.

The Mg/Ca ratio of the lake water may have played an important role in the formation of the Lake Qinghai dolomite (refer to Section 6.5.2.1). Mineralogical results from the examination of the annually trapped sediments clearly indicate that under the current conditions of high Mg/Ca ratios of 62-83, aragonite is the main carbonate mineral precipitating from the lake, although the precipitated carbonate minerals include 3-9% of primary dolomite. Such high Mg/Ca ratios also favour the precipitation of magnesite rather than dolomite (Scoffin, 1987). The fact that hydromagnesite has precipitated today on the shallow water area of Haiyan Bay seems to confirm that a persistent precipitation of dolomite is unlikely to occur if Mg/Ca ratios become too high.

6.5 Brine evolution as deduced from the carbonate mineral record

6.5.1. Mg/Ca ratio

The weight Mg/Ca ratios of Lake Qinghai today are as high as 62-83, which creates conditions favourable for aragonite precipitation. Such high values in Mg/Ca ratio reflect a

long-term deposition of aragonite in the lake because magnesium ions remained in the lake water as calcium ions were removed from the waters with the precipitation of aragonite and calcite. As shown in Figure 6.1f, aragonite turned to be the dominant carbonate phase at the onset of Unit III. This suggests that Mg/Ca ratios were higher than 12 since ~10 ka BP and thereafter the ratios increased progressively to the present high values.

During the deposition of Unit VIb the Mg/Ca ratio of the hydrologically closed lake was probably only around 7, as indicated by the Mg-calcite dominated carbonate mineral composition. A mineralogical change at the boundary between Unit VIb and Unit VIa from a Mg-calcite dominated phase to a phase of calcite and aragonite may indicate a critical change in Mg/Ca ratio of the waters, from which a ratio slightly higher than 12 might occur. In the southern basin waters, the Mg/Ca ratios did not increase substantially during the deposition of Unit V and Unit IVb because a Mg/Ca ratio of around 12 would favour the followed dolomite formation (Unit IVa) in addition to other geochemical conditions required.

The persistent precipitation of aragonite since the early Holocene has led to the enrichment of Mg^{2+} in Lake Qinghai and, as a consequence, Mg/Ca ratio has reached high values of 62-83. Apparently, Mg^{2+}, identified as the most significant inhibitor of aragonite dissolution and calcite precipitation in seawater (Morse, 1983; Carlson, 1983), is as well the chemical species, which favours the precipitation of aragonite. It also inhibits the aragonite to calcite transformation in Lake Qinghai. This is in accord with results from a series of kinetic experiments (Bishoff and Fyfe, 1968; Bishoff, 1968).

The mineralogical data of sediment traps from Lake Qinghai and two peripheral lakes confirm that Mg/Ca ratio plays an important role in determining which carbonate mineral is the dominant precipitate from the water, and that abundant Mg^{2+} may have assisted preventing aragonite, usually a metastable form of $CaCO_3$, from transformation to calcite. The fresh waters of Lake Erhai usually produce calcite. But in 1989, aragonite turns to be the dominant carbonate precipitate, accounting for 52.5% relative to the TCC of 20.8% in the trapped sediments, as Mg/Ca ratio has approached 13. Abundant aragonite was precipitated from Lake Qinghai, accounting for 35.7% in weight percentage of the trapped sediments, as Mg/Ca ratio of the brackish water reached 98 in the summer of 1989. However, the co-existing calcite and dolomite in the trapped sediments, mandates a consideration of other factors controlling the formation of a mixed precipitates of three carbonate minerals other than Mg/Ca ratio during the trapping period from July to October. Involvement of organic carbon from degraded aquatic plants could catalyze dolomite precipitation from the alkaline water with high Mg/Ca ratio, as discussed in Section 6.4. It seems certain that kinetic factors and biological processes play a major role in controlling the precipitation processes (Frisia, 1999).

To sum up, the carbonate mineral record of Q14B provides evidence for reconstructing a brief history of the lake's Mg/Ca ratios in the past 14 ka. The Mg/Ca ratio was about 7 during the deposition of Unit VIb. It increased to 12-13 during the deposition of Unit VIa to Unit IVb. During the formation of the dolomite layer (Unit IVa) the Mg/Ca ratio was around 12. From the onset of the Holocene, the Mg/Ca ratio of the lake turned to be higher than 13, and the persistent precipitation of aragonite and calcite thereafter led to a progressive increase of the ratio, reaching the high values of 62-83 of today.

6.5.2 Carbonate production and salinity

Mineralogical data from both trapped sediments (Table 6.1) and core Q14B (Figure 6.1) indicate that TCC largely reflects past changes in carbonate production, which is related to the carbonate alkalinity of the mesosaline water and to the amount of Ca-input by rivers and rainfall, provided that other factors, such as variations in detrital influx and biogenic ostracod shells, have little effect on the variations of TCC.

The calcite shells of Ostracoda are present throughout the post-glacial sediment sequence of core Q14B. They contribute to the total calcite content of the sediments but the contribution is minor in comparison with the calcite component chemically precipitated from the lake water. This is judged from the following facts. Ostracod shells are sparsely present in the basal sediments (Lister et al., 1991) of Unit VIb, in which an increase in calcite content is obviously not related to ostracod shells, but resulted from an increase in Mg-calcite (Figure 6.1e). Ostracod shells are relatively abundant in the sediments of Unit III, but the calcite contents of the bulk sediment samples are basically the same as those of the Holocene sediments. Clearly, apart from some 2-3 mm thin laminae with abundant ostracod shells, variations in calcite content of the bulk sediments are predominantly caused by chemically precipitated calcite, and the contribution of the minor portion from the calcite shells of ostracoda to the calcite content profile (Figure 6.1e) can be considered to be homogeneous.

The effect on the TCC variation in the Holocene sequence by changes in detrital influx is considered to be insignificant because the site of core Q14 is at the center of the post-glacial deposition and the sedimentation regime has not changed since at least the beginning of the Holocene.

The TCC curve and the carbonate mineral records hence provide an indication of carbonate production of the paleo-lake. They allow us to evaluate the past changes in the lake's alkalinity and related salinity. Carbonate production during the deposition of Unit VI, Unit V and Unit IVb was much lower than that during the Unit III deposition, suggesting that the alkalinity of the lake at about 14-10.5 ka BP was much lower than during the early Holocene. This interpretation is supported by evidence from diatoms in the sediments. Diatoms are abundant in Lake Qinghai today but are not preserved in the sediments throughout the Holocene sequence. Diatom species were however preserved in the sediments of Unit VI and Unit V (diatom analysis by Fritz, S.C.). Lower alkalinity of the lake is apparently the prerequisite conditions preventing fossil diatoms from dissolution and thus for the preservation of diatoms in the sediments. According to Barker (1992), fossil diatoms could not be preserved in the sediment intervals formed under the conditions with a pH value of the water higher than 9 due to selective chemical dissolution. The evidence from both carbonate stratigraphy and fossil diatom lead us to conclude that during the deposition of Units VI, V and IVb, both salinity and alkalinity of the paleo-lake were much lower than today with a pH value slightly lower than 9.

The deposition of dolomite during the highest TCC (Unit IVa) in the record represents the highest alkalinity of the paleo-lake in the past 14 ka BP, indicating a negative P-E water balance for about 300 years due most likely to abruptly enhanced summer evaporation (Yu and Kelts, 2002). The dolomite deposition ceased abruptly around 10 ka BP, which is followed by a negative excursion in TCC and a mineralogical change to a calcite

dominated carbonate phase. This represents a marked change of the brine, which was diluted critically by abruptly enhanced water inflow. The average TCC of Unit IIIb is around 50%, which is about 15% more than that of Unit I. This implies that the carbonate alkalinity of the paleo-lake during the deposition of Unit IIIb was much higher than during the last 4 ka BP, probably higher than that of Lake Gahai today, as suggested by the TCC data.

Carbonate production at ~8-4 ka BP, mainly due to higher aragonite production, was higher than during the late Holocene, implying that carbonate alkalinity of the lake during the mid-Holocene was higher than during the late Holocene. This must have caused by a higher alkalinity and a higher rate of carbonate production, as evidenced by mineralogical data of sediment traps in the three lakes with different alkalinity. Some marked changes in TCC in the past 14 ka BP largely reflect major fluctuations in alkalinity of the paleo-lake, as well as in salinity. Such a relationship between carbonate alkalinity and salinity has also been suggested for highly alkaline Mono Lake (Oxburgh et al., 1991).

6.6 Stable isotope ratios and their covariance

6.6.1 Isotopic covariance

From reviewing the data of stable carbon and oxygen isotope composition in primary carbonate minerals from a number of lacustrine sequences, Talbot (1990) has proposed that a δ^{13}C-δ^{18}O covariance with a high correlation coefficient is a characteristic feature, which can be used for evaluating whether an ancient lacustrine basin was hydrologically closed or not. Lakes with outlets and relatively short residence time, i.e. hydrologically open lakes, often have a narrow range of δ^{18}O close to that of the bulk isotopic composition of inflow waters. Primary carbonates precipitated from open-lakes show only small variations in δ^{18}O within each basin and their isotopic ratios show little or no correlation between δ^{13}C and δ^{18}O, example of this behaviour are among others, Lakes Henderson (Stuiver, 1970), Greifensee (McKenzie, 1985), and Huleh (Stiller and Hutchinson, 1980). The small variations in δ^{18}O probably reflect minor oscillations in temperature and inflow-evaporation balance between periods of carbonate precipitation. For some open-lakes with relatively long residence times, the isotopic ratios of the carbonates may display covariance but the correlation between δ^{13}C and δ^{18}O is poor and the correlation coefficient is less than 0.7 (Talbot, 1990), e.g. Lobsigensee (Siegenthaler and Eicher, 1986) and Little Lake (Turner et al., 1983).

Hydrologically closed lakes lack surface outlets and evaporation causes oxygen isotope composition to become heavier than that of inflows. One feature common to closed-lake carbonates, and a contrast to those from most open-lakes, is the relatively large variation in δ^{18}O within each basin largely because the inflow-evaporation balance, which dominates the isotopic evolution of closed-lakes, is subject to the changes of hydro-climatic conditions. Temperature effects, which influence both the oxygen isotopic composition of rainfall (and thus that of lake inflows), and isotopic fractionation during carbonate precipitation are apparently of secondary importance in closed lakes and are generally masked by evaporative- and residence-related effects (Stuiver, 1970; Gat, 1981; Gonfiantini, 1986; Talbot, 1990). Closed-lake carbonates show a highly correlated covariance between δ^{13}C and δ^{18}O, as shown by the data from modern closed lakes (Fig. 1

in Talbot, 1990). Shifts to more positive $\delta^{13}C$ with increasing evaporative evolution of the water body may be attributed to the preferential outgassing of ^{12}C-rich CO_2 from lake surface to the atmosphere and to changes in primary productivity (McKenzie, 1985). Paleolimnological characteristics of covariant trends and their possible applications for the paleohydrological interpretation of closed basins were concluded by Talbot (1990) as follows: 1) a covariant trend defines a unique isotopic identity of each closed lake, which is a function of the basin's geographical and climatic setting, its hydrology, and the history of the waterbody, 2) within individual basins, covariant trends may have remarkable long-term persistence despite major environmental changes, indicating considerable stability in basin hydrology, 3) any major interruption or realignment of this trend reflects a fundamental change in basin hydrology, 4) covariant trends may be used for correlation purposes, to confirm hydrological connection between basins, and segmentation of basins for tectonic or other reasons.

The compiled data of carbonate stable isotopic records from a number of lacustrine settings has originated a very useful isotopic probe of $\delta^{13}C$-$\delta^{18}O$ covariance for paleohydrological analysis. Further studies are however needed to pursue a better understanding on causal mechanism of $\delta^{13}C$-$\delta^{18}O$ covariance. Meanwhile, new questions arise such as why for the case of Mono Lake the isotopic ratios of the carbonates precipitated during some of the time intervals on the time scales of 60-1400 years of the Holocene show poor $\delta^{13}C$-$\delta^{18}O$ covariance or even no covariance, although the whole sets of the isotopic ratios of the Holocene carbonate samples show fairly good covariance with r = 0.76 (Li and Ku, 1997). The authors suggest that $\delta^{13}C$-$\delta^{18}O$ covariance usually occurs in lake sediments under the condition of hydrological closure for time periods of 5000 years or longer, while breakdowns of the covariance in shorter terms may indicate 1) rapid lake level transgressions (strong covariance) or stable lake-level conditions (absent or poor covariance), and 2) variations in alkalinity (and salinity) because a high ΣCO_2 and carbonate alkalinity impede the $\delta^{13}C$ shift and $\delta^{13}C$-$\delta^{18}O$ covariance.

6.6.2 Isotope results from Lake Qinghai

Carbonate samples selected for stable isotope analysis include: 1) aragonite laminae indicating an isotopic signal parallel to one year or seasonal mean of the ambient waters, 2) bulk aragonitic samples of 1 cm core slices, representing a 20-year mean isotopic signal, 3) bulk calcitic sample of 1 cm slices, and 4) bulk dolomitic samples of 1 cm slices. Table 6.2 shows the data of the stable isotope analyses for all samples available selected from cores Q14B and Q16C. Figure 6.3 (I) shows the data points from Q14B as scatter plots of $\delta^{13}C$ versus $\delta^{18}O$. The sample of aragonite lamina at 22.8-23 cm in Section 5 (Plate 6.2) shows the highest $\delta^{13}C$ value at 4.236‰. Two dolomite samples show the most negative values in $\delta^{13}C$ of all carbonate samples. Bulk aragonitic/calcitic/Mg-calcitic samples display highly correlated covariance between $\delta^{13}C$ and $\delta^{18}O$, except for two samples 14-1 and 14-2, which contain 44% and 12% dolomite relative to TCC, respectively. Stable isotope data from core Q16C exhibit the same characteristics, as shown in Figure 6.3 (II). Sample 16-1, deviating from the isotopic covariant trend, contains 19% dolomite relative to the TCC. The isotopic ratios of all samples selected from the two cores are plotted in Figure 6.3 (III). For the samples 14-1, 16-1 and 14-2, the more dolomite the bulk carbonate sample contains, the larger deviation from the isotopic covariant trend the isotopic ratio is shown.
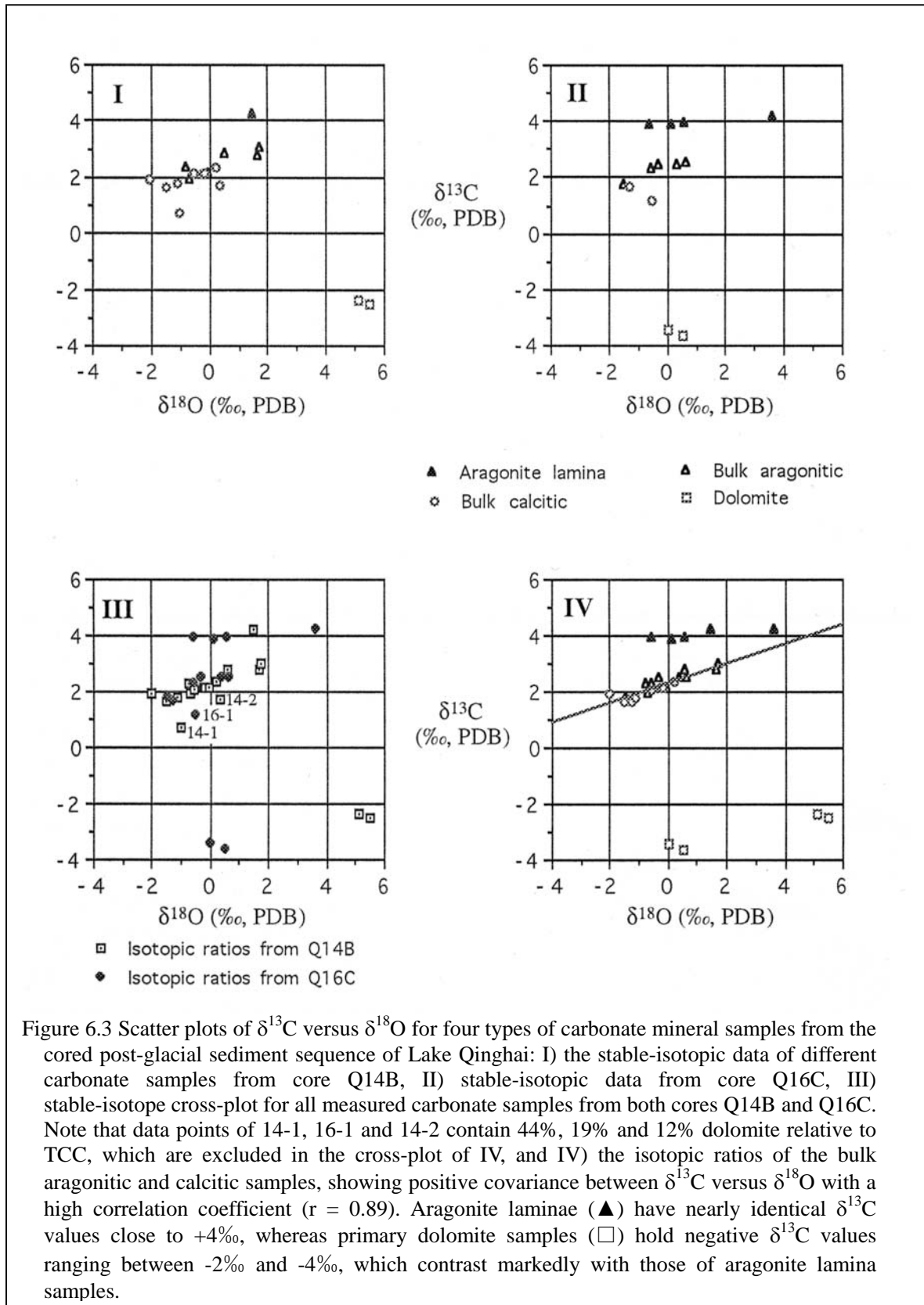
Figure 6.3 Scatter plots of $\delta^{13}C$ versus $\delta^{18}O$ for four types of carbonate mineral samples from the cored post-glacial sediment sequence of Lake Qinghai: I) the stable-isotopic data of different carbonate samples from core Q14B, II) stable-isotopic data from core Q16C, III) stable-isotope cross-plot for all measured carbonate samples from both cores Q14B and Q16C. Note that data points of 14-1, 16-1 and 14-2 contain 44%, 19% and 12% dolomite relative to TCC, which are excluded in the cross-plot of IV, and IV) the isotopic ratios of the bulk aragonitic and calcitic samples, showing positive covariance between $\delta^{13}C$ versus $\delta^{18}O$ with a high correlation coefficient (r = 0.89). Aragonite laminae (▲) have nearly identical $\delta^{13}C$ values close to +4‰, whereas primary dolomite samples (□) hold negative $\delta^{13}C$ values ranging between -2‰ and -4‰, which contrast markedly with those of aragonite lamina samples.

Table 6.2 The oxygen and carbon isotopic composition of different types of carbonate

samples selected from the sediment cores of Q14B and Q16C.

No.	Core/Sect.	Depth interval (cm)	$\delta^{18}O$ (‰, PDB)	$\delta^{13}C$ (‰, PDB)	Dominant carbonate mineral / type / % relative to total carbonate content (TCC)	TCC (%)
315	Q14B/5	39.5-40	5.11	-2.37	Dolomite / bulk / 100%	77.0
316	Q14B/5	42.7-43.2	5.47	-2.51	Dolomite / bulk / 100%	77.0
202	Q16C/5	27.4-28	0.50	-3.68	Dolomite / bulk / 87%	67.5
213	Q16C/5	28-28.5	0.03	-3.46	Dolomite / bulk / 80%	66.4
405	Q14B/5	22.8-23	1.47	4.24	Aragonite / lamina / 90%	78.0
205	Q16C/2.1	15	3.64	4.18	Aragonite / lamina / >80%	
8	Q16C/3	63.5	1.20	3.87	Aragonite / lamina / >80%	
204	Q16C/4	59	0.15	3.89	Aragonite / lamina / >80%	
203	Q16C/4	89	-0.58	3.90	Aragonite / lamina / 100%	98.7
2	Q16C/5	3.6	0.61	3.94	Aragonite / lamina / 87%	82.7
403	Q14B/1	22-23	1.73	3.02	Aragonite / bulk / 53%	33.0
404	Q14B/3	7.3-8	1.64	2.79	Aragonite / bulk / 61%	42.0
402	Q14B/4	3-4	0.56	2.81	Aragonite / bulk / 68%	50.0
215	Q14B/5	21.8-22.4	-0.68	1.92	Aragonite / bulk / 38%	54.0
216	Q14B/5	24-25	-0.03	2.12	Aragonite / bulk / 68%	53.0
217	Q14B/5	28.2-29	-0.76	2.32	Aragonite / bulk / 47%	42.0
106	Q16C/4	74-75	-0.28	2.47	Aragonite / bulk / 88%	69.1
214	Q16C/5	34-35	-0.53	2.28	Aragonite / bulk / 50%	42.5
206	Q16C/5	36-37	0.67	2.50	Aragonite / bulk / 71%	57.5

Table 6.2 continued

No.	Core/Sect.	Depth interval (cm)	$\delta^{18}O$ (%, PDB)	$\delta^{13}C$ (%, PDB)	Dominant carbonate mineral / type / % relative to total carbonate content (TCC)	TCC (%)
212	Q16C/5	37-38	0.37	2.47	Aragonite / bulk / 68%	55.0
307	Q14B/6	15-16	-1.49	1.66	Calcite / bulk / 54%	32.0
306	Q14B/6	35-36	0.20	2.33	Calcite / bulk / 45%	36.0
305	Q14B/6	43-44	-1.11	1.78	Calcite / bulk / 51%	31.0
409	Q16C/6	47-48.5	-1.29	1.65	Calcite / bulk / >50%	27.6
16-1	Q16C/5	85.3-85.4	-0.51	1.15	Calcite / bulk / 45%	31.0
14-2	Q14B/6	8.5-10.5	0.33	1.69	Calcite / bulk / 30%	30.0
14-1	Q14B/5	54-54.5	-1.04	0.70	Dolomite/ bulk/ 44% (calcite 38%)	31.0
218	Q14B/6	61-62	-0.15	2.13	Mg-calcite / bulk / 83%	36.0
219	Q14B/6	87-88	-0.54	2.10	Mg-calcite / bulk / 89%	29.0
220	Q14B/6	95-96	-2.02	1.92	Mg-calcite / bulk / 82%	23.0

These three samples are not used for calculating correlation coefficient of isotopic covariance because of the obvious effect of the distinctly negative value of the dolomite.

As resulted from the regression equation $\delta^{13}C = 2.3178 + 0.3514 * \delta^{18}O$, all isotopic ratios from bulk aragonitic and calcitic samples display a strong covariance between $\delta^{13}C$ and $\delta^{18}O$ with a correlation coefficient r = 0.89 (Figure 6.3 IV). Carbonate samples from aragonite laminae show a nearly identical $\delta^{13}C$ value of 4.0±0.24‰, while their $\delta^{18}O$ values vary. The $\delta^{13}C$ values of dolomite samples range from –2.37‰ to –3.68‰. These $\delta^{13}C$ values are in sharp contrast to those from aragonite laminae, showing distinctly negative values.

6.6.3 Discussion

Stable isotope data from lacustrine dolomite or dolomitic samples usually are not included for the study of isotopic covariance (Talbot, 1990) because of the uncertainty about the formation of primary dolomite in lacustrine environments (Talbot and Kelts, 1986). In the case of Lake Qinghai, the main reason that the dolomite isotope ratios are excluded from the covariant trend is because all dolomite samples have the $\delta^{13}C$ values distinctly negative than those of other primary carbonates, despite a large variation in their

$\delta^{18}O$ values (0.03 to 5.47‰). This might be caused by the incorporation of ^{13}C-depleted CO_2 from the degradation of aquatic plants during the dolomite formation, as suggested by our stratigraphic records (Figure 6.2). A caution must be taken for carbonate samples containing such type of dolomite, giving rise to an influence on the study of isotopic covariance. The extent of the influence depends upon the amount of the dolomite involved. This type of dolomite could be formed in many other closed-basin lakes with mesosaline to hypersaline water chemistry. The carbonate samples mixed with substantial amount of dolomite, such as the samples 14-1, 16-1 and 14-2, should not be included in calculating the correlation coefficient of an isotopic covariant trend. Our data clearly indicate that it is extremely important to obtain detailed mineralogical information for each carbonate samples used for isotopic analysis.

The isotopic ratios of all aragonite lamina samples selected from the Holocene sediments show the most positive $\delta^{13}C$ values (nearly identical to +4‰), while the $\delta^{18}O$ values are widely spread. This clearly indicates that not all endogenic carbonates show the characteristics of covariance between $\delta^{13}C$ and $\delta^{18}O$. The white aragonite laminae, easily visible on core photographs, are direct precipitates from the surface layer. They were formed in summer probably representing whiting, triggered either by intense evaporation or photosynthetic activity of phytoplankton. Four of the five aragonite-laminae samples were selected from the early-Holocene sediments (averaging TCC higher than 50%). The occasional occurrence of aragonite laminae was relatively frequent during the early Holocene when salinity and carbonate production of the lake was higher than in the middle to late Holocene. The average $\delta^{13}C$ value (4.00±0.24‰) of aragonite lamina samples is 0.98-2.35‰ higher than the $\delta^{13}C$ values of the bulk carbonate samples and 6.37-7.68‰ higher than those of the dolomite samples. Under isotopic equilibrium with atmospheric CO_2 (normally -7‰ in $\delta^{13}C$), $\delta^{13}C$ of the calcium carbonate precipitated from a lake would in principle have a value of about +3‰ because calcium carbonate is enriched in ^{13}C by about 10‰ at 20°C relative to CO_2 gas by carbon isotope fractionation in the CO_2 (gas)–carbonate ion (aqueous)–(solid) $CaCO_3$ system (Faure, 1977). The $\delta^{13}C$ values of the bulk $CaCO_3$ samples, ranging between 1.66‰ and 2.80‰, which covary very well with $\delta^{18}O$ values, represent the carbon isotopic identity of Lake Qinghai of the past 14 ka BP. The $\delta^{13}C$ is a function of a number of factors such as $\delta^{13}C$ values of the bicarbonate and carbonate ions, organic productivity, and invasion of atmospheric CO_2 etc. One of the reasons causing the $\delta^{13}C$ of the aragonite lamina samples to be 0.98-2.35‰ higher than those of the bulk samples is the higher amount of atmospheric CO_2 invasion. In other words, the $CaCO_3$ of the laminae were formed in equilibrium with atmospheric CO_2. The aragonite laminae formed in this scenario however can not in principle have $\delta^{13}C$ value higher than +3‰. Another reason causing $\delta^{13}C$ value of aragonite laminae to have reached values as high as 3.88-4.24‰ is photosynthetic activity. It preferentially takes up isotopically light CO_2, which leads to an enrichment in $\delta^{13}C$ of the dissolved inorganic carbon in the surface water, from which aragonite in the white laminae were nucleated. The aragonite laminae occasionally present in the early-Holocene sediments were likely formed by whitings, representing an isotopic signal of the surface water lasting only a few weeks. Their $\delta^{13}C$ values are the result of a relatively strong modification by photosynthetic activities during summer, whereas the $\delta^{13}C$ values of the bulk samples (each representing 10-20 years mean isotopic signal) include contributions from carbonate precipitates

chemically formed at different depths during all seasons of the lake.

The isotopic ratios of all 19 bulk $CaCO_3$ samples correlate with r = 0.9 (13 from core Q14B and 6 from core Q16C), even though the two cores are located at different basin centers 40 km apart. This provides a good example validating the hypothetic application of the covariant trend to the paleohydrological analysis of an ancient lacustrine basin. In other words, such a single covariant trend for the samples from two sections of an ancient closed lacustrine basin defines a spatial continuity of the deposition in the same waterbody (Talbot, 1990).

The isotope covariant trend of Lake Qinghai shows a long-term persistency over the past 14 ka at least, despite marked changes in lake-level and paleolimnological conditions induced by climate changes. The magnitude of lake-level fluctuation was about 30 meters, including the fluctuations from near desiccation to less than eight meter deep across the late-glacial/Holocene transition (Yu and Kelts, 2002) and the gauged variations of about 3 meters in the past 46 years. A short-term disconnection of the eastern basin with the southern basin during 10.3-10 ka BP, when the lake level was occasionally down to less than two meters deep (Yu et al., 2000), has not resulted in the breakdown of the persistent covariant trend. Differences in carbonate mineralogy between sediment units, such as the calcite and Mg-calcite dominated phase of Unit VI and aragonite dominated phase of Unit III through Unit I, provide no effect on the persistency of the single covariant trend. The interval of dolomite deposition did not cause any effect either.

Some further paleoenvironmental signals may be recorded in the isotopic trend. The isotopic ratios of calcite or Mg-calcite dominated samples plot on the negative side of the regression line (Figure 6.3IV). This carbonate phase was formed in a shallow lake environment when salinity, carbonate production and organic productivity were all low (Yu and Kelts, 2002). Three aragonitic samples from the mid to late Holocene sediments deposited in a much deeper lake environment similar to that of today show isotopic ratios near the positive end of the regression line. This suggests that isotopic ratios do not record only lake-level history; rather, they reflect a general trend of isotope composition of the lake water. Because the $\delta^{18}O$ of closed-basin lakes is mainly controlled by the P-E balance, the relatively negative $\delta^{18}O$ values of the pre-Holocene calcitic samples resulted most probably from very low evaporation due to longer winters and cooler summers, even though the effective moisture (P-E) at that time was lower than that of the mid to late Holocene. The reason that $\delta^{13}C$ values of calcitic samples are overall lower than those of the mid to late Holocene is a lower productivity, as indicated by TN, TOC and C/N ratio (Yu and Kelts, 2002). The Lake Qinghai data thus suggest that the isotopic ratios of bulk calcium carbonate samples formed during lower salinity and lower productivity occupy the negative end of the $\delta^{13}C$-$\delta^{18}O$ regression line.

The isotopic ratios of all carbonate samples shown in Figure 6.3 (III) would be considered as $\delta^{13}C$-$\delta^{18}O$ invariant if all the ratios were used for linear regression with no consideration of mineralogical differences in type and origin. Even if the isotopic ratios of dolomite were discarded, the correlation coefficient r would still be less than 0.7, although the isotopic ratios are all from carbonate samples of primary origin. To avoid any misinterpretation on isotopic records in terms of paleohydrological history of a lacustrine basin, each isotopic sample therefore must be characterized mineralogically.

6.7 Summary and conclusions

Post-glacial core composition and sediment trap data show that Lake Qinghai has produced a mixed facies of primary aragonite, calcite and dolomite. Aragonite has been the main carbonate composition in the Holocene sediments, along with calcite and small amounts of dolomite. The proportions of aragonite:calcite:dolomite were within the range of those of the trapped sediments. The Mg/Ca ratio in the $CaCO_3$ supersaturated water has been identified as one of the key kinetic factors determining which carbonate mineral phase forms in the lake.

Dolomite present in amount of 4.9-14.9% precipitates today directly from the alkaline waters of Lake Qinghai and two other peripheral lakes. A deposition event of nearly pure dolomite occurred near the onset of the Holocene. The 13 cm thick calcian dolomite layer was formed under specific environmental conditions in the central southern basin of the lake. Based on the data from petrographic, geochemical and stable isotopic investigations on the fine-grained dolomite, a very shallow lake or a carbonate playa environment with sharply increased alkalinity is one of the prerequisite conditions. A Mg/Ca ratio around 12 and an involvement of organic carbon derived from the decomposition of aquatic plants are two other kinetic factors triggering or catalyzing the precipitation of the dolomite.

The carbonate phase of the pre-Holocene sediments deposited prior to the dolomite deposition is dominated by calcitic mud with TCC (20-36%). This is much lower than that of the Holocene sediments. A threshold change in Mg/Ca ratio, presumably from 8 to 12, occurred at about 13.3 ^{14}C ka BP, as suggested by a shift in carbonate composition at the Unit VIb/Unit VIa boundary from Mg-calcite to aragonite. The sediment evidence of lower TCC, calcitic-dominated mineral phase, and well preserved fossil diatoms all point to a lower alkalinity prior to the dolomite deposition. Most likely, the pH of the paleo-lake was slightly lower than 9.

The deposition of the 13 cm thick primary dolomite represents the most arid phase of the calcareous succession formed in the past 14 ka. The geochemical and environmental conditions favourable for dolomite precipitation ended abruptly as a result of the enhancement of catchment inflow. Such conditions did not occur again in the Holocene, not even in the early Holocene when the lake was relatively shallow with high summer evaporation and increased organic productivity. Instead, aragonite became the dominant carbonate mineral precipitated throughout the Holocene, and its production determined the variations of TCC in the sediments. The persistent precipitation of calcium carbonates since the early Holocene has led to a continued increase in Mg/Ca ratio of the lake water from around 12 to present-day values of up to 98.

In the study I showed the evidence that stable isotope ratios of primary carbonate minerals formed in closed-basin lakes do not necessarily fall into a covariant trend. Identification of mineralogical type and origin of carbonates is extremely important in the study of lacustrine isotopic records, particularly in using isotopic covariance for paleohydrological analysis. Isotopic ratios of aragonite laminae do not fall on the covariant trend, because they display a nearly identical $\delta^{13}C$ value of close to 4‰, while the $\delta^{18}O$ values range from -0.58‰ to +3.64‰. Primary dolomite, on the other hand, shows much more negative $\delta^{13}C$ values, i.e., between -4‰ and -2‰, which contrast sharply with those

of aragonite laminae, placing the isotopic ratios below the covariant trend. These isotopic ratios therefore must be excluded from the group of samples used for the isotopic regression. Apparently, specific processes caused ^{13}C to be either unusually enriched or depleted in the two types of primary carbonates. It is important to note that neither the isotopic ratios of aragonite laminae, which represent seasonal surface water events, nor those of primary dolomite, which reflect isotopic information spanning several hundred years, represents a breakdown of the δ^{13}C-δ^{18}O covariant trend, the essential isotopic identity of the lake. In addition, isotopic ratios from some bulk carbonate samples containing substantial amounts of dolomite must be excluded, otherwise error will be introduced into the δ^{13}C-δ^{18}O correlation coefficient because of the distinctly negative δ^{13}C values of the dolomite involved. The isotopic result from the large closed-basin Lake Qinghai confirms the validity of the application of the isotopic covariant trend to the paleohydrological analysis of ancient lacustrine basins, that is, a single covariant trend for the samples from two sections of a closed lacustrine basin defines a spatial continuity of the deposition in the same waterbody.

7. Paleoclimate evolution since the Marine Isotopic Stage 3 in the N. E. Tibet-Qinghai Plateau: new results from Lake Qinghai and a synthesis

7.1 Introduction

The Marine Isotope Stage 3 is the interval between the two times of maximum ice-sheet extent during the last glaciation, extending from ca. 60 to 25 ka BP, during which global environmental conditions were neither fully glacial nor fully interglacial. In the past 30 years or so, with the help of improved technology of dating, including radiocarbon, U/Th, and luminescence, correlations of Stage 3 paleoenvironmental records on both regional and global scales have become possible. Also, major advances in marine- and ice-core stratigraphy; ice sheet, biome, and climate modeling; and new archeological and paleoanthropological discoveries and analyses have made it possible to interpret the changing environments of Stage 3 in a new light (van Andel, 2002).

A δ^{18}O record from the Guliya ice cap in the western Tibet-Qinghai Plateau suggests that the climate conditions of Stage 3 may be similar to the Holocene and Eemian (Thompson et al., 1997). This led to an investigation on other geological records from the Plateau, focusing on the time window of 30-40 ka (Shi et al., 2001). The investigators indicate that at this time high lake-level stands occurred in large areas of western China, and compared to the present-day vegetation, alpine steppe-forests were shifted ca. 400 km further north and the alpine conifer forest extended ca 400-800 km beyond their present western limits. They estimated that the temperature was 2-4° C higher and precipitation was 40 to over 100% higher than today, based mainly on ice-core δ^{18}O records from the Plateau. The Tengger Desert, with an area of 36,700 km^2 and some 260 km northeast of Lake Qinghai, is located at the junction of the Tibet-Qinghai Plateau, the Loess Plateau of China and the Mongolian Plateau. There are some 400 lakes today in the desert but none of them is perennial. According to Zhang et al. (2002), the Tengger Desert was a Mega-lake at 35-22 ^{14}C ka BP and lake levels then were 20-30 m above the playa surface of today. This interpretation is based on multiple stratigraphic data from ^{14}C dated terrace sections. A contrary interpretation on paleo-lake conditions at Stage 3 in the northwestern China was reported by Ma et al. (2004): U-series dating of the cored lacustrine sequence and stratigraphic records from Balikun Lake, Xinjiang, indicate that the lake was a playa at 62-25 ka BP (corresponding to Stage 3), suggesting an arid paleoclimate. The high-resolution seismic and core stratigraphy from Lake Qinghai may provide key-site evidence to shed more light on the regional paleoclimate conditions during Stage 3.

Large changes of the Earth's climate since the Last Glacial Maximum (LGM) have drastically altered the vegetation, ice volume, and sea surface conditions over the globe (COHMAP Members, 1988; Wright et al., 1993). The LGM is the time period of maximal ice volume of the globe, as measured by deep-sea δ^{18}O records. It lasted for about 3000 years from 21 to 18 ka BP in calibrated years (Bard et al., 1990); the climate then was radically different from that of today (CLIMAP, 1981; Rind and Peteet, 1985; Street-Perrott, 1991; Pollard and Thompson, 1997). A reexamination of the CLIMAP reconstruction suggests that a decrease in eustatic sea level at the LGM was 128 m on average, and that nearly all of the LGM ice sheets were thinner than those postulated in the

CLIMAP maximum model (Clark and Mix, 2002).

While an important paleoclimatic question remains controversial regarding whether or not there existed a unified ice sheet on the Plateau during the LGM (Zheng and Li, 1981; Kuhle, 1987; Shi, Y.F., 1992; Kuhle, 2004), lacustrine records in China retrieved from 1980s started to fill the data gap of paleoclimate reconstruction. Based on these records, Chen et al. (1990) suggested that the paleoclimate between 25-10 ka BP was cold and dry on the Tibet-Qinghai Plateau. This study showed the importance of establishing paleoclimate records by detailed investigation on sediment cores of modern lakes. Based on a survey of available data published in Chinese journals of 1980s, Fang (1991) drew a conclusion that most lake basins were desiccated 20-16 ka BP. A recently completed survey of lacustrine records from 31 sites in China led to a different conclusion: Very dry LGM conditions occurred only in eastern China while western China was in wetter climate conditions (Yu et al., 2000). The wetter climate is attributed to a decrease in evaporation, thus creating a positive anomaly of P-E of 70-95 mm/year between the LGM and today. Further investigations of selected key-sites, in addition to a reevaluation of some proxy records already available, may help to narrow down these uncertainties.

Lake Qinghai is a closed-basin perennial lake and the largest waterbody in China. It lies in an intermountain basin at the NE corner of the Tibet-Qinghai Plateau with an elevation of 3195 m above sea level. The catchment location marks a "triple junction" of climatic influence: the main body of the stable pressure system to the southwest, prevailing winds from the west or northwest and a precipitation gradient to the southeast, which increases steadily towards the ocean (Lister et al., 1991). The reconstruction of the Stage 3 and LGM climate for the site of Lake Qinghai may therefore provide valuable paleoenvironmental information in relation to the glacial history. This information also helps to gain insight into the deglaciation pattern of the NE Tibet-Qinghai Plateau.

This chapter reports new results based on 3.5 kHz seismic records of the sub-bottom sediments across the eastern basin of Lake Qinghai, and from the investigation of a 26-m drill core. The drill core, named Q87, represents the deepest cored sediment sequence recovered until now from pelagic centers of the lake. Discussions based on the results are centered on the Marine Isotope Stage 3 (MIS 3) and the LGM climatic conditions in the NE Tibet-Qinghai Plateau. For the climate reconstruction of the Holocene, new stratigraphic records of core Q14B are reported and discussed here in this chapter. Note that the paleoclimate of the late-Glacial/Holocene transition has been discussed in Chapter 5.

7.2 Results and interpretations

7.2.1 Seismic reflection Profile No. 1

The reflection Profile No. 1 (Figure 7.1) begins at a site near the Factory No. 151, heading N20°E towards Haiyan Bay (refer to Figure 4.1 for locations). It surveys the sub-bottom sediment structures across the eastern basin of Lake Qinghai. Among a series of reflectors, a most notable and strong reflection extends over the eastern basin. This reflection shows the same characteristic feature as the one named Q-reflector (refer to Section 4.2, and also Kelts et al., 1989 and Lister et al., 1991). The distribution of the Q-reflector in the eastern basin confirms its ubiquity in all basins of Lake Qinghai.
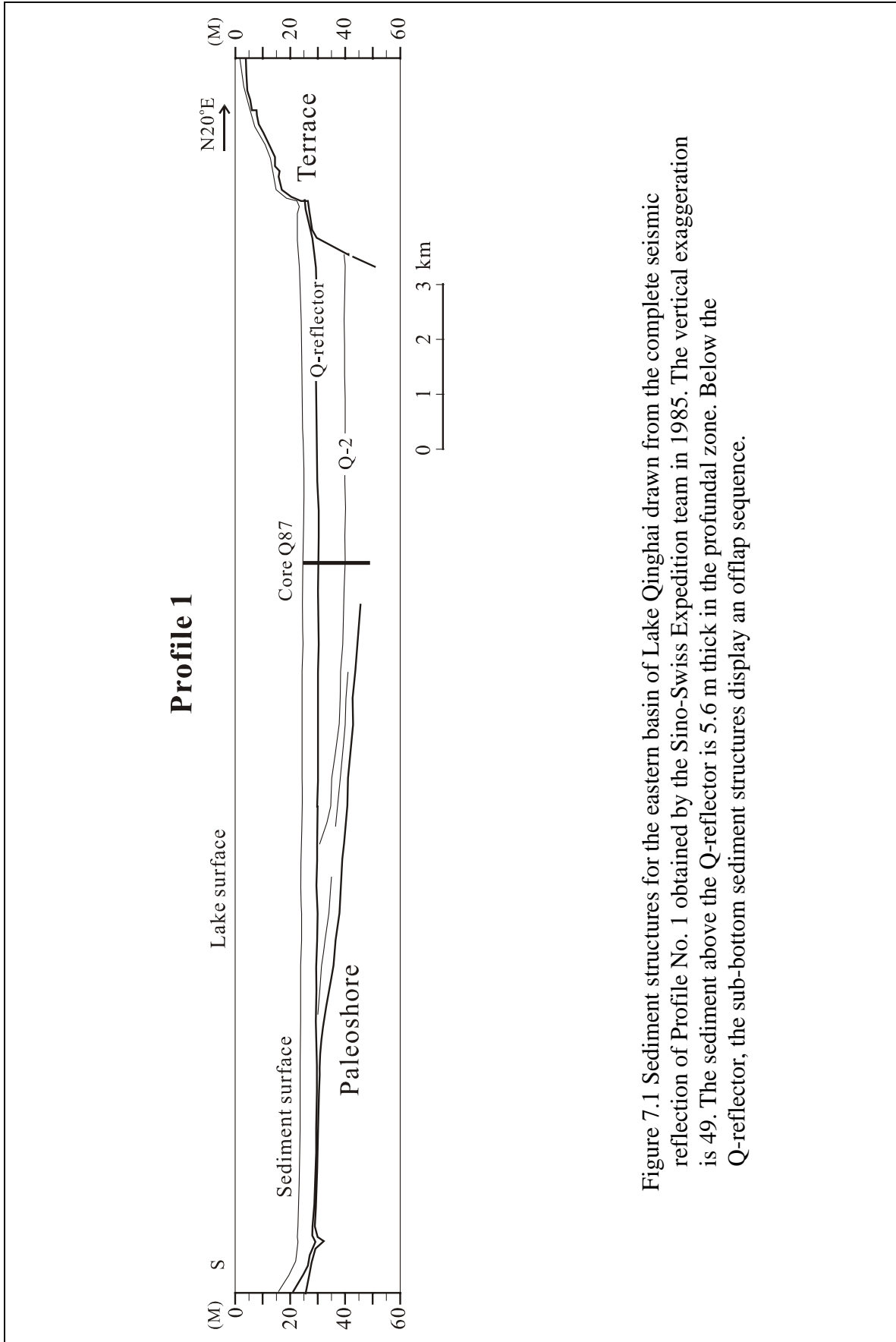
Figure 7.1 Sediment structures for the eastern basin of Lake Qinghai drawn from the complete seismic reflection of Profile No. 1 obtained by the Sino-Swiss Expedition team in 1985. The vertical exaggeration is 49. The sediment above the Q-reflector is 5.6 m thick in the profundal zone. Below the Q-reflector, the sub-bottom sediment structures display an offlap sequence.

Although quite flat, the Q-reflector falls by 3.5 m from near-shore to the central eastern basin. Above the Q-reflector, parallel, closely-spaced reflectors represent a 4.8-6 m thick sequence of deposits. They rest unconformably on underlying deposits. Below the Q-reflector, the seismic reflection profile displays an offlap sequence. Another reflector named Q-1 (refer to Figure 4.3 and also Lister et al., 1991) is not shown in Profile No. 1, based on a comparison with other seismic profiles such as Profile No. 10 from the southern basin of the lake.

Plate 7.1 A rotary drilling rig set on a 90-ton barge fixed with 4 anchors, used for retrieving core Q87 from the water depth of 25 m in the middle of the eastern basin of Lake Qinghai.

7.2.2 Sediment core Q87

A rotary drilling rig set on a 90-ton barge was used in the summer of 1987 for taking sediment cores from the middle of the eastern basin of Lake Qinghai (Plate 7.1). A sediment core 26.07 m long, named Q87, was successfully recovered (Plate 7.2). The recovery rate of the core is about 50% due to considerable difficulties encountered with storms during the drilling operation. The core can be distinguished into ten lithostratigraphic units (Figure 7.2):

Unit 10 (26.01-26.07 m, 6 cm thick), the basal sediment of the drill core, consists of greenish-gray clay with the total carbonate content (TCC) of 24% and the total organic carbon content (TOC) of 0.11%. The sediment is well laminated on a mm scale. The

precise age of Unit 10 is unknown, but estimated ^{14}C age for Unit 10 deposition are between 68.5 and 68.7 ka BP, based on the sedimentation rate of 0.38 mm/a extrapolated from five AMS ^{14}C dates (see Chapter 7.2.3).

Plate 7.2 Colour photograph of core Q87 to 26.07 m depth in the sediments from the central eastern basin of Lake Qinghai.

Unit 9 (22.35-26.01 m, 3.66 m thick) is characterized by tan to gray mud overall homogeneous with faint laminations. The sediment contains 17.5% TCC and 0.33% TOC.

Unit 8 (20.78-22.35 m, 1.57 m thick) comprises olive-gray mud with TCC (around 13.4%) and TOC (about 0.21%) lower than Unit 9. Irregular stringers of sandy sediments and FeS spots are common.

Unit 7 (16.08-20.78 m, 4.7 m thick) is characterized by olive-gray laminated couplets of finer and sandy sediments. The finer thin layers of the couplets are usually thicker than sandy thin layers. Unit 7 also contains intervals laminated on the scales of 1-3 mm. A loose, sandy layer 20-cm-thick is present at 17.65-17.45 m. This soil-like layer shows no grading and contains bits of shell.

Unit 6 (12.25-16.08 m, 3.83 m thick) consists of olive-gray, muddy silts laminated on the scales of 1-3 mm. Total carbonate content of the bulk sediments is about 16%, mostly calcite. TOC and TN contents of the sediments are as low as 0.15% and 0.055%, respectively. A 2.5-cm-thick layer composed of well-sorted coarser sand with quartz and
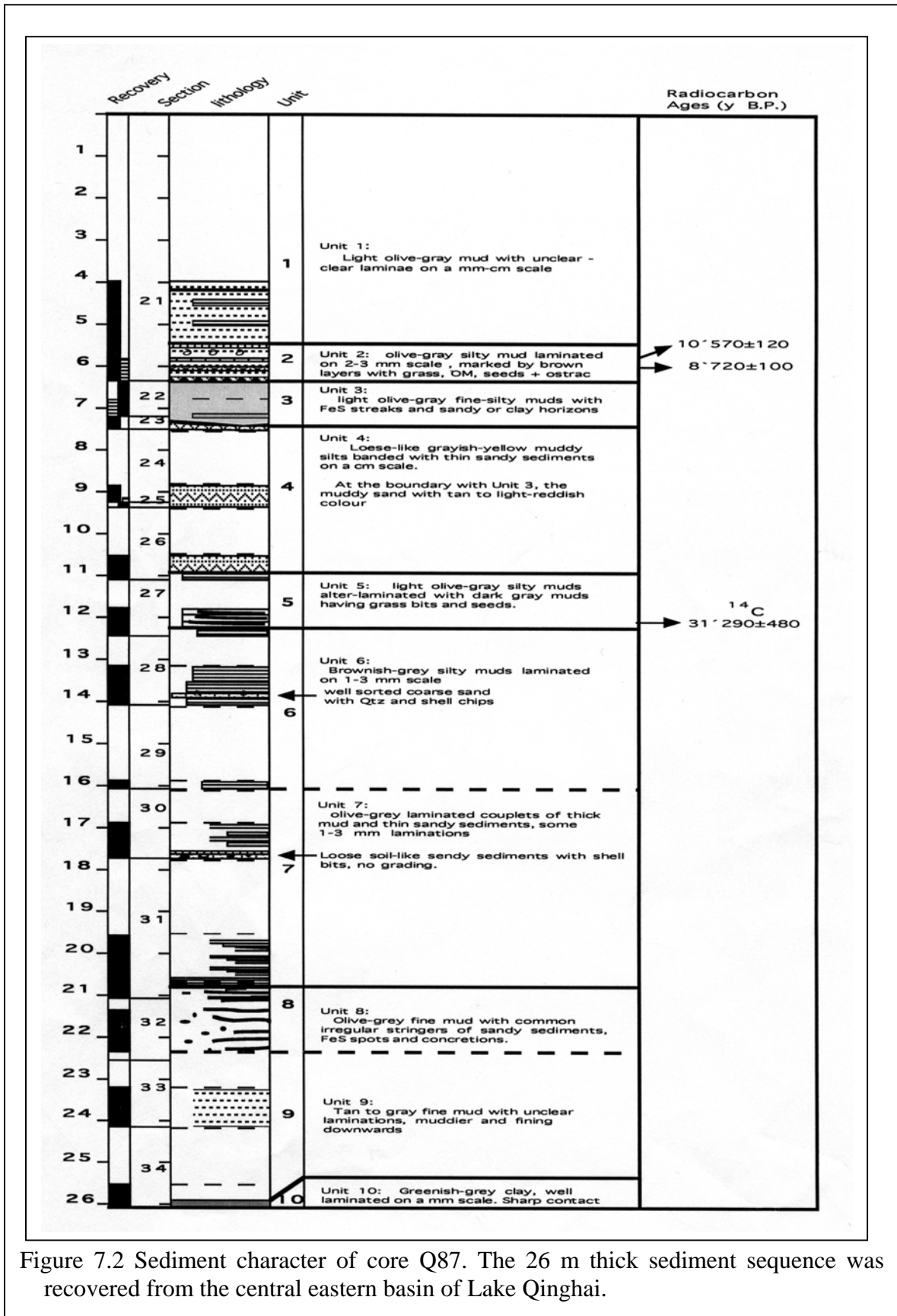
Figure 7.2 Sediment character of core Q87. The 26 m thick sediment sequence was recovered from the central eastern basin of Lake Qinghai.

shell chips is present at the core depth of 13.8 m.

Unit 5 (10.93-12.25 m, 1.32 m thick) is characterized by irregular couplets of dark and light gray laminae, 2-5 mm thick. The dark laminae contain iron sulfide, bits of grass, and seeds from aquatic plants. The carbonate content of the sediments is low and ranges between 13.3% and 15.2%. Calcite is the dominant carbonate mineral. TOC content ranges from 0.09% to 0.51%, much lower than that of the Holocene sediments.

Unit 4 (7.31-10.93 m, 3.62 m thick) comprises grayish-yellow silts, banded with coarser thin layers on a 0.5-cm scale. The loess-like sediment contains the lowermost TOC content in comparison with those of all sediment samples measured for core Q87. The sediment near the contact with the upper unit is a muddy sand layer with a tan to light-reddish hue.

Unit 3 (6.34-7.31 m, 0.97 m thick) is composed of light olive-gray, muddy silts with FeS streaks, and sandy or clay horizons. There are cm-scale layered zones with exotic rock fragments or scattered quartz pebbles.

Unit 2 (5.55-6.34 m, 0.79 m thick) comprises olive-gray muddy silts laminated on a 2-3 mm scale. It includes brownish layers with grass remains, fossil seeds from aquatic plants and ostracod shells. The sediment has 22.5% TCC, mainly calcite. Aragonite is detected from the sediments, accounting for 22% relative to the content of total carbonate.

Unit 1 (0-5.55 m, 5.55 m thick) consists of the light olive-gray muddy silts with faint to well-defined laminations and bands rich in algal filaments.

7.2.2.1 Lithologic correlation of Q87 with Q16C and Q14B

The sediment Unit I and Unit II of core Q87 can be basically correlated with the Unit I through Unit VI of core Q14B (refer to Sections 4.4.2 and 4.4.1). The lithologic correlation between the two cores is difficult to have a detailed match according to their coring depth, mainly because of the insufficiency of the rotary drilling device for retrieving the soft sediments of upper five meters with quality as good as Kullenberg corer. For the reconstructions of paleoenvironment and paleoclimate in the past 14 ka B.P., we therefore rely on data from core Q14B and core Q16C.

7.2.3 AMS ^{14}C dating

Fossil seeds from rooted aquatic plant were picked from the sediments of Q87 at the depth of 5.78 m, 5.99 m and 12.12 m. The AMS ^{14}C ages of the three selected samples are shown in Table 7.1 The age control for the sediments of the upper 6 m relies on radiocarbon ages of piston core Q14B as shown in Table 4.1. The radiocarbon calibration program (Calib Rev 5.0.1) was used to convert the AMS ^{14}C ages to calibrated (cal) ages (Stuiver et al., 1998; Stuiver and Reimer, 1993). The lack of sufficient amount of organic matter in samples for radiocarbon dating of Q87 led to a poor age control for the sediment sequence below 6 m. Only one AMS radiocarbon age from Q87 at the depth of 12.12 m is reliable for the chronology of the core.

The Holocene sedimentation rate of Lake Qinghai is estimated to be between 0.40 and 0.42 mm/a, based on extrapolations between each pair of AMS radiocarbon ages (refer to

Figure 4.4). The extrapolation yields an average sedimentation rate of 0.38 mm/year for the late Pleistocene deposition in Lake Qinghai. The age of deposition at the base of core Q87

Table 7.1 Radiocarbon ages of core Q87, measured by AMS facility at ETH-Hönggerberg.

Laboratory number	Sample No. /core depth (m)	AMS ^{14}C age (yr BP)	Calibrated ^{14}C age (2σ) (cal yr BP)	Dating material	δ^{13}C (‰)
ETH-5506	Q87-27-1/12.12	31,290±380	Not obtainable	Seeds	-6.8
ETH-5507	Q87-21-3/5.99	8720±100	9532-9956	Seeds	-12.0
ETH-5508	Q87-21-3/5.78	10,570±120	12,146-12,823	Seeds	-11.5

is estimated at ~52-68 ka BP if calculated by using the sedimentation rates of 0.50-0.38 mm/a (based on the extrapolation of five AMS radiocarbon dates).

7.2.4 Carbonate mineral record

In core Q87, the carbonate content (TC) ranges from 13.3-24% in the sediments of 5.73-26.07 m, with calcite as dominant carbonate mineral (Table 7.2). The TC content and carbonate composition are similar to those in the sediments deposited at ~10.7-14 ka BP (Figure 5.2 c and d). They are however distinctly different from those of the Holocene sediments, in which TC is mostly between 40% and 60%, with aragonite as the dominant carbonate mineral. This marked difference provides mineralogical evidence reflecting a large difference of the lake's chemistry between the late Pleistocene and the Holocene.

Shifts in carbonate composition were remarkable across the late glacial/Holocene transition, briefly from a calcite-dominated phase to dolomite phase and then to the Holocene aragonite dominated phase (see Figure 5.2d). These shifts, in combination with changes in TC, indicate marked changes in P-E balance mainly as a consequence of increased summer temperature and abrupt enhancement of monsoon rainfall (refer to Chapter 5).

A complete carbonate mineral record of core Q14B includes the down-core variations in TC, carbonate mineral composition, and content of each carbonate mineral, as shown in Figure 6.3. These variations provide indication of the brine evolution of the past 14 ka BP in relation to changes in Mg/Ca ratio, carbonate alkalinity and salinity of the paleo-lake (refer to Section 6.5). The sediments of Unit VI and Unit V in core Q14B contain 20-36% TC, which suggests the lowermost alkalinity and salinity of the paleo-lake in the past 14 ka B.P. (Yu and Kelts, 2002). The calcite and Mg-calcite dominated composition of the

sediments suggests that the Mg/Ca ratios of the lake were between 7 and 10 at ~10.7-14 ka BP. The high Mg/Ca ratio 100:1 of today has been brought about by a long-term evaporative concentration of the brine over the Holocene. At 10.6-14 ka BP the alkalinity and salinity were lower and the lake was shallower than they were in the Holocene. This is attributed to a cold climate with longer ice-cover of the year and lower summer evaporation.

In core Q87 the contents of TC and aragonite in the sediments deposited at ~15.2-58.7 ka BP are, by comparison, lower than those in the sediments deposited at ~10.7-14 ka BP. This suggests that alkalinity and salinity of the paleo-lake in the late Pleistocene was much lower than the Holocene, and even lower than that at ~10.7-14 ka B.P. It moreover implies that climate conditions remained colder throughout the period of ~15.2-58.7 ka BP than the Holocene.

Table 7.2 Data from mineralogical and geochemical analyses for sediment samples selected from core Q87

Depth m	% (relative to TC)			% of sediment weight			C/N
	Calcite	Dolomite	Aragonite	TC	TOC	TN	
5.73	64	14	22	22.50	0.16	0.02	8.0
5.80	67	16	17	19.60	0.27	0.05	5.4
8.87	80	20	0	14.40	0.07	0.03	2.3
11.94	84	16	0	13.30	0.26	0.04	6.5
12.18	75	18	7	14.40	0.09	0.04	2.3
12.23	77	14	9	15.20	0.51	0.05	10.2
13.29	82	18	0	16.50	0.12	0.05	4.0
13.36	88	12	0	16.00	0.18	0.06	3.0
21.30	84	16	0	13.40	0.21	0.04	5.3
23.84	85	15	0	17.80	0.32	0.06	5.3
23.91	86	14	0	17.30	0.33	0.04	8.3
26.04	94	6	0	24.00	0.11	0.08	1.4

7.2.5 Total organic carbon, total nitrogen and C/N ratio

The data of TOC, TN and C/N from core Q14B are plotted against sediment depth in Figure 7.3. The C/N ratios range from 5 to 14, indicative of an autochthonous origin of the organic matter from algae and aquatic macrophytes, which have C/N ratios of 5 to 12. TOC and TN increased after 10.7 ka BP by a factor of three. The two negative excursions of TN

and TOC in Unit IIIb are associated with two aragonite layers.

Table 7.2 shows the measurements of TOC and TN for selected sediment samples in depth below 5.73 m from core Q87. These TOC and TN values are as low as those of the detrital sediments of Unit V in core Q14B, suggesting that the organic productivity of Lake Qinghai throughout the late Pleistocene remained on a very low level. This also implies cold climate conditions with lower summer evaporation. The sharp increase in TOC and TN at the onset of the Holocene suggests an abrupt and substantial increase in organic productivity of the paleo-lake, which is interpreted as the evidence of increased summer temperature (Yu and Kelts, 2002).
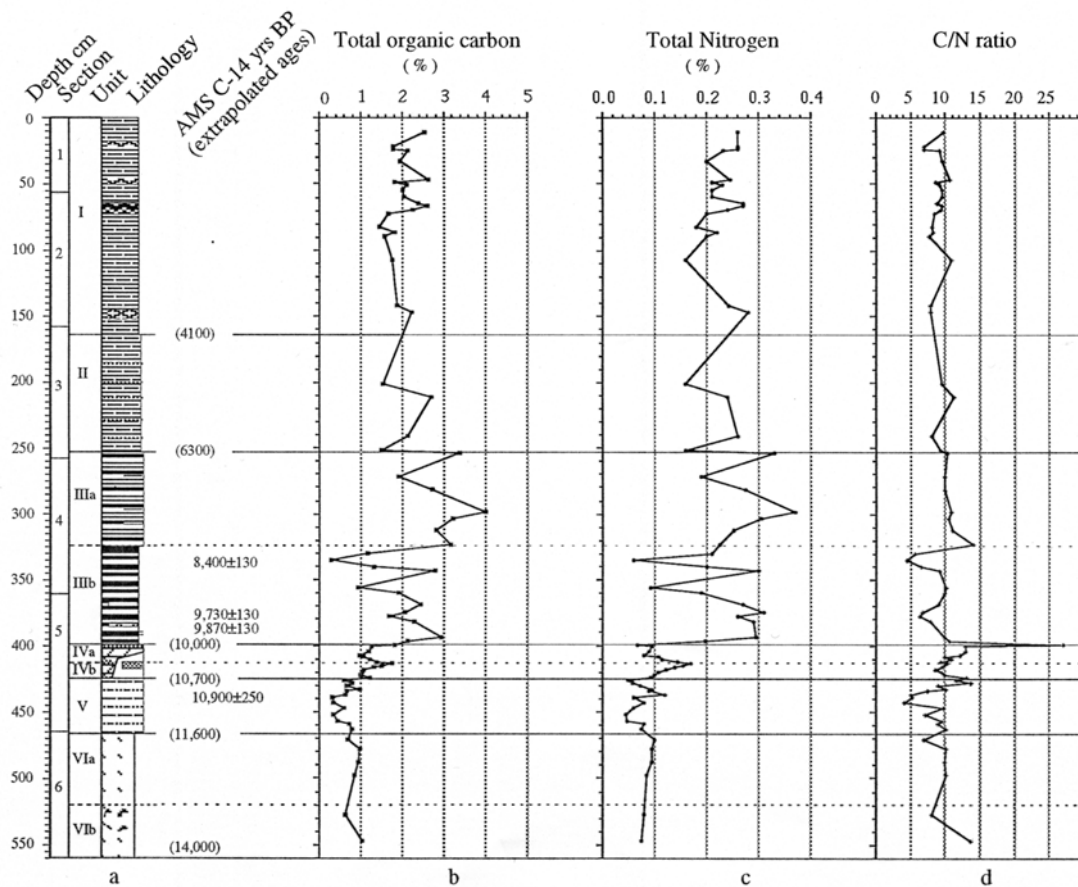
Figure 7.3 Paleolimnological variables of total organic carbon (TOC), total nitrogen (TN) and C/N ratio against sediment depth in core Q14B. Refer to Figure 4.8 for detailed description of the legends of lithology.

7.2.6 Pollen record

The pollen record of core Q14C shows that the vegetation history of the past ~11 ka BP (Du et al., 1989) can be divided into five zones (Figure 7.4). Zone I (450-400 cm, ~11-10 ka BP) is dominated by the pollen of shrubs and herbs with minor percentages of *Betula*, *Picea* and *Pinus*. Zone II (400-320 cm, ~10-8 ka BP) is characterized by the increase of tree pollen taxa, especially of *Betula*. Zone III (320-140 cm, ~8-3.5 ka BP) shows the predominance of tree pollen, mostly over 50% relative to the total pollen,

including *Pinus*, *Picea*, *Betula* and *Abies*. Zone IV (140-60 cm, ~3.5-1.5 ka B.P.) displays marked fluctuations and a decreasing trend in tree pollen while herb and shrub pollen increased. Zone V (60-0 cm) is the top interval spanning the last 1.5 ka BP, in which herbs and shrubs are predominant (over 75%), whereas tree-pollen grains usually are less than 20%.

The pollen record indicates that at ~11-10 ka BP patches of woody plants such as *Betula* and *Picea* existed in the catchment of Lake Qinghai although shrubs and herbs dominated the vegetation. A marked increase of *Betula*, a woody plant favoured by a relatively dry, temperate climate, occurred from Zone I to Zone II and reached a maximum percentage at ~9.2 ka BP. The consistent high percentage of over 50% in tree pollen (Zone III) reflects a substantial expansion of forest between 8 and 3.5 ka B.P. *Picea* and *Pinus* then turned to be the dominant trees mixed with *Betula*. The vegetation in the lake basin may have been similar to that in the today's drainage basin of the Huangshui River to the east of Lake Qinghai, where the present climate is warmer and wetter. Forest cover declined in general, with some fluctuation, since 3.5 ka BP, as suggested by the sporo-pollen assemblage in Zone IV, and steppe vegetation expanded. Most likely, the vegetation cover in the lake basin became similar to that of today since about 1.5 ka BP.

7.3 Climatic conditions at Stage 3 and the LGM

Below the upper 7-m of the sediments, the sub-bottom sediment structure in the eastern basin shows an offlap sequence of about 25-m-thick deposits, as revealed by the 3.5 kHz seismic Profile No. 1 (Fig 7.1). This indicates an offshore regression of the paleo-lake, which is in agreement with the interpretation for the seismic reflection profiles from the southern basin of the lake (Lister et al., 1991). The deposition of the well-laminated greenish-gray clay with 24% TC (Unit 10) and the subbottom structure imply a rapid expansion of the paleo-lake occurred approximately 65 ka B.P. The dimension of the expanded lake, however, did not reach that of the Holocene, as indicated by the seismic structures of the subbottom sediment sequence. The maximum expansion around 65 ka BP was at least 6 km off the shore of today on the southern lakeside (Figure 7.1). As revealed by the AMS ^{14}C dated lithostratigraphy of core Q87, the sediments of Unit 9 through Unit 4 deposited approximately from 67 to 18.3 ka BP are characterized by clastic deposition with TC, TOC and TN contents much lower than those of the Holocene sediments. This indicates both organic and carbonate production of the paleo-lake were much lower than in the Holocene. A cold climate at ~67-18.3 ka BP is suggested by the proxy record. Also, the expansion of the lake from 65 ka B.P. indicates wetter climate conditions. In the semi-arid region, a cold but wetter climate could induce an expansion of mountain glaciers and permanent ice field in the drainage basin of Lake Qinghai. The sediments deposited between 59 and 32 ka BP show the texture of alternating coarser and fine-grained layers with TOC lower than 0.33%. This implies a depositional environment with seasonal variation in meltwater supply from the expanded mountain glaciers.

The lake began to recede at ca. 44 ka BP and terminated with a marsh environment, as suggested by the sediments (Unit 5) with the alternating light olive-gray and darker layers having grass bits and macrophyte seeds and a relatively high content in TOC (0.51%). The marsh environment lasted 3200 years (from ~32 –28.8 ka BP). The following deposit of yellowish-gray silty sand (Unit 4) is water-lain loess (core depths 10.93 m and 7.31 m). It implies a severe cold and arid climate at ~28.8-18.3 ka BP, during which large areas of
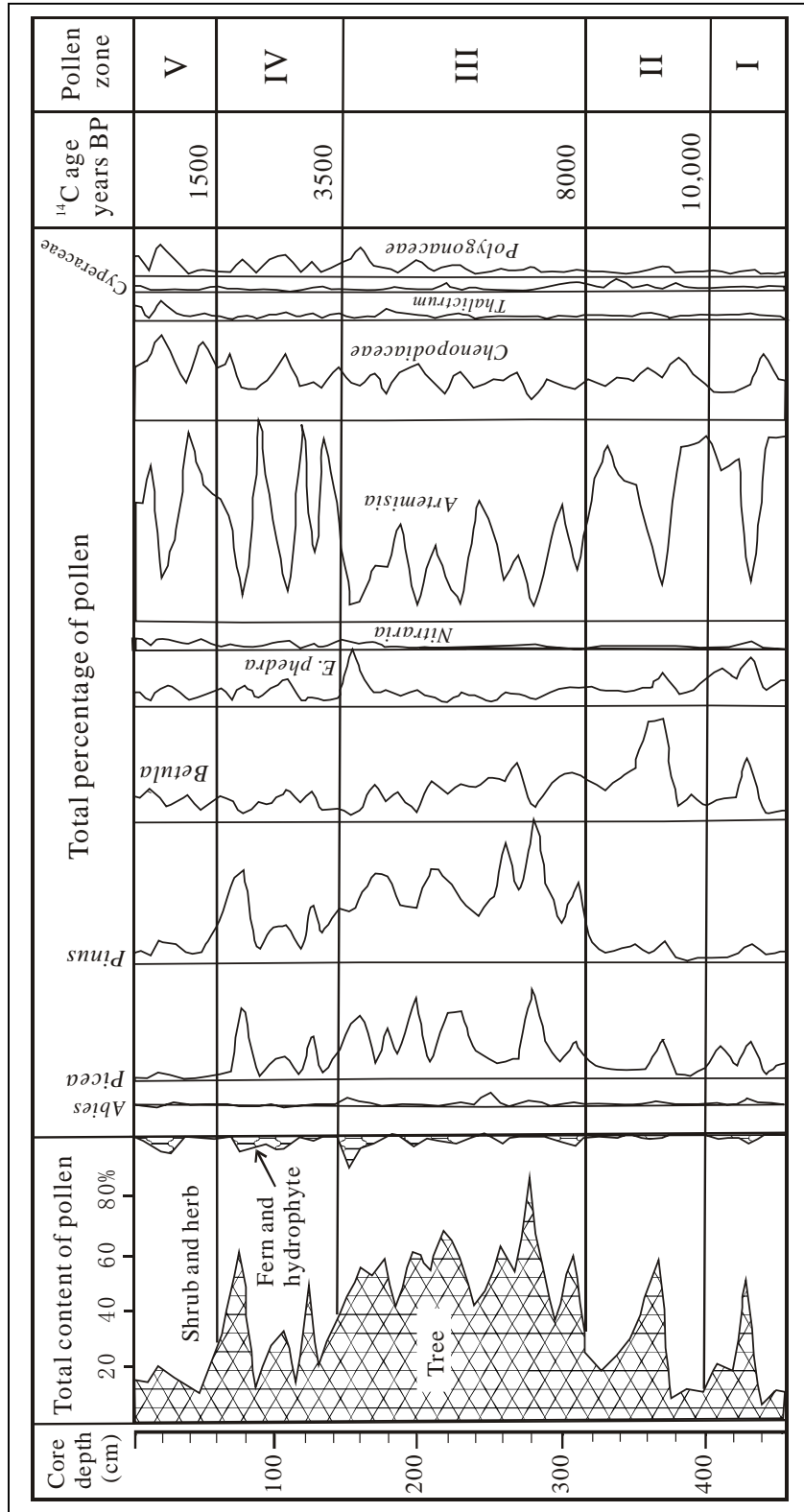
Figure 7.4 The Holocene pollen percentage diagram of selected taxa from core Q14C recovered from the central southern basin of Lake Qinghai (after Du et al., 1989).

the paleo-lake dried up or turned to be separate small lakes.

The lack of a glacial moraine deposit in the drilled sediment sequence of Q87 indicates that glaciers on the northern slope of Qilian Mountain have not advanced down to the central area of the eastern basin (3160 m a.s.l.) of Lake Qinghai, not even during the wetter period of ~59-32 ka BP, let alone in the most cold and arid period of ~28.8-18.3 ka BP. The expansion of the paleo-lake, as suggested by the Q-reflector and the deposition of the post-glacial sequence, occurred in about three thousand years after the LGM. This may be attributed to meltwater, representing a major step of the last deglaciation in the region before the influence of monsoon started.

7.4 A paleoclimate record of the Holocene from Lake Qinghai

A wet pulse at ~10-9.8 ka BP, that terminated the carbonate playa and resulted in the negative excursion of TC (Figure 7.5e and f), marked the beginning of the early-Holocene warm and wetter climate conditions. It was preceded by oscillating hydro-climate conditions across the late Glacial/Holocene transition (Yu and Kelts, 2002). The increase of the lake's organic productivity was substantial right after the onset of the Holocene, as indicated by TN, TOC and the C/N ratio. This may be attributed to a marked increase of summer temperature in the Holocene, as TOC and TN have been used as a distinctive proxy record for climate reconstruction, such as Lake Biwa, Japan (Meyer and Horie, 1993), Lake Huangqihai, Inner Mongolia (Yu et al., 2003) and Lake Xinyun, Yunnan Province (Hodell et al., 1999). Warm summer temperatures also resulted in the enhancement of evaporation, thus the increased carbonate production of the lake. Although monsoonal precipitation has enhanced as suggested by the wet pulse from 10 ka BP, the reconstructed early-Holocene lake depths did not exceed 8 m with large fluctuation, based also on the evidence of fossil seeds from *Ruppia* preserved in several thin layers of Unit IIIb. High evaporation due largely to high summer insolation may be responsible for preventing the lake from a further increase in lake level. Therefore, the effective moisture was lower than during any later stages of the Holocene. This interpretation is supported by the pollen record (Figure 7.4), which indicates that during 10.7-8 ka BP, woody plants distributed as patches in the catchment were mainly *Betula*, a species growing preferably in a dry and warm climate.

An increase in effective moisture and lake level occurred at 8 ka BP, as suggested by the following evidence: 1) a substantial decrease in TC along with the absence of the laminae rich in dolomite which were present in Unit IIIb, and 2) an expansion of evergreen trees, mainly pine and spruce, accompanied by a decrease in birch in the drainage basin of Lake Qinghai. Organic productivity was increasing from 8 ka BP, as indicated by the increase of TN and TOC contents, suggesting that the summer temperature and evaporation remained high since the Holocene. It was the increase of precipitation in the catchment that resulted in the increase of effective moisture.

As suggested by the high percentage of tree pollen and the data of the modest contents of TN, TOC and TCC, effective moisture and lake level during middle Holocene between 7 and 4.1 ka BP were higher than the early Holocene. The TN, TOC and TC contents were lower in comparison with those of the early Holocene. This implies that summer temperature and evaporation decreased, which may be associated with the gradual decrease of summer insolation during that period. The P-E then could increase providing that

precipitation remained as high as during the early Holocene, let alone a possible increase.

The sediment character of Unit I deposited in the past 4.1 ka BP is basically uniform in terms of colour, structure, algal remains and ostracod shell species, suggesting stable lake environmental conditions. The fluctuation of the lake level may have not exceeded 8 m, based on the evidence of paleoshoreline. Carbonate production and organic productivity were lower than in the other stages of the Holocene but apparently higher than in the pre-Holocene stages. The lowered temperature and enhanced aridity of the last 4 ka B.P. is also documented by the marked decrease of tree pollen. However, there is no clear evidence of lowered lake levels in the past 4000 years if compared with those in the early stages. On the contrary, the ostracod $\delta^{18}O$ record shows an essentially vertical to weakly negative trend with values scattered around 3‰. This is a marked change from the former trend of overall steady positive shift for $\delta^{18}O$ values of some 6‰, through the early to middle Holocene (Lister et al., 1991).

7.5 Paleoclimate evolution: a correlation of Lake Qinghai record with other proxy records in the region

7.5.1 The Marine Isotope Stage 3 (MIS 3)

An ice core record from the Dunde ice cap, about 200 km west of Lake Qinghai, yielded little detailed information about the glacial stage because the pre-Holocene ice was confined to the bottom 10 m of the core (Thompson et al., 1989). A 308.6-m ice core was drilled from the Guliya ice cap at the site with the elevation of 6200 m above sea level in the far western Kunlun Mountains on the Tibet-Qinghai Plateau and the Guliya isotopic record shows a positive $\delta^{18}O$ excursion in the ~ 30-40 ka BP interval during MIS 3 with the isotopic values as high as those of the Holocene, suggesting similar temperatures as in the Holocene (Thompson et al., 1997). A later assessment of proxy records including ice cores and lake-levels from the Plateau put forward an interpretation that the paleoclimate during 40-30 ka BP was 2-4 °C warmer with 40-100% more precipitation than in the Holocene (Shi et al., 2001). This is however incoherent with the Lake Qinghai record. Our data suggest that the overall environmental conditions during MIS 3 were neither fully glacial nor fully interglacial in the NE Tibet-Qinghai Plateau.

7.5.2 The Last Glacial Maximum (LGM)

The paleoenvironmental conditions of Lake Qinghai was severely cold and dry during the LGM, as suggested by the 3.62 m thick wind-blown sand deposited in the central eastern basin at ~28.8-18.3 ka BP. According to Chen and Bowler (1986), the Qarhan salt lake, the largest salt flat of the Qaidam basin to the southwest of Lake Qinghai, was in humid lacustrine conditions at about 40-30 ka B.P.; desiccation began from 25 ka BP and remained cold and arid until about 9 ka BP. Sediment cores from Lake Luanhaizi, which is a small fresh-water lake with the altitude of 3200 m a.s.l. in the eastern Qilian Mountains, also revealed cold and arid climate conditions, as indicated by a playa deposit (Zone 5) (Mischke et al., 2005). Sediment evidence from the three sites of the arid to semiarid region near the outer margin of the Asian summer monsoon all point to cold and arid climate conditions during the LGM. Although severely cold, the high aridity of the region might have prevented a large advance of mountain glaciers; hence the formation of a

unified ice sheet on the Plateau is unlikely. This is proved by the lack of moraine deposits in the sediment sequences of both Lake Qinghai and Lake Luanhaizi. Despite reduced snowfall, the severity of cold temperature during the LGM might have resulted in a positive mass balance of mountain glaciers, as implied by relict cirques in Mt. Qinghai Nanshan. The elevation of the relict cirques suggests a snowline decline of 800-900 m in the catchment of Lake Qinghai (Yu and Kelts, 2002). Results from Lake Qinghai are in general agreement with those of newly dated and reassessed glacial successions in the Anyemaqen and Nianbaoyeze mountains of NE Tibet-Qinghai Plateau, where glaciation was more restricted during the LGM but much more extended during MIS 3 (Owen et al., 2003).

Synchronous and coherent records, like those from the NE Tibet-Qinghai Plateau with regard to MIS 3 and MIS 2 environmental conditions, are also documented in the sediment archive of lakes in the Yunnan Province, SW China (Hodell et al., 1999) and in newly dated moraine successions in the Himalayas (Owen et al., 2002). Paleoclimate interpretations of the proxy records of both lacustrine and glacial successions appear undesignedly to have converged. It seems clear that the pattern of the last glaciation and deglaciation since the MIS 3 on the Tibet-Qinghai Plateau was determined more importantly by the availability of moist air masses and not so much by temperature. This is somewhat different from that in other continents, particularly from the European pattern. The data and interpretation presented here may act as a benchmark and help to form a consensus on the pattern of paleoclimate change on the Tibet-Qinghai Plateau.

7.5.3 The post-glacial climate evolution

Sediment evidence from Lake Qinghai revealed two abrupt enhancements of catchment inflow, which occurred at 11.6 and 10 ka BP, respectively. They represent two events of monsoon rain penetration, as a consequence of reorganization of the Asian monsoon circulation. The temperature on the Plateau was an important factor of the land surface boundary conditions causing the summer monsoon penetration. Major shifts in temperature across the late Glacial/Holocene transition played an important role in affecting the changes of the P-E balance of Lake Qinghai (Yu and Kelts, 2002).

Based on the correlation of the proxy record of Lake Qinghai with records from closed-basin lakes with different dimensions and geographic locations in China, we found one common but profound and most interesting feature, that is, the early-Holocene warming along with lake expansion occurred in all selected lake sites at approximately 10 ka BP. These sites, other than Lake Qinghai, include 1) Lake Sumxi, western Tibet-Qinghai Plateau (Gasse et al., 1991), Lake Daihai (Xiao et al., 2004), Lake Huangqihai, Inner Mongolia (Yu et al., 2003; Li and Yu, 2002), and Lake Xinyun, Yunnan Province, SW China (Hodell et al., 1999). In addition, the Guliya ice core $\delta^{18}O$ record (Thompson et al., 1997) and the well-dated proxy record of the Baxie loess-paleosol section near Lanzhou (An et al., 1993) also point out an early-Holocene warming, which started at around 10 ka B.P. The Lake Qinghai record of relative dry conditions with high summer evaporation in the early Holocene is in general agreement with the pollen record of Lake Daihai and the carbonate and stable isotopic records of Lake Sumxi and Lake Huangqihai.

From 8 ka B.P., an increase in effective moisture at Lake Qinghai, as indicated by carbonate and pollen records, occurred synchronously at the site of Lake Daihai, Inner

Mongolia, where an expansion of forests is suggested by the pollen record (Xiao et al., 2004) similar to that from Lake Qinghai. From 7–4.1 ka BP, forest expanded to the largest extend in the area of Lake Qinghai, as suggested by the persistency of total tree pollen of around 50%. This indicates humid and warmer conditions, for the Lake Qinghai area today is dominated by steppe vegetation and almost treeless. However, the data of TCC, TN and TOC suggest that the ascending lake level along with a possible increase in temperature started from ~8 ka BP. Taking humidity as an important factor, we define the so-called "Holocene Climatic Optimum" on the NE Tibet-Qinghai Plateau as in the period between 8 and 4.1 ka BP.

The Holocene Climatic Optimum may have been punctuated by a severe cold and dry phase that affected climates across northern Africa, southern Asia, Europe, the Americas and Antarctica about 7.5 ^{14}C ka B.P., perhaps lasting for a century or two before a return to warmer and wetter conditions (Stager and Mayewski, 1997). The sediment evidence of Lake Qinghai shows a decreasing trend in TOC and TN from around 7.5 ^{14}C ka BP, implying a possible cool-down from the highest summer temperature of the Holocene, but definitely not a severe cold and dry phase. The temperatures during the period of 10-8 ka BP were considered to be overall similar to or somewhat higher than those at ~8-4.1 ka BP in the Lake Qinghai area. But effective moisture at ~8-4.1 ka was definitely lower, as evidenced by the lake-levels some 20 m shallower than those of today (Yu and Kelts, 2002). Therefore, the relatively dry phase at 10-8 ka B.P. (although wetter than the earlier phase between 10.7-10 ka BP) is excluded from the Holocene Climate Optimum at Lake Qinghai. In addition, it is not surprising to see differences among proxy records from different continents regarding timing of the "optimum", because climate systems and shifts of seasonality associated with insolation differ in different continents, latitudinal zones and hemispheres. Different interpretations for the Holocene Optimum of China (Shi et al., 1993; An et al., 2000) may also be related to difference in terms of definition of the "optimum". Nevertheless, the mid-Holocene climate provides an interesting period of the Holocene, highlighted as a direct analog for the study of contemporary climate change.

The lake level, water chemistry and limnological conditions of the last 4.1 ka are relatively stable, particularly if compared with the period of Late Glacial-to-Holocene transition. The magnitude of lake-level fluctuation in the last 4.1 ka could exceed 3 m that occurred in the past 40 years. The 40-year instrumental record shows a decreasing trend with a rate of 10 cm/a. An annual rate of lake-level change may however exceed 0.5 m, such as that occurred in the warm summer of 1989, when an abnormal but substantial increase in precipitation resulted in a 0.5 m increase of the lake level. While the detection by sediment proxy of the changes in the past 40 years requires further investigation, marked changes in sediment character present at the intervals of 64-75 cm in Q14B and of 66-78.5 cm in Q16C may indicate an event with more pronounced changes of the lake conditions in the past 4.1 ka.

The change of water depth in the past 4.1 ka ranged within ±4 m, as suggested by the sediment evidence from cores and paleoshorelines. This lake extent indicates much higher effective moisture than in the early Holocene and in the pre-Holocene stages, based on a comparison of paleo-lake levels reconstructed for each environmental stage. Yet, it is uncertain from sediment evidence that the lake level (also effective moisture) of the late Holocene is lower than that of the mid-Holocene, although pollen record implies a warmer
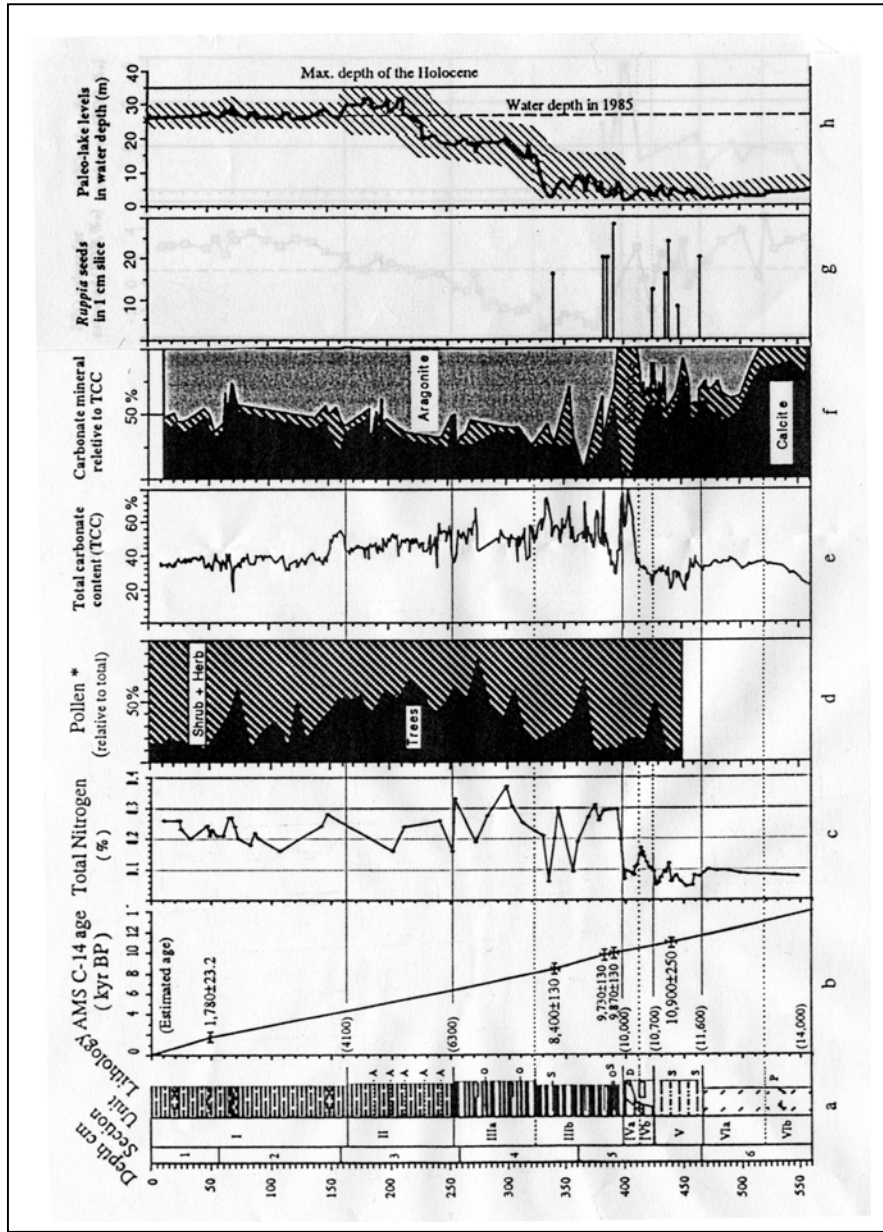
Figure 7.5 Multiple stratigraphic records of core Q14B and reconstructed water depth in the past 14 ka BP.

and probably wetter mid-Holocene climate. The late-Holocene alkalinity and salinity of the lake were lower than the early to mid-Holocene ones, as suggested by lowered TC and ostracod $\delta^{18}O$ values turning out to be essentially vertical to weakly negative (Lister et al., 1991). This may imply a deeper lake environment in addition to lowered summer evaporation as a consequence of decreased air temperature during the past 4.1 ka, due to the decline of solar insolation. The ostracod data from Lake Huangqihai suggest deeper lake conditions of the late Holocene until the 1950s, when the lake depth decreased, due to human disturbance (Li and Yu, 2002). The proxy data of carbonate content from Lake Xinyun, Yunnan province, NW China (Hodell et al., 1999) imply that the lake remained closed for most of the time between 10-3 ka BP with no connection to Lake Fuxian via the Gehe River like that of today. A number of proxy records in China proved that the climate of the late Holocene was colder than that of the mid-Holocene, but the state of effective moisture and in particular precipitation in the past 3-4 ka may require further investigations.

7.6 Summary and conclusions

Two high-quality piston cores (Q14B and Q16C) recovered from the central areas of the southern and eastern basins of Lake Qinghai are investigated using a multi-proxy approach in order to establish a continuous record of paleoenvironmental and paleoclimate changes on the NE Tibet-Qinghai Plateau for the past 14 ka. The sub-bottom sediment structures of the eastern basin, as revealed by a 3.5 kHz seismic profile, show an offlap sequence between two onlap sequences, suggesting that several major shifts in size and lake-level occurred during the deposition of the ca. 30 m sequence. Core Q87, drilled down to 26 m from the lake bottom at a site on the seismic profile near the center of the eastern basin, was then studied in order to test the hypothesis of a unified ice cover on the Plateau and for investigating paleoclimate conditions during the last Ice Age on the outer margin of today's Asian summer monsoon.

The seismic data and the AMS ^{14}C dated lithostratigraphic record suggest that during the period between ~68.7-28.8 ^{14}C ka BP, equivalent to the Marine Isotopic Stage 3 (MIS 3), Lake Qinghai was in wet but not in full glacial conditions. The MIS 3 here was relatively warmer, if compared with the LGM (MIS 2), but definitely colder than the Holocene. The lake began to shrink at approximately 44 ^{14}C ka BP. The deposition of windblown, loess-like sand (Unit 4) reflects extremely cold and arid climate conditions at ~28.8-18.3 ^{14}C ka BP. The drilling did not encounter any glacial moraine deposits, implying that glaciers on the NE Plateau did not advanced down to the elevation of 3160 m a.s.l. since the time of the MIS 3. The data imply that the glaciated areas during the MIS 3 were much larger than in the LGM. This interpretation is undesignedly in full agreement with that drawn from the evidence of newly dated glacial successions on the NE Tibet-Qinghai Plateau (Owen et al., 2002; Owen et al., 2003).

Sediment evidence excluded the possibility of large meltwater input into Lake Qinghai since ~14 ka BP, which might be the consequence of extreme aridity during the LGM. Three abrupt shifts in P-E balance across the late-Glacial-to-Holocene transition were clearly documented in the high-resolution record of the two piston cores. An arid event at ~10.7-10 ^{14}C ka BP is clearly archived, which is synchronous with the European Younger Dryas but not entirely coherent because cooling is not evident at the Lake Qinghai site

(refer to Chapter 5). The onset of a warm and wetter climate regime is dated at 10 ^{14}C ka B.P., which also marked the beginning of the Holocene expansion of Lake Qinghai. A correlation with proxy records from other closed-basin lakes in China indicates that this marked shift occurred also in Lake Huangqihai and Lake Daihai, Inner Mongolia; in Lake Sumxi, western Tibet-Qinghai Plateau; and in Lake Xinyun, Yunnan Province, SW China. The coherence and synchronousness of the abrupt shift represents a prominent change probably associated with the Asian monsoon circulation.

The abrupt onset of the early-Holocene climate regime is followed by a relative dry phase between 10-8 ^{14}C ka BP., if compared with conditions in the mid-Holocene. Relatively shallow lake conditions resulted from the highest summer evaporation with precipitation lower than that in the mid-Holocene. Warmer summer and colder winter brought about the deposition of the better-laminated sediments in the early to middle Holocene. The optimal Holocene conditions lasted from 8 to 4.1 ^{14}C ka BP. This is in general agreement with pollen records from northern China, where forests expanded northward as precipitation rose to values about 100 mm higher than today in the region (Winkle and Wang, 1993; An et al., 2000), although Gasse and Van Campo (1994) find evidence from lakes in Tibet and Rajasthan of a major dry phase somewhere between around 8 and 7 ka BP.

The conditions of Lake Qinghai since ~4.1 ka BP. remained similar to what it is today. The effective moisture is evidently higher than that of the early Holocene, as indicated by the reconstructed lake-levels. We are yet unconvinced by the evidence available regarding the question whether the effective moisture of the late Holocene is lower than that of the mid-Holocene. Further investigation may shed more light on this interesting issue.

8. Acknowledgement

In the autumn of 2000, I gave an oral presentation on the paleoclimate of Lake Qinghai in a PAGES conference in Prague, where I met Prof. Stephan Kempe. In the meeting, our common interest on paleoclimate of large, closed-basin lakes aroused my enthusiasm to resume the thesis study on Paleoenvironment and Paleoclimate of Lake Qinghai. The resume did not become a reality until the January of 2004, following a 3-month visit to TU-Darmstadt. My sincere thanks go to Prof. Fuess, the Dean of the time, Department of Material and Geosciences, University of Technology, Darmstadt, for granting me admission into the doctoral program, and to Profs. Stephan Kempe, Andreas Hoppe, Matthias Hinderer for a strong backing of the admission.

I had wonderful time during my stay in the Institute of Applied Geosciences for the thesis study. I wish to thank all professors, research associates, administrative and technical staff, and graduates for being always friendly and helpful. In particular, I would like to thank Prof. Hinderer for allowing me using his book collections on sedimentology and for helpful discussions, Thomas Nix and Christian Lerch for sharing their experience on the procedural completion of a TUD thesis, Stephan Lang for technical assistance in improving my knowledge of using CorelDRAW, Jens Hartmann for introducing the PHREEQC, Petra Kraft for prompt assistance in getting copies of some published papers, Monika Hofmann for providing GIS information, Ulrike Simons, Sunita Saggu, Markus Schmitt, and Andreas Koppe for technical assistance, Frau Hirsmueller for her help with scanning materials. I am grateful to Frau Herrmann for her help with finding accommodation, and to Frau Relaford at the Dean's office and Frau Pooya at the university administration for their help in my gaining a better understanding on the TUD regulations.

Above all appreciations, my grateful thanks are due to Prof. Kempe for all his help. The dissertation could not be substantially improved without his making careful corrections and suggestions. Hospitality generously provided by both Stephan and Christhild made my first visit to TUD like at home: warmly meeting me and seeing me off at the Frankfort airport, touring me around Frankfurt and adjacent areas, and organizing home parties in Dieburg, inviting me having dinners in restaurants and so on. I appreciate it.

My graduate students, Ziting Liu, Wei Cai and Liang Chen, helped with collecting papers from Chinese Journals. I thank my wife, Lisa, for her unconditional support. During my absence from China, my daughter, Lucy, managed by herself and obtained admission into the Master's program of actuarial science at University of Wisconsin-Madison. I am proud of her!

Finally, I would like to dedicate this thesis to Prof. Kerry Kelts, former director (1990-2000) of Limnological Research Center, University of Minnesota, in memory of his great contribution to Limnogeology. He guided me into the field of Past Global Changes in using lake sediments as environmental archives.

9. REFERENCES

An, Z.S., S.C. Porter, W. Zhou, Y. Lu, D.J. Donahue, M.J. Head, X. Wu, J. Ren & H. Zheng, 1993. Episode of strengthened summer monsoon climate of Younger Dryas age on the Loess Plateau of Central China. Quaternary. Research, 39: 45-54.

An, Z.S. and S. Porter, 1997. Millennial-scale climatic oscillations during the last interglaciation in central China. Geology, 25: 603-607.

An, Z.S. 2000. The history and variability of the East Asian paleomonsoon climate. Quaternary Science Reviews, 19: 171-187.

An, Z.S., S.C. Porter, J. E. Kutzbach, X.H. Wu, S.M. Wang, X.D. Liu, X.Q. Li, W.J. Zhou, 2000. Asynchronous Holocene optimum of the East Asian monsoon. Quaternary Science Reviews, 19: 743-762.

An, Z.S., J.E. Kutzbach, W.L. Prell, S.C. Porter, 2001. Evolution of Asian monsoons and phased uplift of the Himalayas-Tibetan Plateau since Late Miocene times. Nature, 411: 62-66.

Andrews, J.T. and A.E. Jennings, 1987. Influence of sediment source and type on the magnetic susceptibility foird and shelf deposits, Baffin Island and Baffin Bay, N.W.T. Canadian Journal of Earth Sciences, 24: 1386-1401.

Appleby, P.G. and F. Oldfield, 1992. Application of ^{210}Pb to sediment studies. In: M. Ivanovich and R. Harmon (Editors), Uranium Series Disequilibrium: Application to Earth, Marine, and Environmental Studies. Clarendon Press, Oxford, 731-738.

Barker, P., 1991. Differential diatom dissolution in late Quaternary sediments from Lake Manyara, Tanzania: an experimental approach. Journal of Paleolimnology, 7: 235-251.

Bush, A.B.G., 2001. Pacific sea surface temperature forcing dominates orbital forcing of the early Holocene monsoon. Quaternary Research, 55: 25-32.

Bengtsson, L. & M. Enell, 1986. Chemical analysis. In B. E. Berglund (ed.), Handbook of Holocene Palaeoecology and Palaeohydrology. John Wiley & Sons, Chichester: 423-451.

Bennett, K.D., S.G. Haberle, S.H. Lumley, 2000. The last glacial-Holocene transition in southern Chile. Science, 290: 325-328.

Berger, W.H., 1990. The Younger Dryas cold spell — a quest for causes. Palaeogeogr., Palaeoclimatol., Palaeoecol. 89: 219-237.

Bishoff, J.L. and W.S. Fyfe, 1968. Catalysis, inhibition, and the calcite-aragonite problem. The aragonite-calcite transformation. Am. J. Sci., 266: 65-79.

Bishoff, J.L., 1968. Temperature controls on aragonite-calcite transformation in aqueous solution. Am. Mineral., 54: 149-155.

Bond, G., W.S. Broecker, S. Johnson, J. McManus, L. Labeyrie, J. Jouzel, G. Bonani, 1993. Correlation between climate records from North Atlantic sediments and Greenland ice. Nature, 365: 143-147.

Brenner, M. K. Dorsey, X. Song et al., 1991. Paleolimnology of Qilu Hu, Yunnan Province, China, Hydrobiologia, 214: 333-340.

Brenner, M., T.J. Whitmore, X. Song et al., 2000. Sediment records from Qilu Hu and Xingyun Hu, Yunnan Province, China: late Pleistocene to present. In: E.H. Gierlowski-Kordesch and K. Kelts (Editors), Lake Basin through Space and Time. The American Association of Petroleum Geologists, Tulsa, Oklahoma, USA. 619-624.

Brock, M.A. & J.A. K. Lane, 1983. The aquatic macrophyte flora of saline wetlands in Western Australia in relation to salinity and permanence. Hydrobiologia 105: 63-76.

Broecker, W.S., M. Andree, W. Woelfli, H. Oeschger, G. Bonani, J. Kennett and D. Peteet, 1988. The chronology of the last deglaciation: implications to the cause of the Younger Dryas event. Paleoceanography, 3: 1-19.

Broecker, W.S., 2000. Abrupt climate change: causal constraints provided by the paleoclimate record. Earth-Science Reviews, 51: 137-154.

Carlson, W.D., 1983. The polymorphs of $CaCO_3$ and the aragonite-calcite transformation. Rev. Mineral., 11: 191-225.

Chai, L., A. Navrotsky and R.J. Reeder, 1995. Energetics of calcium-rich dolomite. Geochimica et Cosmochimica Acta, 59: 939-944.

Chang, C.-P. (editor), 2004. East Asian Monsoon. World Scientific, 572pp.

Chao et al, 1981. Origion and evolution of schizothracine fishes in relation to the upheaval of Qinghai-Xizang Plateau. Proceedings on the Qinghai-Xizang (Tibet) Plateau. Geological and Ecological Studies 2: 1053-1060. Science Press, Beijing (in Chinese).

Chen, K.Z. and J.M. Bowler, 1986. Late Pleistocene evolution of salt lakes in the Qaidam Basin, Qinghai Province, China. Palaeogeography, Palaeoclimatology, Palaeoecology, 54: 87-104.

Chen, K.Z., J.M. Bowler, K. Kelts, 1990. Paleoenvironmental evolution in the past 40 ka in the Tibet-Qinghai Plateau, Quaternary Sciences, 1990/1: 21-31 (in Chinese).

Chen, M.-T., H.-W. Ho, T.-D. Lai, L.F. Zheng, Q.M. Miao, K.-S. Shea, M.-P Chen, P.X. Wang, K.-Y. Wei, C.-Y. Huang, 1998. Recent planktonic foraminifers and their relationships to surface ocean hydrography of the South China Sea. Marine Geology, 146: 173-190.

Chen, M.-T., C.-H. Wang, C.-Y. Huang, P. Wang, L. Wang, M. Sarnthein, 1999. A late Quaternary planktonic foraminifer faunal record of rapid climatic changes from the South China Sea. Marine Geology, 156: 85-108.

Clemens, S., P.X. Wang, W. Prell, 2003. Monsoon and global linkages on Milankovitch and sub-Milankovitch time scales. Marine Geology, 201: 1-3.

CLIMAP members, 1981. Seasonal reconstruction of the earth's surface at the last glacial maximum. Geol. Soc. Am. Map Chart Ser. MC-36. Geological Society of America Boulder, Colorado, USA.

COHMAP Members, 1988. Climatic changes of the last 18,000 years: Observations and model simulations. Science, 241: 1043-1052.

Colman, S. (Editor), 1996. Continental Drilling for Paleoclimatic Records. PAGES Workshop Report 96-4.

Craig, H., 1965. The measurement of oxygen isotope paleotemperature. In E. Tongiorgi (ed.), Stable isotopes in oceanographic studies and paleotemperatures.Cons. Naz. Rich. Lab. Geol. Nucl., Pisa: 9-130.

Dansgaard, W., H. Clausen, N. Gundestrup, C. Hammer, S. Johnson, P. Kristinsdottir & N. Reeh, 1982. A new Greenland ice core. Science 218: 1273-1277.

Dansgaard, W., J. W.C. White & S. J. Johnson, 1989. The abrupt termination of the Younger Dryas climate event. Nature 339: 532-534.

De Deckker, P., 1988. Biological and sedimentary facies of Australian salt lakes. Palaeogeography, Palaeoclimatology, Palaeoecology, 62: 237-270.

De Deckker, P. and R.M. Forester, 1988. The use of ostracodes to reconstruct continental paleoenvironmental records. In: De Deckker, P., J.P. Colin and J.P. Peypouquet (Editors), Ostracoda in the Earth Sciences. Elsvier, New York, 175-199.

Ding, Z.L., N.W. Rutter, J.T. Han, 1992. A coupled environmental system formed at about 2.5 Ma over East Asia. Palaeogeography, Palaeoclimatology, Palaeoecology, 94: 223-242.

Ding, Z.L., Z. Yu, N. Rutter, and T.S. Liu, 1994. Towards and orbital time scale for Chinese loess deposits. Quaternary Science Reviews, 13: 39-70.

Dodson, J.R., D. Taylor, Y. Ono, P. Wang, 2004. Climate, human, and natural systems of the PEP II transect. Quaternary International, 118-119: 3-12.

Du, N.Q., Z.C. Kong, F.S. Shan, 1989. A prelimilary investigation on the vegetational and climatic changes since 11,000 years in Qinghai Lake — An analysis based on palynology in core QH85-14C. Acta Botanica Sinica, 31: 803-814 (in Chinese).

Engstrom, D.R. and S.R. Nelson, 1991. Paleosalinity from trace metals in fossil ostracodes compared with observational records at Davils Lake, North Dacoda, USA. Palaeogeography, Palaeoclimatology, Palaeoecology, 83: 295-312.

Eugster, H. and K. Kelts, 1983. Lacustrine chemical sediments. In: A.S. Goudie and K. Pye (Editors), Chemical Sediments and Geomorphology, Academic Press, London, p 321-368.

Fang, J.Q., 1991. Lake evolution during the past 30,000 years in China, and its implications for environmental change. Quaternary Research, 36: 37-60.

Faure, G. 1986. Principles of Isotope Geology. John Wiley. New York, 486 pp.

Flohn, H., 1968. Contributions to a meterorology of the Tibetan Highlands. Journal of Atmospheric Sciences Papers, 130, 120pp.

Fontes, J.C., F. Melidres, E. Gibert et al., 1993. Stable isotope and radiocarbon balances of two Tibetan lakes (Sumxi Co, Longmu Co) from 13,000 B.P. Quaternary Science Reviews, 12: 875-887.

Frisia, S. 1999a. Dolomite and dolomitization. In: Clare P. Marshall, Rhodes W. Fairbridge (editors), Encyclopedia of Geochemistry. Kluwer Academic Publishers, Dordrecht.

Frisia, S., 1999b. Calcium carbonate and the carbonic acid system. In: Clare P. Marshall, Rhodes W. Fairbridge (editors), Encyclopedia of Geochemistry. Kluwer Academic Publishers, Dordrecht.

Gagan, M.K., E.J. Hendy, S.G. Haberle, W.S. Hantoro, 2004. Post-glacial evolution of the Indo-Pacific Warm Pool and El Niño-Southern oscillation. Quaternary International, 118-119: 127-143.

Gasse, F., M. Arnold, J.C. Fontes, M. Firt, E. Gibert, A. Huc, B.Y. Li, Y.F. Li, Q. Liu, F. Melieres, E. Van Campo, F. B. Wang & Q. S. Zhang, 1991. A 13,000-year climate record from western Tibet. Nature, 353: 742-745.

Gasse, F., J. Ch. Fontes, E. Van Campo, K. Wei, 1996. Holocene environmental changes in Bangong Co Basin (Western Tibet). Part 4: Discussion and conclusions. Palaeogeogr., Palaeoclimatol., Palaeoecol., 120: 79-92.

Gasse F. & Van Campo E. (1994). Abrupt post-glacial climate events in west Asia and North Africa monsoon domains. Earth and Planetary Sciences Letters, 126: 435-456.

Gat, J.R., 1981. Lakes. In: J.R. Gat and R. Gonfiantini (Editors), Stable Isotope Hydrology: Deuterium and Oxygen-18 in the Water Cycle. I.A.E.A. Tech. Rep., 210: 203-221.

Geological Survey of QHP, 1991. Regional Geology of Qinghai Province. Geological Memoirs Series 1, No 24, Geological Publishing House, Beijing. pp. 661 (in Chinese).

Gierlowski-Kordesch, E.H. and K.R. Kelts (Editors), 2000. Lake Basins through Space and Time. The American Association of Petroleum Geologists, Tulsa, Oklahoma, USA. 648pp.

Goldsmith, J.R. and D.L. Graf, 1961. Relation between lattice constants and composition of the Ca-Mg carbonates. Am. Minerl., 43: 84-101.

Gonfiantini, R., 1986. Environmental isotopes in lake studies. In: Fritz P, Fontes J C, eds. Handbook of environmental isotope geochemistry, Vol. 2, The terrestrial environment. Amsterdam: ELSEVIER, pp. 113-168.

Grossman, E.L. & T.-L. Ku, 1986. Oxygen and carbon stable isotope fractionation in biogenic aragonite: temperature effect. Chemical Geology, 59: 59-74.

Guo, Z.T., W.F. Ruddiman, Q.Z. Hao, H.B. Wu, Y.S. Qiao, R.X. Zhu, S.Z. Peng, J.J. Wei, B.Y. Yuan, T.S. Liu, 2002. Onset of Asian desertification by 22 Myr ago inferred from loess deposits in China. Nature, 416: 159-163.

Hahn, D.G., and S. Manabe, 1975. The role of mountains in the south Asian monsoon circulation. Journal of Atmospheric Sciences, 32: 1515-1541.

Hammer, U.T, J.M. Heseltine, 1988. Aquatic macrophytes in saline lakes of the Canadian prairies[J]. Hydrobiologia, 158:101-116.

Hardie, L.A. 1987. Dolomitization: A critical view of some current views. Journal of Sedimentary Petrology, 57: 166-183.

Heller, F. and T.S. Liu, 1982. Magnetostratigraphic dating of loess deposits in China. Nature, 300: 431-433.

Herzschuh, U., C.Zhang, S. Mischke et al., 2005. A Late Quaternary lake record from the Qilian Mountain (NW China): evolution of the primary production and the water depth

reconstructed from macrofossil, pollen, biomarker and isotope data. Global and Planetary Change, 46: 361-379.

Hodell, D.A., M. Brenner, S.L. Kanfoush, J.H. Curtis, J.S. Stoner, X.L. Song, Y. Wu, T.J. Whitmore, 1999. Paleoclimate of southwestern China for the past 50,000 yr inferred from lake sediment records. Quaternary Research, 52: 369-380.

Holms, J.A., 1996. Trace-element and stable isotope geochemistry of non-marine ostracod shells in Quaternary paleoenvironmental reconstruction. Journal of Paleolimnology 15: 223-235.

Huang, C.-Y., P.-M. Liew, M.-X. Zhao, T.-C. Chang, C.M. Kuo, M.-T. Chen, C.-H. Wang, L.-F. Zheng, 1997. Deep-sea and lake records of the southeast Asian paleomonsoons for the last 25 thousand years. Earth and Planetary Science Letters, 146: 59-72.

Jian, Z.M., B. Huang, W. Kuhnt, H.-L. Lin, 2001. Late Quaternary upwelling intensity and east Asian monsoon forcing in the South China Sea. Quaternary Research, 55: 363-370.

Jiang, X.Z., X.D. Tang, S.M. Wang, 1999. Sedimentary characteristics and climatic evolution of core HQ in Heqing basin, Yunnan province. Journal of Geomechanics, 4: 6-81.

Kazmierczak, J. And S. Kempe, 1990. Modern cyanobacterial analogues of Paleozoic stromatoporoids. Science, 250: 1244-1248.

Kelts, K., K.Z. Chen, G.S. Lister, J.Q. Yu, Z.H. Gao, F. Niessen & G. Bonani, 1989. Geological fingerprints of climate history: a cooperative study of Qinghai Lake, China. Eclogae Geol. Helv., 82: 167-182.

Kelts, K.R., U. Briegel, K. Ghilardi & K.J. Hsu, 1986. The limnogeology-ETH coring system. Schweiz. Z. Hydrol. (Swiss Journal of Geosciences) 48: 104-116.

Kempe, S. and J. Kazmierczak, 1990. Chemistry and stromatolites of the sea-linked Satonda Crater Lake, Indonesia: A recent model for the Precambrian Sea? Chemical Geology, 81: 299-310.

Kempe, S. and J. Kazmierczak, 1990. Calcium Carbonate Supersaturation and the Formation of in situ Calcified Stromatolites. In Ittekkot, V., S. Kempe, W. Michaelis. A. Spitzy (Editors): "Facets of Modern Biogeochemistry". 255-278, Berlin, Springer -Verlag.

Kempe, S., J. Kazmierczak, G. Landmann, T. Konuk, A. Reimer and A. Lipp, 1991. Largest known microbialites discovered in Lake Van, Turkey. Nature, 349: 605-608.

Kempe, S., Landmann, G. & Müller, G., 2002. A floating varve chronology from the Last Glacial Maximum terrace of Lake Van/Turkey. – Zeitschr. Geomorphol., Supplem. 126 Research in Mountains and Deserts of Africa and Central Asia: 97-114.

Kempe, S. and J. Kazmierczak, 2003. Modern Soda Lakes: Model Environments for an Early Alkaline Ocean. – In: Müller, T. & Müller, H. (editors.) "Modelling in Natural Sciences; Design, Validation and Case Studies": 309-322; Springer Verlag, Berlin, Heidelberg.

Kong, Z.Z., N.Q. Du, F.S. Shan, 1990. Vegetational and climatic changes in the last 11,000 years in Qinghai Lake—numerical analysis based on palynology in core QH85-14C. Marine and Quaternary Geology, 10: 79-90 (in Chinese).

Krishnaswamy, S. and Lal, D., 1971. Goechronology of lake sediments. Earth Planetary Science Letters, 11:407-414.

Kudrass, H.R., H. Erlenkeuser, R. Vollbrecht and W. Weiss, 1991. Global nature of the Younger Dryas cooling event inferred from oxygen isotope data from Sulu Sea cores. Nature, 349: 406-409.

Kuhle, M., 1987. Subtropical Mountain- and Highland-Glaciation as Ice Age Triggers and the Waning of the Glacial Periods in the Pleistocene. In: GeoJournal 14 (4): 393-421.

Kuhle, M., 2003. New geomorphological indicators of a former Tibetan ice sheet in the central and northeastern part of the high plateau. Zeitschrift für Geomorphologie N.F. Suppl.-Vol. 130: 75-97.

Kuhle, M., 2004. The High Glacial (Last Ice Age and LGM) ice cover in High and Central Asia. In: Ehlers, J.; and P.L. Gibbard, (Editors). Quaternary Glaciation - Extent and Chronology, Part III: South America, Asia, Africa, Australia, Antarctica, 175-199. Elsevier B.V., Amsterdam.

Kukla, G., and Z.S. An, 1989. Loess stratigraphy in central China. Palaeogeography, Palaeoclimatology, Palaeoecology, 72: 203-223.

Landmann, G., A. Reimer, G. Lemcke. S. Kempe, 1996. Dating late glacial abrupt climate changes in the 14,470 yr long continuous varve record of Lake Van, Turkey. Palaeogeography, Palaeoclimatology, Palaeoecology, 122: 107-118.

Lanzhou Institute of Geology et al., 1979. Qinghai Lake Monograph of the 1961 Expedition. Science Press Series, Beijing (in Chinese).

Last, W. 1990. Lacustrine dolomite: an overview of modern, Holocene, and Pleistocene occurrences. Earth-Science Reviews, 27: 221-263.

Last, W.M., J.P. Smol (Editors). 2001. Tracking Environmental Change Using Lake Sediments, Volume 2: Physical and Geochemical Methods. Kluwer Academic Publishers, Dordrecht/Boston/London, 504pp.

Last, W.M., J.P. Smol (Editors). 2001. Tracking Environmental Change Using Lake Sediments, Volume 1: Basin Analysis, Coring, and Chronological Techniques. Kluwer Academic Publishers, Dordrecht/Boston/London, 548pp.

Lau, K.M. and M.T. Li, 1984. The monsoon of East Asia and its global association—A survey. Bulletin of American Meteorological Society, 65: 114-125.

Liew, P.-M. and S.-Y. Huang, 1994. A 5000-year pollen record from Chitsoui Lake, central Taiwan. TAO, 5: 411-419.

Liew, P.-M., C.M. Kuo, S.Y. Huang, M.H. Tseng, 1998. Vegetation change and terrestrial carbon storage in eastern Asia during the last Glacial Maximum as indicated by a new pollen record from central Taiwan, Global and Planetary Change, 16-17: 85-94.

Li, J. and Yu, J.Q., 2002: Lake Huangqihai, Inner Mongolia: A palaeoenvironmental record deduced from Ostracoda and stable isotope composition of Ostracods shells. Journal of Salt Lake Research 10 (4): 13-18 (in Chinese).

Li, S.H., 1959. A preliminary investigation on the type, biological productivity and evolution of Lake Qinghai. Proceedings of 2nd Congress of the West Pacific Fishery Society.

Linsley, B.K. and R.C. Thunell, 1990. The record of deglaciation in the Sulu Sea: Evidence for the Younger Dryas event in the tropical western Pacific. Paleoceanography, 5: 1025-1036.Li, H.-C. and T.-L. Ku, 1997. $\delta^{13}C$-$\delta^{18}O$ covariance as a paleohydrological indicator for closed-basin lakes. Palaeogeography, Palaeoclimatology, Palaeoecology, 133: 69-80.

Lister, G.,K. Kelts, K.Z. Chen, J.Q. Yu & F. Niessen, 1991. Lake Qinghai, China: closed-basin lake levels and the oxygen isotopic record for ostracoda since the latest Pleistocene. Palaeogeogr., Palaeoclimatol., Palaeoecol. 84: 141-162.

Lister, G.S. 1988. Stable isotopes from lacustrine Ostracoda as tracers for continental paleoenvironments. In: De Deckker, P., J.P. Colin and J.P. Peypouquet (Editors), Ostracoda in the Earth Sciences. Elsvier, New York: 201-218.

Lister, G.S., K.R. Kelts, R. Schmidt, G. Bonani, M. Nessi, M. Suter & W. Woelfli, 1984. Correlation of paleoclimatic record in lacustrine sediment sequences: ^{14}C dating by AMS. Nucl. Instrum. Methods Phys. Res. B5: 389-393.

Liu, J.H., H.X. Xiao F.M. Lei et al., 2005. Highly pathogenic H5N1 influenza virus infection in migratory birds. Science, July 6, 2005 (in press).

Liu, G.X., Y.P. Shen, W. Rui, S.M. Wang, 1995. The vegetation and climatic changes in Zoige during the last 20,000 years determined by pollen records. Journal of Glaciology and Geocryology, 17: 132-137 (in Chinese).

Liu, G.X., Y.P. Shen, P.Z. Zhang, S.M. Wang, 1994. Pollen record and its palaeoclimatic significance between 800-150 ka B.P. from RH-core in Zoige basin in Qinghai-Xizang (Tibet) Plateau. Acta Sedimentologica Sinica, 12: 101-109.

Liu, X.M., T.S. Liu, T.C. Xu, C. Liu, M.Y. Chen, 1988. The Chinese loess in Xifeng, I. The primary study on magnetostratigraphy of a loess profile in Xifeng area, Gansu province. Geophysical Journal, 92: 345-348.

Liu, T.S. (editor), 1985. Loess and Environment. China Ocean Press, Beijing, 234pp.

Liu, T.S. and Z.L. Ding, 1998. Chinese loess and the paleomonsoon. Annual Review of Earth and Planetary Sciences, 26: 111-145.

Liu, T.S., Z.L. Ding and N. Rutter, 1999. Comparison of Milankovitch periods between continental loess and deep sea records over the last 2.5 Ma. Quaternary Science Reviews, 18: 1205-1212.

Liu, Z.F., A. Trentesaux, S.C. Clemens, C. Colin, P.X. Wang, B.Q. Huang, S. Boulay, 2003. Clay mineral assemblages in the northern Southern China Sea: implications for East Asian monsoon evolution over the past 2 million years. Marine Geology, 201: 133-146.

Liu, Z.T. and J.Q. Yu, 2005. Application of *Ruppiaceae* L. to the the study of lake-level reconstruction and environmental change. Journal of Salt Lake Research, 13: (in press).

Lowe, J.J., J.M. Gray & J.E. Robinson, (Editors), 1980. Studies in the Late-Glacial of North-West Europe. Pergamon, Oxford.

Lu, H.Y., F.Q. Zhang, X.D. Liu, R.A. Duce, 2004. Periodicities of paleoclimatic variations recorded by loess-paleosol sequences in China. Quaternary Science Reviews, 23: 1891-1900.

Ma, Z.B., Z.H. Wang, J.Q. Liu, B.Y. Yuan, J.L.Xiao, G.P. Zhang, 2004. U-series chronology of sediments associated with Late Quaternary fluctuations, Balikun Lake, northwestern China. Quaternary International, 121:89-98.

Maloney, B.K., 1996. Evidence for the Younger dryas climatic event in South-east Asian. Quaternary science Reviews, 14: 949-958.

McKenzie, J. 1991. The Dolomite Problem: An outstanding controversy. In: D.W. Muller, J.A. McKenzie, H. Weissert (Editors), Controversies in Modern Geology, Academic Press, London, pp. 35-54.

McManus, J.F., G.C. Bond, W.S. Broecker, S. Johnson, L. Labeyrie, S. Higgins, 1994. High resolution climate records from the North Atlantic during the last interglacial. Nature, 371: 326-327.

Meyer P A & Horie S. 1993. An organic carbon isotopic record of glacial-postglacial change in atmospheric pCO2 in the sediments of Lake Biwa, Japan. Palaeogeography, Palaeoclimatology, Palaeoecology, **105**: 171-1178.

Mingram, J., J.R.M. Allen, C. Bruechmann et al., 2004. Maar- and crater lakes of the Long Gang Volcanic Field (N.E. China)—overview, laminated sediments, and vegetation history of the last 900 years. Quaternary International, 123-125: 135-147.

Mingram, J., G. Schettler, N. Nowaczyk et al., 2004. The Huguang maar lake—a high-resolution record of palaeoenvironmental and palaeoclimatic change over the last 78,000 years from South China. Quaternary International, 122: 85-107.

Mischke, S., U. Herzschuh, C. Zhang, J. Bloemendal, F. Riedel, 2005. A late Quaternary lake record from the Qilian Mountain (NW China): lake level and salinity changes inferred from sediment properties and ostracod assemblages. Global and Planetary Change, 46: 337-359.

Molnar, P. and P. Tapponnier, 1975. Cenozoic tectonics of Asia. Science, 189: 419-426.

Morse, J.W., 1983. The kinetics of calcium carbonate dissolution and precipitation. Rev. Mineral., 11: 227-264.

Müller, G., G. Irion and U. Forstner, 1972. Formation and diagenesis of inorganic Ca-Mg carbonates in the lacustrine environment. Naturwissenschaften, 59/4: 158-164.

O'Neil, J.R., and S. Epstein, 1966. Oxygen isotope fractionation in the system dolomite-calcite-carbon dioxide. Science, 152: 198-201.

Owen, L.A., R.C. Finkel, M.W. Caffee, 2002. A note on the extent of glaciation throughout the Himalaya during the global Last Glacial Maximum. Quaternary Science Reviews, 21: 147-157.

Owen, L.A., R.C. Finkel, H.Z. Ma, J.Q. Spencer, E. Derbyshire, P.L. Barnard, M.W. Caffee, 2003. Timing and style of late Quaternary glaciation in northeastern Tibet. Geological Society of America Bulletin, 115: 1356-1364.

Oxburgh, R., W.S. Broecker, R.H. Wanninkhof, 1991. The carbon budget of Mono Lake. Global Biogeochem. Cycles, 5: 359-372.

Peck, J.A., J.W. King, S.M. Colman, V.A. Kravchinsky, 1994. A rock-magnetic record from Lake Baikal, Siberia: Evidence for late Quaternary climate change. Earth and Planetary Science Letters, 122: 221-238.

Peteet, D., 1992. The palynological expression and timing of the Younger Dryas event —Europe versus eastern North America. In: Bard, E., and W. Broecker (Editors), The Last Deglaciation and Radiocarbon Chronologies, Springer-Verlag Berlin Heidelberg. pp. 327-344.

Plummer, L.N., Parkhurst, D.L., Fleming, G.W., and Dunkle, S.A., 1988, A computer program incorporating Pitzer's equations for calculation of geochemical reactions in brines: U.S. Geological Survey Water-Resources Investigations Report 88-4153, 310 pp.

Porter, S.C. and Z.S. An, 1995. Correlation between climate events in the north Atlantic and China during the last glaciation. Nature, 375: 305-308.

Prell, W.L. and J.E. Kutzbach, 1992. Sensitivity of Indian monsoon to forcing parameters and implication for its evolution. Nature, 360: 647-653.

Roberts, N., 1989. The Holocene – An Environmental History. Basil Blackwell, Oxford, UK. 227pp.

Ruddiman, W.F., (editor), 1997. Tectonic Uplift and Climate Change, Plenum Press, N.Y.

Scoffin, T.P. 1987. An Introduction to Carbonate Sediments and Rocks. Blackie, New York.

Shackleton, N.J., J. Backman, H. Zimmerman, D.V. Kent, M.A. Hall, D.G. Roberts, D. Schneiter, J.G. Baldauf, A. Desrairies, P. Homrighhausen, P. Huddlestun, J.B. Keene, A.J. Kaltenback, K.A.D. Krumsiek, A.C. Morton, J.W. Murray, J. Westberg-Smith, 1984. Oxygen isotope calibration of the onset of ice-rafting and history of glaciation in the North Atlntic region. Nature, 307: 620-623.

Shen Ji, R. Matsumoto, S.M. Wang, Y.X. Zhu, Quantitative reconstruction of the paleosalinity in the Daihai Lake, Inner Mongolia, China. Chinese Science Bulletin, 2001, 46(1): 73-76.

Shen, J., X.Q. Liu, S.M. Wang, R. Matsumoto, Y.X. Zhu, 2002. Quantitative reconstruction of the lake water paleotemperature of Daihai Lake, Inner Mongolia, China and its significance in paleoclimate. Science in China Series D, 45(9): 792-800.

Shen, J., L.Y. Yang, X.D. Yang, R. Matsumoto, G.B. Tong, Y.X. Zhu, Z.K. Zhang, S.M. Wang, 2005. Lake sediment record on climate change and human activities since the Holocene in Erhai catchment, Yunnan Province, China, Science in China Series D, 48(3): 353-363.

Shi, Y.F., Z.Z Kong, S.M. Wang, L.Y. Tang, F.B. Wang, T.D. Yao, X.T. Zhao, P.Y. Zhang, S.H. Shi, 1993. Mid-Holocene climates and environments in China. Global and Planetery Change, 7: 219-233.

Shi, Y.F., B.X. Zheng, S.J. Li, 1992. Last glaciation and maximum glaciation in the Qinghai-Xizang (Tibet) Plateau: A controversy to M. Kuhle's ice sheet hypothesis. Zeitschrift fur Geomorphologie. N.F. Supplement Band 84: 19-35.

Shi, Y.F., 1992. Glaciers and glacial geomorphology in China. Zeitschrift fur Geomorphologie. N.F. Supplement Band 86: 51-63.

Shi, Y.F., G. Yu, X.D. Liu, B.Y. Li, T.D. Yao, 2001. Reconstruction of the 30-40 ka BP enhanced Indian monsoon climate based on geological records from the Tibetan Plateau. Palaeogeography, Palaeoclimatology, Palaeoecology, 169: 69-83.

Shi, Y.F., 2002. Characteristics of late Quaternary monsoonal glaciation on the Tibetan Plateau and East Asia. Quaternary International, 97-98: 79-91.

Siegenthaler, U., U. Eicher, H. Oeschger & W. Dansgaard, 1984. Lake sediments as continental [18]O records from the glacial/post-glacial transition. Ann. Glaciology, 5: 149-152.

Siegenthaler, U. and U. Eicher, 1986. Stable carbon and oxygen isotope analyses. Handbook of Holocene Palaeoecology and Palaeohydrology. Wiley, Chichester. 407-422.

Singer, C., J. Shulmeister, B. McLea, 1998. Evidence against a significant Younger Dryas cooling event in New Zealand. Science, 281: 812-814.

Smol, J., H.J.B. Birk, W.M. Last (Editors). Tracking Environmental Change Using Lake Sediments, Volume 3: Terrestrial, Algal, and Siliceous Indicators. Kluwer Academic Publishers, Dordrecht/Boston/London, 371pp.

Snowball, I. F., 1993. Geochemical control of magnetite dissolution in subarctic lake sediments and the implications for environmental magnetism. Journal of Quaternary Science, 8 (4): 339-346.

Stage 3 Project, 2002. Editorial: The Stage 3 Project. Quaternary Research, 57: 1.

Stager, J.C. and P.A. Mayewski, 1997. Abrupt Early to Mid-Holocene Climatic Transition Registered at the Equator and the Poles. Science, 276: 1834-1836.

Steinke, S., M. Kienast, U. Pflaumann, M. Weinelt, K. Stattegger, 2001. A high-resolution sea surface temperature record from the tropical South China Sea (16,500-3000 yr B.P.). Quaternary Research, 55: 352-362.

Steig, E.J., 1999. Mid-Holocene climate change. Science, 286: 1485-1487.

Stein, R., 1991. Accumulation of organic carbon in marine sediments. Springer-Verla, Berlin.

Stiller, M., G.E. Hutchinson, 1980. The Waters of Merom: a study of Lake Huleh, 1. Stable isotopic composition of carbonates of a 54 m core: Paleoclimatic and paleotrophic implication. Arch. Hydrobiol., 89: 275-302.

Street-Parott, F.A. and S. Harrison, 1985. Lake levels and climate reconstruction. In: A.D. Hecht (Editor), Paleoclimate Analysis and Modeling. Wiley New York, NY, pp. 291-340.

Stuiver, M. 1970. Oxygen and carbon isotope ratios of freshwater carbonates as climatic indicators. J. Geophys. Res. 75: 5247-5257.

Stuiver, M., P. J. Reimer, E. Bard, J. W. Beck, G. S. Burr, K. A. Hughen, B. Kromer, F. G. McCormac, J. v.d. Plicht & M. Spurk, 1998. INTCAL98 Radiocarbon age calibration 24,000-0 cal BP. Radiocarbon, 40: 1041-1083.

Stuiver, M., and Reimer, P. J., 1993, Extended 14C database and revised CALI radiocarbon calibration program, Radiocarbon 35:215-230.

Sun, X.J., X. Li, H.-J. Beug, 1999. Pollen distribution in hemipelagic surface sediments of South China Sea and its relation to modern vegetation distribution. Marine Geology, 156: 211-226.

Sun, X.J., Y. Luo, F. Huang, J. Tian, P. Wang, 2003. Deep-sea pollen from the South China Sea: Pleistocene indicators of East Asian monsoon. Marine Geology, 201: 97-118.

Talbot, M.R., 1990. A review of the paleohydrological interpretation of carbon and oxygen isotopic ratios in primary lacustrine carbonates. Chemical Geology, 80: 261-279.

Talbot, M.R. & K.R. Kelts, 1990. Paleolimnological signatures from carbon and oxygen stable isotopic ratios in carbonates from organic carbon-rich lacustrine sediments. In B. J. Katz & B. R. Rosendahl (ed.), Lacustrine Basin Exploration: Case Studies and Modern Analogues. Am. Assoc. Pet. Geol., 99-112.

Thompson, L.G., M. Thompson, E. Davis, J.F. Bolzan, J. Dai, T.D. Yao, N. Gundestrup, X. Wu, L. Klein & Z. Xie, 1989. Holocene-late Pleistocene climatic ice core records from Qinghai-Tibet Plateau. Science, 246: 474-477.

Thompson, L.G., T. Yao, M. E. Davis, K. A. Henderson, E. Mosley-Thompson, P.-N. Lin, J. Beer, H.-A. Synal, J. Cole-Dai & J. F. Bolzan, 1997. Tropical climate instability: the last glacial cycle from a Qinghai-Tibetan ice core. Science, 276: 1821-1825.

Thompson, R. & F. Oldfield, 1986. Environmental Magnetism. Allen & Unwin., Londen.

Thunell, R., D. Anderon, D. Gellar, Q. Miao, 1994. Sea surface temperature estimates for the tropical western Pacific during the last glaciation and their implications for the Pacific warm pool. Quaternary Research, 41: 255-264.

Tucker, M. and P.V. Wright, 1990. Carbonate Sedimentology. Oxford London, Blackwell Scientific Publications. 496 pp.

Turner, J.V., P. Fritz, P.E. Karrow, B.G. Warner, 1983. Isotopic and geochemical composition of marl lake waters and implications for radiocarbon dating of marl lake sediments. Can. J. Earth Sci. 20: 599-615.

van Andel, T.H., 2002. The climate and landscape of the Middle part of the Weichselian glaciation in Europe: the Stage 3 Project. Quaternary Research 57: 2-8.

Vasconcelos, C., J. Mckenzie, S. Bernasconi, D. Grujic and A.J. Tian, 1995. Microbial mediation as a possible mechanism for natural dolomite formation at low temperatures. Nature, 377: 220-222.

Vasconcelos, C. and J. McKenzie, 1997. Microbial mediation of modern dolomite precipitation and diagenesis under anoxic conditions (Lagoa Vermelha, Rio de Janeiro, Brazil). Journal of Sedimentary Research, 67: 378-390.

Verhoeven J T A., 1979. The ecology of *Ruppia*-dominated communities in Western Europe. I. Distribution of *Ruppia* representatives in relation to their autecology. *Aquat. Bot*, 6:197-268.

Walker, K.F., I.G. Dunn, D. Edwards, T. Petr, and H.Z. Yang, 1996. A fishery in a changing lake environment: the naked carp *Gymnocypris przewalskii* (Kessler) (Cyprinidae: Schizothoracinae) in Qinghai Hu, China. International Journal of Salt Lake Research, 4/3: 169-222.

Wang, L. and P. Wang, 1990. Late Quaternary paleoceanography of the South China Sea: glacial-interglacial contrast in an enclosed basin. Palaeoceanography, 5: 77-90.

Wang, L., M. Sarnthein, H. Erlenkeuser, J. Grimalt, P. Grootes, S. Heilig, E. Ivanova, M. Kienast, C. Pelejero and U. Pflaumann, 1999. East Asian monsoon climate during the

Late Pleistocene: high-resolution sediment records from the South China Sea. Marine Geology, 156: 245-284.

Wang, P.X. and X.J. Sun, 1994. Last glacial maximum in China: comparison between land sea. Catena, 23: 341-353.

Wang, P.X., L. Wang, Y. Bian, Z. Jian, 1995. Late Quaternary paleoceanography of the South China Sea: surface circulation and carbonate cycles. Marine Geology, 127: 145-165.

Wang, P.X., 1999. Response of Western Pacific marginal seas to glacial cycles: paleoceanographic and sedimentological features. Marine geology, 156: 5-39.

Wang, W. and K.Z. Chen, 1990. Alkaline earth elemental compositions of Holocene lake deposits and environmental implications for Qinghai Lake, China. China Earth Sciences, 1 (3): 233-239.

Wang, P.X., S. Clemens, L. Beaufort, P. Braconnot, G. Ganssen, Z.M. Jian, P. Kershaw, M. Sarnthein, 2005. Evolution and variability of the Asian monsoon system: state of the art and outstanding issues. Quaternary Science Reviews, 24: 595-629.

Wang, Y.S., R.J. Gonzalez, M.L. Patrick et al., 2003. Unusual physiology of scale-less carp, Gymnocypris przewalaskii, i Lake Qinghai: a high altitude alkaline saline lake. Comparative Biochemistry and Physiology Part A 134: 409-421.

Webster, P.J., 1994. The role of hydrological processes in ocean-atmospheric interactions. Review of Geophysics, 32: 427-476

Wehausen, R and H.-J. Brumsack, 2002. Astronomical forcing of the East Asian monsoon mirrored by the composition of Pliocene South China Sea sediments. Earth and Planetary Science Letters, 201: 621-636.

Wei, K.Q. and F. Gasse, 1999. Oxygen isotopes in lacustrine carbonates of West China revisited: implications for post glacial changes in summer monsoon circulation. Quaternary Science Reviews. 18: 1315-1334.

Whitmore, T.J., M. Brenner, X. Song et al., 1994. Environmental implications of the late Quaternary diatom history from Xingyun Hu, Yunnan Province, China, Memoirs of the California Academy of Sciences, 17: 525-538.

Whitmore, T.J., M. Brenner, Z. Jiang et al., 1997. Water quality and sediment geochemistry in lakes of Yunnan Province, southern China, Environmental Geology, 32: 45-55.

Winkler M.G. and P.H. Wang, (1993), Late-Quaternary vegetation and climate of China. p.221-264, Ch.10 In: H.E. Wright et al. (Editors), Global Climates Since the Last Glacial Maximum. University of Minnesota Press, USA.

Woelfli, W., G. Bonani, M. Suter, R. Balzer, M. Nessi & C. Stoller, 1983. Radioisotope dating with the ETHZ-EN-tandem accelerator. Radiocarbon 25: 745-753.

Wright, H.E. Jr,, 1989. The amphi-Atlantic distribution of the Younger Dryas paleoclimatic oscillation. Quaternary Science Reviews, 8: 295-306.

Wright, H.E. Jr, et al. (Editors), 1993. Global Climates since the Last Glacial Maximum. University of Minnesota Press. 542 pp.

Wu, Y.F., 1984. Systematic studies on the cyprinid fishes of the subfamily Schizothoracinac from China. Acta Biologica Plateau Sinica 3: 119-140 (in Chinese).

Xiao, J.L., Q.H. Xu, T. Nakamura, X.L. Yang, W.D. Liang, Y. Inouchi, 2004. Holocene vegetation variation in the Daihai Lake region of north-central China: a direct indication of the Asian monsoon climatic history. Quaternary Science Reviews, 23: 1669-1679.

Xue, B., S.M. Wang, Y.H. Wu et al., 1999. Palaeoenvironmental reconstruction of Zoige basin of eastern Tibetan Plateau during the past 140 ka. Journal of Lake Sciences, 11: 206-212 (in Chinese).

Yan, J.P., M. Hinderer, G. Einsele, 2002. Geochemical evolution of closed-basin lakes: general model and application to Lake Qinghai and Turkana. Sedimentary Geology, 148: 105-122.

Yu, J.Q., K. Kelts and G. Lister, 1992. Paleoenvironmental signatures from carbonate minerals and their stable isotopic ratios from the closed-basin Lake Qinghai, China. Unpublished workshop report, Environmental Isotopes in Lacustrine Archives, University of Minnesota.

Yu, J.Q., K.R. Kelts, K.Z. Chen, P.X. Zhang, Z.S. An, 2000: An arid event at the Younger Dryas time window in the N. E. Tibet-Qinghai Plateau. Geolines, 11: 36-39.

Yu, J.Q., X.Y. Wang, J. Li and Z.S. An, 2001. Paleoenvironmental interpretations on organic carbon isotopic records from lake sediments: A critique. Journal of Lake Sciences. 13: 72-78 (in Chinese).

Yu, J.Q. and K. Kelts, 2002. Abrupt changes in climatic conditions across the late-glacial/Holocene transition on the N. E. Tibet-Qinghai Plateau: evidence from Lake Qinghai, China. Journal of Paleolimnology, 28/2: 195-206.

Yu, J.Q. and K.R. Kelts, 2002: Climatic change in the northeast Qinghai-Tibet Plateau during the glacial/Holocene transition. Quaternary Sciences 22 (5): 413-423 (in Chinese).

Yu, J.Q., Z.S. An, J. Li, X.Y. Wang and C. Zeng, 2003: A post-glacial paleolimnological record from Lake Huangqihai, Inner Mongolia, Proceedings of the 3rd International Limnogeology Congress, Tucson, Arizona.

Yu J.Q., C. Zeng, L.S. Zhang and Z.T. Liu, 2004. Evaluation of oxygen stable-isotope fractionation among co-existing carbonates in the sediments of Lake Qinghai. Journal of Lake Sciences. 16 (3): 223-226 (in Chinese).

Zhang, H.C., B. Wuennemann, Y.Z. Ma, J.L. Peng, H-J. Pachur, J.J. Li et al., 2002. Lake level and climate changes between 42,000 and 18,000 14C yr. B.P. in the Tengger Desert, Northwestern China. Quaternary Research, 58: 62-72.

Zhang, P.X. et al, 1989: On the model of post-glacial palaeoclimatic fluctuation in Qinghai Lake region. Quaternary Sciences 1989/1: 66-77.

Zhang, P.X. et al, 1989: Environmental evolution of the water body of Qinghai Lake since the postglacial age. Chinese Journal of Geochemistry 8/2: 112-125.

Zhang Z.K. et al.,2001. Climatic variations recorded by the sediment from Erhai Lake, Yunnan Province, Southwest China during the past 8000 years. Chinese Science Bulletin, 2001,44 (Suppl.): 80-82.

10. LIST OF ILLUSTRATIONS

Figure captions

Plate captions

11. LIST OF TABLES

Table captions

CURRICULUM VITAE

Born: 17.05.1954, Dongtai, Jiangsu Province, China

1972.5 –1975.7:   Nanjing University, Major: Hydrogeology & Engineering Geology.

1975.9 –1985.9:   Research assistant/Associate, Institute of Salt Lakes, Chinese Academy of Sciences (CAS).

1985.9 –1987.6:   Visiting scholar, Swiss Federal Institute of Water Resources (EAWAG).

1987.6 –1989.8:   ETH diplom (equivl.): ^{210}Pb and ^{137}Cs dating.

1987.6 –1991.10:   Research assistant, Geologisches Institut, ETH-Z, Zürich, Switzerland.

1991.11-1995.6:   Research Fellow, Limnological Research Center, University of Minnesota, USA.

1995.12-1998.2:   Associate professor, Institute of Salt Lakes, CAS.

1996.9 –1996.12:   Visiting scholar, Swiss Federal Institute for Environmental Sciences and Technology (Dübendorf).

1998.3-2001.3:   Guest professor, State Key Laboratory of Loess and Quaternary Geology, CAS.

1998.2-present: Research professor, Institute of Salt Lakes, CAS.

2002.5-present: Professor, the Graduate School of Chinese Academy of Sciences.

2003.10-2005.12: Institute of Applied Geosciences, University of Technology, Darmstadt.